TRANSLATION

THE PRODUCTION AND TREATMENT OF STEEL AND ALLOYS, SYMPOSIUM 38

By Various Authors

November 1960

PART II (pages 228-456)

PREPARED BY
LIAISON OFFICE
TECHNICAL INFORMATION CENTER
MCLTD
WRIGHT-PATTERSON AIR FORCE BASE, OHIO

This translation was prepared under the auspices of the Liaison Office, Technical Information Center, Wright-Patterson AFB, Ohio. The fact of translation does not guarantee editorial accuracy, nor does it indicate USAF approval or disapproval of the material translated.

Comments pertaining to this translation should be addressed to:

Liaison Office
Technical Information Center
MCLTD
Wright-Patterson Air Force Base, Ohio

Prof. Dr. of Tech. Sciences V. I. YAVOYSKIY, Engineers D. P. CHERENGA, S. A. TELESOV, Ya. L. TROSKUNOV, A. M. OFENGENDEN, I. I. REKKER.

DEGASSING OF STEEL IN LADLES AND MOLDS BY MEANS OF DIRECT ELECTRIC CURRENT.

A large mass of liquid metal was degasified by means of direct current on the basis of the fact that hydrogen is to be found in liquid steel in the form of electrically charged particles (1, 2, 3, 4, 5). The experiments were carried out in the Stalin Metallurgical Works. A welding machine with current strength up to 1000 A and 30-60 v voltage served as a generator of direct current.

All preceding laboratory tests (4, 5, 6, 7, 8) have shown that a high current density is required to attain intensive degassing of metal. V. G. Korotkov (7), for instance, brought the density of current up to 6 A/cm^2.

In our tests the current density for metal degasification in ladles amounted to 0.02 A/cm^2 and to 0.25-0.30 A/cm^2 in the molds.

Steel was melted in 125-ton capacity open-hearth furnaces fueled by a mixture of blast-furnace and gas-oven gases. Degassed were carbon and low-alloy steels (65G, 55S2, 10G2A, 40Kh, 50KhGA, St.45 and other grades).

Samples to check the content of hydrogen were taken during teeming from the ladle nozzle by means of an assay spoon. The metal was immediately poured into thick-walled cast-iron molds.

During the crystallization of the ingots in the molds, the hydrogen contents in the dead head sections were checked in samples drawn in by quartz tubes provided with copper foil tips. The quartz tubes were dipped into the metal to a depth of 160-150 mm. The percentage of hydrogen was determined in apparatus similar to those proposed by G. I. Batalin (9).

The contents of nitrogen and oxygen were checked in the process of teeming. For this purpose, metal previously deoxidized by aluminum (0.8% Al) was

poured into test beakers. In mold degassing tests samples for nitrogen and oxygen determination were taken from the ingots. A check could thereby be made of the distribution of these elements in the ingots.

To verify the contents and the composition of non-metallic inclusions, a sample weighing 6-7 kg was poured directly from the ladle. The sample was forged, and the inclusions were then separated by the electrolytic method.

DEGASSING OF STEEL IN THE MOLDS.

The tests were carried out with 3.1-3.4 t. bottom-poured ingots. The metal in the risers was heated up by "lunkerite". Current was supplied to the test ingot metal by one of the following methods: 1) by means of a graphite beaker and a copper busbar (Fig. 1-a). In this case the mold was insulated from the bottom plate by asbestos sheets, and from the beaker - by a chamotte mass; 2) by supplying current to the stool well insulated from the bogie by asbestos and chamotte bricks (Fig. 1-b). The anode was connected to the lower part of the ingot. A graphite electrode suspended from a special bracket, braced to the supporting pillar of the shop premises, served as the cathode (Fig. 2). The electrode was insulated from the bracket, and, consequently, also from the pillar by means of textolite disks.

The current was passed through the metal for 10-30 minutes, beginning from the second part of the process of mold filling, or from the moment when teeming was ended. The effect of the current action was checked by measurements of hydrogen concentration in the top section of the ingot during the process of crystallization. For purposes of comparison samples were simultaneously taken from the adjacent control ingot cast on the same stool. It was thereby assumed that under the influence of liquation hydrogen should accumulate in the upper part of both ingots with approximately the same intensity. This method of checking had a considerable drawback. There occurred a current-induced escape of hydrogen into the atmosphere after its energetic

Figure 1. Mold for tests of steel degassing by current:
a - supply of current through graphite beaker:
1 - clay solution; 2 - graphite beaker; 3 - asbestos;
4 - copper busbar 60 x 10 mm; 5 - 1665 to the top of the mold.
b - supply of current through bottom plate:
1 - clay solution; 2 - chamotte beaker; 3 - chamotte bricks; 4 - asbestos; 5 - copper lead.

concentration in the top section of the test ingot. This resulted in a levelling of the hydrogen contents in the test and control ingots.

Furthermore, the effect of electrolytic separation of hydrogen was also checked by the quality of the rolled stock (by its susceptibility to flake formation, macrostructure, surface flaws, content of sonims, etc.).

A comparison of the metal of the test and check ingots was made for each of these indices. This method is also not entirely without shortcoming due to the fact that the crystallization of the ingot takes 1 h. and 10 min., whereas the current was passed only for a period of 20-30 minutes after completion of teeming (lest the top section of the ingot become excessively carburized). Consequently, the free diffusion of hydrogen might lead to a certain equalization of its concentration over the entire volume of the ingot and efface the effect produced by direct current.

Figure 2. Diagram of layout for mold tests:
1 - textolite washer; 2 - stopper tube; 3 - contact; 4 - steel rod; 5 - graphitized electrode; 6 - control mold; 7 - test mold; 8 - windlass for electrode shifting; 9 - metal sheet fastened to a shop pillar; 10 - turning bracket.

Figure 3 shows the variation of hydrogen concentration in the top portion of the test and check ingots.

In a number of tests an energetic boil of metal and the evolution of fuel gas was observed near the suspended electrode. Obviously hydrogen also formed a component part of these gases. The hydrogen contents curves for test ingots show clearly expressed peaks followed by sags caused by the

evolution of hydrogen into the atmosphere. Thus the effect of direct current could be evaluated only after a determination has been made of the quantity of the released gases and after their analysis.

The data recorded in Table 1 indicate that there is no relationship between the difference in hydrogen concentrations in the top sections of the control and test ingots, on the one hand, and the amount of electricity passed through the ingots, on the other hand. This is to be attributed to the escape of hydrogen into the atmosphere.

For a 200-210-A current, i.e. when the current density is 0.06-0.07 A/cm^2, there is almost no intensified accumulation of hydrogen in the top part of the test ingot as compared to the control ingot. A considerable enrichment of the upper section of the ingot with hydrogen is to be observed at 500-600 A current (with 0.14-0.17 A/cm^2 density) in spite of its intensified evolution into the atmosphere.

A 1000-A current (density 0.25-0.30 A/cm^2) causes the process of hydrogen accumulation in the ingot dead head section to develop faster than the process of hydrogen liberation into the atmosphere, and leads to a higher concentration of it in the test ingot head.

In the case of inverse polarity the contents of hydrogen in the upper section of the test ingot is approximately the same as in the check ingot.

A Study of the Metal in the Test and Control Ingots.

A number of samples ranging from 100 x 100 mm to 160 x 160 mm in section were cut from rolled metal. They were cooled in a draft to check the susceptibility of steel to flake formation. Sensitivity to flakes was studied in macrosections of transversely cut disks and by longitudinal fractures of quenched samples.

Investigations have shown that the head part of the test ingots is not distinguished by a higher sensitivity to flakes than that of the check ingots, even though the accumulation of hydrogen in the upper section of the test

Figure 3. Variation of hydrogen concentration in the heads of the test and standard control ingots in the process of crystallization:
——— test ingot; ----- standard ingot.
a) Current on; b) Current off; c) Heat d) Time, min.

ingots and its more intensive escape into the atmosphere under the influence of current should have affected the sensitivity of the metal to flakes. It may have been caused by a considerable carbon enrichment of the head portions of test ingots resulting from the dissolution of the electrode.

It is well known that an increase of carbon concentration in iron (at a temperature lower than that of $\alpha \rightarrow \gamma$ -transformation) diminishes considerably the rate of hydrogen diffusion (10), augmenting thereby the sensitivity to flakes.

The chemical inhomogeneity of both the test and check ingot metal was studied in order to determine the effect of direct current on the distribution of impurities in the test ingots.

Samples were taken by boring the top and bottom ends of bars A, C, and O. From each bar section samples were taken from the section center and at one quarter length of one of the diagonals.

Some of the results obtained in studying the samples are recorded in Table 2. The samples marked by indices A, C, and O, were taken from the upper,

third from the top, and bottom (6 to 7) bars. Samples with index H were taken from the bottom end of the bars. Index Ц signifies that the samples were taken from the center of the sections (samples without that index were taken at one-quarter length of the sectional diagonal).

Table 1.

Concentration of Hydrogen in the Upper Part of the test and check Ingots.

Heat No.	Time from the beginning of test, min.	Current A	Quantity of flowing electricity coulomb x 60	Difference in hydrogen contents in the upper parts of test and check ingots, $cm^3/100$ g.

Test at inverse polarity (the upper electrode serving as anode)

During casting of test ingots the metal contained 0.15% C, 0.029% S, and 0.019% P. Similar results were obtained from other analyses of the test and check ingots.

Table 2.

Chemical Inhomogeneity of the Test and Check Steel Ingots.
(Grade of Steel 10G2A, Heat 4173)

Index	Contents, %					
	C		S		P	
	Test	Check	Test	Check	Test	Check

A considerable carburization of metal streaming from the electrodes was to be observed in the upper part of the test ingots. Phosphorus distribution in the test and check ingots was identical.

As seen from Table 2, the concentration of sulfur under the cathode is slightly lower as compared with its contents in the check ingot. Although the difference in concentrations is very small, it still exceeds the magnitude of the error in the analysis. The reduced percentage of sulfur at the cathode does not contradict the postulate concerning its existence in the metal in the ion form (11).

The control specimens cut from the upper and bottom ends of bars A, C, and O were subjected to deep etching and were used for the study of the macrostructure of the test and check ingots. It was established that the test ingots have a somewhat denser structure. This is particularly noticeable in bars C and at the bottom ends of bars A.

The segregation ghost in the majority of cases was less pronounced in the bars of the test ingots than in those of the check ingots.

The distribution of gases in the rolled metal of the test and check ingots

was also studied. The gases were identified by the method of vacuum extraction during melting in a unit designed by the TsNIIChM (Central Scientific-Research Institute of Ferrous Metallurgy). In addition to this, nitrogen was determined in samples taken from the bars by method of dissolution.

The content of oxygen in bar A is, ordinarily, higher than in bar C. No appreciable difference was to be observed in the character of oxygen distribution in the test and control ingots.

The percentage of residual oxygen in the test ingots was always markedly higher in bar A than in bar C. This was almost never observed in the check ingots. Thus there exists a considerable difference in the character of hydrogen distribution in the test and check ingots. On the other hand, in the tests at inverse polarity the contents of residual oxygen in bar A was smaller than in bar C, resembling the distribution of hydrogen in the check ingot. It is characteristic, though, that the proportion of hydrogen in both sections of the test ingot is lower than in the check ingot. This indicates that the hydrogen tends to shift in the direction of the cathode (Fig. 4).

Nitrogen distribution turned out to be different in the test and check ingots (Fig. 5).

A positive liquation of nitrogen was registered in the check ingots, while in the test ingots, there was no positive liquation; a tendency was even discerned towards migration of nitrogen to the lower levels of the ingot.

The residual, predominantly molecular, hydrogen reflects, as it were, in a certain measure the total contents of hydrogen in metal during the crystallization of a steel ingot, since the growth of the latter (hydrogen content) enhances the possibility for the separation of the gas phase within the metal. As to the migration of nitrogen into the lower levels of test ingots, this factor still calls for verification. Unlike V. M. Prosvirin (11), Seitz and Dauer were also able to observe the movement of nitrogen to the anode, and not to the cathode, during the electrolysis of solid steel samples.

A detailed study of the character of distribution and the composition of non-metallic inclusions in test and check ingots was also made in this investigation. For this purpose the following methods were used: a) microscopic evaluation of the oxide and sulfide inclusions with an estimate of contamination according to a standard five-mark scale, and b) electrolytic separation of inclusions and their subsequent analysis.

Investigations show that direct electric current produces practically no effect on the distribution and the chemical composition of the oxide and sulfurous inclusions.

Figure 4. Distribution of residual hydrogen in the upper half of the ingots (figures indicate the contents of hydrogen in hundred-thousandth fractions of one percent):
a - steel 50KhGS; b - steel 65G of heats 1188, 5199, 3172; c - average results of heats with direct polarity; d - steel 40Kh of heat 7171 with inverse polarity; the unshaded rectangles refer to check ingots.
1) Bar A; 2) Bar C.

DEGASSING OF STEEL IN LADLES

Owing to the difficulties involved in the evaluation of the degassing effect of current passed through the metal in the ladle, two different procedures were used in the investigation.

The first procedure consisted in a comparison of the degree of gas saturation, contamination by nonmetallic inclusions, and the other character-

istics of metal obtained in ordinary heats and in runs conducted, whenever possible, under the same conditions but involving treatment of the liquid steel by electric current in the ladle, while holding the latter under the runner after tapping.

Figure 5. Nitrogen distribution in test (with direct polarity) and check ingots (averages for 6 ingots).
———test ingots ------ check ingots.

For comparison of the current-treated metal with the ordinary metal, samples were taken from the furnace before deoxidation and prior to tapping, as well as in the process of teeming from each bottom plate. The ladles were grounded. The corresponding safety regulations were duly observed.

The current was supplied to the metal by means of coils cut from carbon electrodes. The location of the pseudo-stoppers and the carbon coils in the ladlesis shown in Figures 6 and 7. The carbon coil of the pseudo-stopper (the lowest on the stopper) usually served as the anode.

One of the upper coils of the opposite stopper served as the cathode. An electric contact between the stopper rod and the coil was obtained by filling the clearance between the rod and the coil with fine graphite powder,

Figure 6. Location of the stopper-electrodes in the ladle: 1 - flange; 2 - steel pipe; 3 - protective hood; 4 - beaker with textolite washers; 5 - bracket; 6 - bush; 7 - stopper tubes of the "anode" with a carbon cap at the end; 8 - stopper tubes of the "cathode"; 9 - bush; 10 - bracket; 11 - carbon tubes of the "cathode"; 12 - runner lip.

carried out during assembly of the stoppers.

The second test procedure involved casting with the current on. The possibility of a return passage of hydrogen into the degasified volumes of metal was thereby excluded. This could not be achieved in the first variant, since from the moment of switching the current on and up to filling the molds on the first bottom plate there elapsed 18 to 30 minutes. Moreover, the passage of current during the filling of part of the bottom plates made it possible

to compare the hydrogen contents in metal subjected to electrolysis with the proportion of hydrogen in the remaining metal of the same heat.

The tests were conducted in the same manner as in the first procedure, but the pseudo-stopper which usually served as the cathode had two carbon tubes (the upper tube partially embedded in slag, and the other situated 0.8-1.0 m lower). This made it possible to pass the current during furnace tapping and during teeming of metal into the molds of the first bottom plate.

The first method was used in 6 heats, the second - in 2 heats, and 4 heats were run for control purposes.

The data on the contents of hydrogen in the test and check heats will be found in Table 3 and Figures 8 and 9. On the first bottom plate the contents of hydrogen in the metal of the check heats was increased owing to ladle additions of ferroalloys, and also because of the contact between the metal and the insufficiently dried ladle lining (the ladle was not specially calcinated). In teeming silicon steel, i. e. after introducing up to 2.5% ferrosilicon into the ladle, a rise in hydrogen content takes place in the metal of the first stools as against the respective value in the furnace samples.

As teeming progresses the proportion of hydrogen in metal shows a slight drop caused by its evolution into the atmosphere.

A lower content of hydrogen in metal of the first bottom plate, as compared with the furnace samples, was observed in the test heats carried out according to the first procedure. In view of this fact the proportion of hydrogen in the silicon steel of the test heats in the molds of the first bottom plate was by 1-1.5 $cm^3/100$ g lower than in the metal of the check heats.

The hydrogen contents in the metal of the test heats diminishes somewhat in the process of further teeming, or becomes almost constant. Consequently, the difference in hydrogen percentage between the metal of the test and check heats decreases on the subsequent bottom plates (see Fig. 8). This

indicated the return of hydrogen into the previously degassed regions and, possibly, even the penetration of hydrogen from slag to metal after the current has been switched off. Thus, the first procedure does not fully reveal the degasifying effect of the current. During the 20-40 minutes elapsing

Figure 7. Ladle with stoppers:
1 - pseudo-stopper "anode"; 2 - acting stopper;
3 - pseudo-stopper "cathode".

Figure 8. Variation of hydrogen contents in the process of steel teeming:
a - steel 60S2; b - steel 55S2; 1 - check heat 7689;
2 - test heat 7677 (inverse polarity); 3 - check heat 8758; 4 - test heat 8749 (direct polarity).
1) Furnace sample; 2) Numbers of bottom plates in the process of teeming.

from the moment of current cut-off to the drawing of the first sample, the unevenness in the distribution of hydrogen (caused initially by the action of the current) disappears. During the teeming of silicon steel (60S2 and 55S)

Table 3.

Hydrogen Contents in Test and Check Heats

No. of Heat & Grade of Steel	Hydrogen contents in 100 g of metal, cm^3									
	Before Tapping	during teeming (in terms of bottom plates)								
		numbers of bottom plates in the process of teeming								
		1	2	3	4	5	6	7	8	9
									Inverse polarity	
									Direct polarity	
									Check heat	
									Check heat	
									Direct polarity	
									Direct polarity	
									Direct polarity	
									current for the first three bottom plates	
									current under the runner 8-9 m.	
									Control heat	
									Control heat	
									Current for the first three bottom plates	

Note: In heats 7677, 8749, 8744, 8755, and 8765 the current was passed through the metal for 10-21 min., while the ladle was held under the runner; in heats 8839 and 8831 - with the ladle under the runner and also during teeming into the molds of the first three bottom plates.

a considerable reduction in hydrogen percentage was observed in it, both in the case of direct and inverse polarity, i.e. when the lower carbon tube served as the cathode as well as when it served as the anode.

Figure 9. Variation of hydrogen concentration in the test steels :
a - steel D and 45, current was passed while the ladle was held under the runner; b - steel 20 Kh and D, current was passed while the ladle was held under the runner and during teeming:
1 - check heat 6712; 2 - heat 8765; 3 - heat 8744; 4 - heat 8755; 5 - steel 20Kh, heat 8831; 6 - steel D, heat 8839; 7 - Sampled before tapping; 8 - End of current flow; 9 - bottom plate numbers in the process of teeming.

The above data coincide with the results of the tests carried out with solid silicon steel samples by V. Ya. Yavoysky and D. F. Chernega. This justifies the assumption that hydrogen is to be found in silicon steel (with about 2% Si) not only in the form of proton H^+, but also in the form of negatively charged ions.

Of practical interest is the fact that the average contents of hydrogen during teeming was less in the test heats than in the check runs, and that the drop of average hydrogen contents in the poured metal, as compared with the hydrogen contents in the last sample was far greater for the test heats than for the check heats.

The carbon steel in all heats had practically the same composition, and besides, the same method of deoxidation was used. All heats of carbon steel, cast according to the first method, will therefore be considered together.

A certain reduction of hydrogen contents was always registered in the metal of the first bottom plate of these heats, as compared to the furnace sample (see Figure 9).

Later on throughout the teeming operation the proportion of hydrogen remained approximately constant or showed a slight drop. This pertains both to the test and the check heats (Table 4). In spite of the higher hydrogen

Table 4.

Variation of Hydrogen Contents in Carbon Steel During Teeming in Test and Check Heats.

Number of the heat and its characteristic.	Hydrogen contents in the furnace sample, $cm^3/100$ g.	Average concentration of hydrogen during teeming, $cm^3/100$ g.	Difference of hydrogen concentrations
test			
"			
"			
"			
"			
check			
"			

percentage in samples taken from the furnace during test heats, as compared with check heat samples, the average hydrogen contents in the metal in the teeming process turned out to be lower for these heats than for the check runs. In teeming in conformity with the second version a decline in the percentage of hydrogen was observed throughout the entire period of current flow. The contents of hydrogen as registered in heat 8839 by the moment the current was turned off (4.24 $cm^3/100$ g) occurs rarely in the operating conditions prevailing at the Stalin Metallurgical Works. The same applies to the chromium steel heat No. 8831. Characteristic is the gradual rise of hydrogen contents in metal cast after the cut-off of current. In the check heats, and in the heats repeatedly observed in other plants, an increase in hydrogen concentration as a result of its transfer from the slag was to be registered only in the metal on the last bottom plate. Consequently, the gradual rise of hydrogen concen-

tration beginning with the fourth bottom plate may be explained only by a re-transfer of the hydrogen into the areas of metal previously degassed by the current. Thus, the considered data indicate that a well-defined, though not of major significance, degassing effect is produced by direct electric current.

To study the effect of current on the behavior of oxygen and nitrogen three samples were taken (from the ladle) during teeming. A part of these samples was deoxidized by aluminum; the other part was not. On the basis of the data obtained by us it may be maintained that direct current with 0.02 A/cm^2 density fails to produce any effect on the distribution of oxygen and nitrogen in liquid steel.

With regard to oxygen distribution a similar situation was revealed in the tests conducted with the use of current in the process of steel crystallization. The behavior of nitrogen in tests carried out in molds and ladles turned out to be different. This fact, most probably, may be attributed to the low density of the current passed through the metal during teeming.

CONCLUSIONS

1. The possibility of steel degassing in ladles and molds on an industrial scale by means of direct current was proven in tests.

2. In the process of steel degasification in molds there occurs: a) a more intensive accumulation of hydrogen in the top section of the ingot; b) a positive segregation of hydrogen remaining in the metal after the passing of current in tests with direct polarity; c) a certain improvement of the macrostructure in the metal of test ingots as against that of control ingots; d) a weakening of the positive segregation of nitrogen in test ingots with direct polarity.

3. Degasification of steel by means of direct current in the ladle, with conditional current density not exceeding 0.02-0.25 A/cm^2, has resulted in a 1.5-2 $cm^3/100$ g drop of the average hydrogen contents in the ladle metal

in comparison with the hydrogen contents in the metal from the furnace; there was also a 0.5-1 $cm^3/100$ g drop of the average contents of hydrogen in the ladle metal of test heats as compared with the respective content in the ladle metal of check heats. This was observed even in those cases, when the metal of the test heats showed a higher degree of gas saturation in the furnace than the metal of the control runs.

The most effective method of degassing by means of direct current is to pass the current through the metal in the ladle not only while it is held under the runner, but also in the process of teeming.

5. During degasification the direct current does not affect the contents and distribution of oxygen and nonmetallic inclusions in the ingot, nor does it affect the contents of oxygen, nitrogen, and nonmetallic inclusions in the ladle metal. The composition of oxide nonmetallic inclusions doesn't change under the influence of current.

REFERENCES

1. A. I. Krasnikov, Izvestiya AN SSSR /News of the Academy of Sciences of the USSR/ OTN, No. 1, 1946.
2. N. A. Galaktionova, Ibid, No. 11, 1949.
3. V. I. Yavoyskiy, Gazy v vannakh staleplavil'nykh pechey /Gases in the Baths of Steelmaking Furnaces/, Metallurgizdat, 1952.
4. V. I. Yavoyskiy, G. I. Batalin, Stal' /Steel/, 1954, No. 6.
5. V. I. Yavoyskiy, G. I. Batalin, Trudy nauchno-tekhnicheskogo obshchestva chernoy metallurgiyi /Transactions of the Scientific and Technical Society of Ferrous Metallurgy/ v. 4, 1955, Metallurgizdat.
6. D. P. Lovtsov, Liteynoye proizvodstvo /Foundry Work/, 1955, No.9.
7. B. G. Korotkov, Avtoreferat dissertatsiyi /Author's Report on Dissertation/ 1955, Sverdlovsk, Polytechnical Institute.
8. V. I. Yavoyskiy, D. F. Chernega, Stal', 1956, No. 9.
9. G. I. Batalin, Trudy instituta chernoy metallurgiyi AN USSR /Transactions of the Institute of Ferrous Metallurgy of the Academy of Sciences of the Ukrainean SSR/ v. 6, 1953.

10. N. M. Chuyko, Nauchnyye trudy Dnepropetrovskogo metallurgicheskogo instituta /Proceedings of the Dnepropetrovsky Metallurgical Institute/ v. 28, Electrometallurgy, Metallurgizdat, 1955.

11 O. A. Yesin, P. V. Gel'd, Uspekhi khimiyi /Progress of Chemistry/, 1953.

Engineer V. K. Zhuravlyev & Professor A. A. Zhukhovitskiy

Department of Physical Chemistry

TO THE THEORY OF METALLOID SOLUTIONS IN METALS.

Little is known at the present time about the effect of a substance dissolved in liquid iron on the thermodynamic activity of another substance. These data are nonetheless important in connection with the development of the theory of solutions in metals and have a practical significance for steelmaking.

The thermodynamics of sulfur in various iron solutions had been studied most of all.

Chipman and Ta Li (1), White and Skelly (2) have studied the equilibrium of sulfur with the gas phase of H_2 and H_2S in liquid iron. They were able to determine that the ratio $P_{H_2S}/P_{H_2} \cdot (\%\ S)$ is constant up to 1.2% S. Maurer, Hammer, and Mobius (3) have investigated a wider range of sulfur concentration: up to 36.5% S, i.e. up to the theoretical composition of FeS. These investigators have also found that the solution of sulfur in liquid iron is ideal up to 1% S. It is important, however, to emphasize that in the work of Chipman and Ta Li and in that of White and Skelly the heats were contaminated by silicon (over 2%). Moreover, the induction furnace used in Chipman's and Ta Li's experiments showed a high temperature gradient which led to thermal diffusion in the mixture of H_2 and H_2S gases.

I. A. Kitchener, J. Bockris and A. Liberman (4) succeeded in making an indirect evaluation of the effect of carbon on the activity of sulfur. A direct measurement was carried out by them in a heat saturated with carbon. The results show that in this case the activity of sulfur is doubled. Morris and Williams (5) have thoroughly investigated the effect of silicon on the thermodynamic activity of sulfur in iron at 1615°. At the same time these authors were able to determine the equilibrium constant of the reaction

$(S) + H_{2(gas)} = H_2S_{(gas)}$ for the pure Fe-S system. They have found that up to 1% S the Fe-S system is ideal within these limits.

$$K = \frac{P_{H_2S}}{P_{H_2}[\%S]} = 0.00256 \text{ at } 1615^\circ.$$

In studying the effect of silicon on the activity of sulfur the contents of silicon was found to be attaining 9.4%, the activity coefficient being equal to 6.9.

Morris and Buehl (6) studied the influence of carbon on sulfur activity. Most of the tests were carried out at 1600°. When iron was saturated with carbon the activity coefficient of sulfur turned out to be higher than six. The temperature dependence of sulfur activity was insignificant. However, it must be noted that only a few tests were carried out at different temperatures (2 tests at 1415°, two at 1200°, and one at 1800°.

Chipman and Sherman (7) completed an inquiry into the effect of phosphorus on the activity of sulfur in liquid iron at 1600°. It was established that phosphorus actually increases the activity of sulfur, but less than carbon and silicon. The sulfur activity coefficient in the Fe-P-S system with phosphorus contents at 8.04% was equal to 2.34.

The effect of temperature on the activity of sulfur in the Fe-S system was studied, in particular, by Sherman, Elvander, and Chipman (8). According to their data, the rise in temperature causes a higher deviation from ideality. However, the authors do not believe this temperature effect to be solidly established. A detailed study of the influence of manganese on sulfur activity in the Fe-Mn-S system at 1600° is described in a paper by Sherman and Chipman (9). The contents of manganese was brought to 8.2%, with the sulfur activity coefficient amounting in this case to 0.6. The same paper contains data on the effect of aluminum on sulfur activity, as well as on the influence produced by silicon. With aluminum contents at 2.78% the coefficient of sulfur activity was 1.42.

V. A. Karasev and A. M. Samarin (10) determined the activity of sulfur at 1600° in silicon-containing liquid iron. The authors used the method of sulfur evaporation in vacuo. The existence of a linear relationship between the contents of sulfur in the solution and the rate of its evaporation justify the conclusion that the coefficient of sulfur activity does not depend on the contents of sulfur over the investigated range of its concentrations. The varying slope of the straight lines evidences the dependence of the sulfur activity coefficient upon the contents of silicon in the metal. The ratio of sulfur volatilization rate in a solution with a given proportion of silicon to the rate of sulfur volatilization in a silicon-free solution determines the numerical value of the sulfur activity coefficient. The data of these authors show a considerable disagreement with the data presented by Morris and Williams (5) who studied the effect of silicon on sulfur activity on the basis of equilibrium

$$/S/ + H_{2(gas)} = H_2S_{(gas)}$$

For 3.5%Si, according to the Morris' and Williams' data, $\gamma_S^{Si} \approx 1.7$, whereas according to V. A. Karasev and A. M. Samarin $\gamma_S^{Si} \approx 4$, where γ_S^{Si} is the sulfur activity coefficient in the Fe-Si-S system.

A theoretical interpretation of the solutions under review was given by M. I. Temkin and L. A. Shvartsman (11). It is assumed that the observed growth of the sulfur activity coefficient with increasing concentration of sulfur is associated with the formation of an interstitial solution. The authors feel that since the gamma-iron lattice is face-centered cubic, and the carbon atoms are situated in it in the centers of the cubes, then for ν_1 atoms of iron there must be $\frac{1}{4}\nu_1$ vacancies for carbon atoms. If the actual number of carbon atoms is equal to ν_2, then they may be arranged in the $\frac{1}{4}\nu_1$ vacancies in the following number of ways:

$$W = \frac{\left(\frac{1}{4}\nu_1\right)!}{\nu_2!\left(\frac{1}{4}\nu_1 - \nu_2\right)!} \qquad (1)$$

For any fixed arrangement the entropy comprises

$$S = \nu_1 S_1 + \nu_2 S_2, \qquad (2)$$

where S_1 and S_2 are constant.

For a given composition, at any possible distribution of carbon atoms, the entropy will be

$$S = \nu_1 S_1 + \nu_2 S_2 + k \cdot \ln W. \qquad (3)$$

Whence, using the Stirling formula ln n! = n ln - n, we obtain

$$\bar{S}_2 = \frac{\partial S}{\partial \nu_2} = S_2 + k \cdot \ln \frac{\frac{1}{4}\nu_1 - \nu_2}{\nu_2}. \qquad (4)$$

The authors consider the partial molar heat contents of the H_1 and H_2 components to be independent from the solution concentration. Then

$$\mu_2 = \bar{H}_2 - T\bar{S}_2 = \bar{H}_2 - TS_2 - kT \ln \frac{\frac{1}{4}N_1 - N_2}{N_2}. \qquad (5)$$

Assuming further that

$$\mu_2^0 = \bar{H}_2 - TS_2 - kT \ln \frac{1}{4}, \qquad (6)$$

and comparing expressions (5) and (6), one finds that

$$\mu_2 = \mu_2^0 + kT \ln a_2, \qquad a_2 = N_2\gamma_2 = \frac{N_2}{N_1 - 4N_2},$$

whence the variation of the sulfur activity coefficient with sulfur concentration in γ-iron may be described by the following formula

$$\gamma_C = \frac{1}{1 - 5N_C}. \qquad (7)$$

This formula was checked by the authors on the basis of R. Smith's (12) experimental data for equilibria

$$C_{(\gamma\text{-Fe})} + CO_2 = 2CO,$$
$$C_{(\gamma\text{-Fe})} + 2H_2 = CH_4.$$

Formula (7) shows a satisfactory agreement with the experimental data on the activity of carbon dissolved in liquid iron (up to 3% C). A. M. Samarin and L. A. Shvartsman (13) made use of the conclusions drawn in this work for a theoretical explanation of the effect produced by carbon on the activity of sulfur dissolved in liquid iron. Proceeding from the fact that the number of vacancies for sulfur and carbon is always equal to one-fourth the iron atoms, and that carbon and sulfur occupy these places on an equal basis, the authors obtain

$$f_S = \frac{1}{1 - 6(N_C + N_S)} \qquad (8)$$

This equation is in good accord with the experimental data (6), at any rate for carbon contents up to 3%.

O. A. Yesin and P. V. Gel'd (14), in referring to V. I. Arkharov, justifiably remark that the figure of ¼ is taken without sufficient substantiation. If one should take into account not only the atoms of carbon situated in the center of a given cube, but also those in the centers of the adjacent cubes, their number will become considerably higher. Consequently expression (8) should be regarded as semi-empirical.

The solutions of non-metals in iron present a great theoretical interest because they form a little known intermediate class between the metallic and ionic melts. There still is no quantitative theory of interaction between substances dissolved in liquid iron, since the molecular structure of such solutions is, so far, insufficiently known. Nevertheless, the reciprocal effect of the dissolved substances may be studied on a simple structural model. As already stated above (11, 13), the concept of interstitial solutions has been resorted to in the interpretation of the properties of metalloid solutions. However, the a-priori considerations and the test data seem to indicate that real solutions, particularly those liquid, do not, as a rule, fit into this pattern.

The experiments were carried out with Fe-S, Fe-C-S, Fe-Si-S, and Fe-P-S

systems in which the thermodynamic activity of sulfur and the influence exerted upon it by the concentrations of sulfur, carbon, and silicon were studied. The experimental method involved was described in an earlier paper (15). The method was based on the application of the radioactive isotope of sulfur S^{35}. A refractory ZrO_2 cylinder was brought into contact with the mirror of metal containing sulfur together with its radioisotope. The amount of sulfur which passed from the metal into the refractory cylinder was proportional to the thermodynamic activity of sulfur in metal. Electrolytic iron, commercial silicon and ferrophosphorus containing 16.05% P, 0.082% S, 0.2% Si, and 0.047% C were used in this work. Carbon was added in the form of synthetic cast iron, which was manufactured by holding molten electrolytic iron in a graphite crucible.

Figure 1. Sulfur activity coefficient as a function of sulfur contents in iron in the Fe-S system, for various temperatures:
0 - Fe-C-S system; □ - Fe-Si-S system; Δ - Fe-P-S system.
1) Contents (S), %.

For the study of the Fe-S system a number of iron ingots was prepared with different contents of sulfur. Sulfur was introduced in the form of FeS. In all tests FeS had an identical proportion of radioactive sulfur.

Each heat was run for three temperatures. Up to 10 refractory cylinders

were used for each temperature. The data pertaining to the Fe-S system are recorded in Figure 1. Each point in the diagram represents an average of 6-10 tests. The data on systems Fe-C-S, Fe-Si-S, and Fe-P-S are shown in Figure 2 and Tables 1-3.

The activity coefficients which deviated slightly from unity were measured with particular care. Each such coefficient represents an average of 10 or more tests. The computation of the sulfur activity coefficient in the Fe-C-S system containing 0.49% C at 1550° may be set as an example. The metal for which the activity coefficient was taken to be unity contained 0.082% S and 0.01% C. The radiation intensity produced by the refractory cylinders was equal to $I^* = 96$ ppm on the average for ten tests. The relative radiation intensity of metal $I_M^* = 1560$ ppm. The effect of carbon on the thermodynamic activity of sulfur was studied at 0.081% S and 0.49% C contents in metal. The relative radiation intensity of metal $I_M = 1500$ ppm. The data on radiation intensity produced by the refractory cylinders are listed in Table 4.

Table 1.

Sulfur Activity Coefficient Values for Fe-C-S System.

Contents %		γ_S^C - sulfur activity coefficient.		
S	C	1550°	1600°	1650°

According to the previously derived relationship, the coefficient of sulfur activity in liquid iron containing 0.081% S and 0.049% C may be calculated from formula

$$\gamma_S^C = \frac{I \cdot I_M^* \cdot [\%\,S]^*}{I^* I_M \cdot [\%\,S]} = \frac{106 \cdot 1560 \cdot 0{,}082}{96 \cdot 1500 \cdot 0{,}081} = 1{,}16,$$

where I - radiation intensity produced by refractory cylinders in the tests involving the Fe-C-S system;

I_M - relative radiation intensity of metal in tests involving the Fe-C-S system;

I^* - radiation intensity produced by refractory cylinders in tests involving the Fe-S system;

I_M^* - relative radiation intensity of metal in tests involving the Fe-S system;

$[\%S]$ - sulfur contents in metal in tests involving the Fe-C-S system;

$[\%S]^*$ - sulfur contents in metal in tests involving the Fe-S system.

Table 2.

Sulfur Activity Coefficient Values for Fe-Si-S System.

Contents, %		γ_S^{Si} - sulfur activity coefficient		
S	Si	1560°	1620°	1670°

As calculated from experimental data, the least quadratic deviation in determining the activity coefficients amounts to 3.5%.

On the basis of the obtained experimental data calculations were made of $\Delta \overline{H}$, $\Delta \overline{F}$, and $\Delta \overline{S}$. As is well known, activity and the activity coefficient vary with temperature in accordance with equation

$$RT^2 \frac{\partial \ln a}{\partial T} = -(\lambda - \lambda_c); \qquad (9)$$

$$\Delta \overline{H} = \lambda - \lambda_c,$$

where λ_c and λ are respectively the heats of evaporation of one mole of dissolved sulfur in the standard and in the investigated states.

Table 3.

Sulfur Activity Coefficient Values for Fe-P-S System

Contents, %		γ_S^P - sulfur activity coefficient		
S	P	1550°	1600°	1675°

Table 4.

Radiation Intensity of Refractory Cylinders

Numbers of the refractory cylinders	1	2	3	4	5	6	7	8	9	10
Radiation intensity, p.p.m.		I_{cp} = 106 p.p.m								

Considering that the 1-% solution of sulfur in pure iron is very closely approaching the ideal solution, it may be taken as the standard state.

The free energy variation was calculated by formula

$$\Delta \overline{F} = RT \ln a_S. \qquad (10)$$

The entropy variation was computed according to equation

$$\Delta \overline{F} = \Delta \overline{H} - T \Delta \overline{S}. \qquad (11)$$

The computed thermodynamic values are to be found in Tables 5-7 and in Figures 3 and 4.

Figure 2. Sulfur activity coefficient as a function of the contents of carbon, silicon, and phosphorus in the Fe-C-S, Fe-Si-S, Fe-P-S systems, for various temperatures:
1 - Fe-C-S; 2 - Fe-Si-S; 3 - Fe-P-S.
1) Contents [C], [Si], [P], %.

THE THEORY OF THE PROBLEM

In considering the solutions of metalloids in solid and liquid iron M. I. Temkin and L. A. Shvartsman (11), A. M. Samarin and L. A. Shvartsman (13) assumed that they form interstitial solutions. However, for a case of liquid solution it is natural to visualize that the solvent affords to the atoms of the dissolved substance both the lattice points and definite sites between them. In other words the solution is envisaged as a combination of an interstitial and substitutional solutions.

Let us consider the statistical theory of such a solution.

Let M_1 be the number of atoms of the solvent;

M_2 - the number of atoms of the dissolved substance;

x - the number of atoms of the dissolved substance located in the lattice points;

(M_2-x) - the number of atoms of the dissolved substance located in the interstices;

h - heat of transition of one atom of the dissolved substance from the interstice into the lattice corner;

z - number of sites in the interstitial solution per one atom of solvent.

Table 5.

Values of $\Delta\bar{H}$, $\Delta\bar{F}$, and $\Delta\bar{S}$ of Sulfur in Fe-C-S System

C, %	$\Delta\bar{H}$ cal/g-atom	1550°		1660°		1650°	
		$\Delta\bar{S}$ cal/g-atom degree	$\Delta\bar{F}$ cal/g-atom	$\Delta\bar{S}$ cal/g-atom degree	$\Delta\bar{F}$ cal/g-atom	$\Delta\bar{S}$ cal/g-atom degree	$\Delta\bar{F}$ cal/g-atom

Table 6.

Values of $\Delta\bar{H}$, $\Delta\bar{F}$, and $\Delta\bar{S}$ of Sulfur in Fe-Si-S System

Si%	$\Delta\bar{H}$ cal/g-atom	1560°		1620°		1670°	
		$\Delta\bar{S}$ cal/g-atom degree	$\Delta\bar{F}$ cal/g-atom	$\Delta\bar{S}$ cal/g-atom degree	$\Delta\bar{F}$ cal/g-atom	$\Delta\bar{S}$ cal/g-atom degree	$\Delta\bar{F}$ cal/g-atom

Figure 3. Partial molar heat contents of sulfur versus carbon, silicon, and phosphorus contents in systems:

1 - Fe-C-S; 2 - Fe-Si-S; 3- Fe-P-S.

a) $\Delta \bar{H}$ cal/g-atom; b) Contents [C], [Si], [P], %

Figure 4. Partial molar entropy of sulfur versus carbon, silicon, and phosphorus contents in systems:

1 - Fe-C-S; 2 - Fe-Si-S; 3 - Fe-P-S.

a) $\Delta \bar{S}$ cal/g-atom degree; b) [O], [C], [Si], %

Then

$$F = xh - T\,k \ln W, \tag{12}$$

$\frac{dF(x)}{x} = 0$ according to the condition of thermodynamic equilibrium.

Consequently,

Table 7.

Values of $\Delta\bar{H}$, $\Delta\bar{F}$, and $\Delta\bar{S}$ in the Fe-P-S system

P%	$\Delta\bar{H}$ cal/g-atom	1550°C		1600°C		1675°C	
		$\Delta\bar{S}$ cal/g-atom degree	$\Delta\bar{F}$ cal/g-atom	$\Delta\bar{S}$ cal/g-atom degree	$\Delta\bar{F}$ cal/g-atom	$\Delta\bar{S}$ cal/g-atom degree	$\Delta\bar{F}$ cal/g-atom

or,

$$h - kT\frac{\partial \ln W}{\partial x} = 0$$

$$\frac{\partial \ln W}{\partial x} = \frac{h}{kT}. \qquad (13)$$

The thermodynamic probability for such a solution will be equal to

$$W = \sum_{x=0}^{x=M_2} \cdot C_{zM_1}^{M_2-x} \cdot C_{M_1+x}^{x}, \qquad (14)$$

whence

$$W = \frac{zM_1!}{(M_2-x)!\,(zM_1-M_2+x)!} \cdot \frac{(M_1+x)!}{M_1!\,x!}. \qquad (15)$$

Applying the logarithm according to Stirling's formula ln n! = n ln n - n and differentiating with respect to x, we obtain, as restricted to the main term:

$$\frac{\partial \ln W}{\partial x} = \ln\frac{(M_1+x)(M_2-x)}{x(zM_1-M_2+x)}. \qquad (16)$$

Comparing (13) and (16) we see that

$$\ln\frac{(M_1+x)(M_2-x)}{x(zM_1-M_2+x)} = \frac{h}{kT}.$$

or

$$\frac{(M_1 + x)(M_2 - x)}{x(zM_1 - M_2 + x)} = e^{\frac{\varepsilon}{kT}}. \tag{17}$$

We shall prove that computation of the logarithm of a statistical sum may be limited to the main term. We introduce the following supplementary designations:

p - a-priori probability for an atom of the dissolved substance to occupy a nodal point in the lattice;

q - a-priori probability to occupy an interstitial space

$$q = 1 - p \qquad \frac{p}{q} = \omega.$$

The thermodynamic probability W of the solution:

$$W = \sum W_x = \sum_{x=0}^{x=M_2} C_{zM_1}^{M_2-x} \cdot C_{M_1+x}^{x} \cdot p^x \cdot q^{M_2-x}. \tag{18}$$

Let there be a sum $W = \sum_{x=0}^{k} a_x$, composed of positive addends, so that for

$$x < x_0 \quad \frac{a_x}{a_{x+1}} < r < 1;$$

for

$$x > x_0 + 1 \quad \frac{a_{x+1}}{a_x} < r < 1;$$

it is obvious that a_{x_0} is the maximum term, then

$$\ln W = \ln a_{x_0} + \ln \sum_{x=0}^{k} \frac{a_x}{a_{x_0}}.$$

We compare the remaining sum with a geometric progression with the common ratio r:

Thus,

$$\left| \ln \sum_{x=0}^{k} \frac{a_x}{a_{x_0}} \right| < \left| \ln \left(\sum_{n=0}^{x_0} r^n + \sum_{n=0}^{k-x_0} r^n \right) \right| < \left| \ln \frac{2}{1-r} \right|$$

actually constitutes a limited quantity, provided r does not tend to unity. Since the main term of the sum grows infinitely with increasing M and $\ln \frac{2}{1-r}$

is limited, then in computing the sum it suffices to take the principal term. For $W_x = W_{x+1}$ we have

$$\frac{(M_1 + x)(M_2 - x)\omega}{x(zM_1 - M_2 + x)} = 1. \tag{19}$$

Comparing (19) and (17) we find that

$$\omega = l^{-\frac{h}{kT}}.$$

If one takes an infinitely dilute solution, then in it

$$x \ll M_1 \quad \text{and} \quad M_2 \ll M_1.$$

Ignoring x and M_2 in equation (19) as compared with M_1, we obtain

$$x = \frac{M_2\omega}{z + \omega}, \text{ but } \quad a_2 = \frac{x}{M_1} \text{ and } N_2 = \frac{M_2}{M_1},$$

then,

$$a_2 = N_2 \frac{\omega}{z + \omega}. \tag{20}$$

In reality $a_2 = N_2$ in an infinitely dilute solution. Hence, in order to obtain the true activity, it is necessary to multiply the activity from equation (2) by $\frac{z + \omega}{\omega}$. Thus, the true activity

$$a_2^1 = a_2 \frac{z + \omega}{\omega}. \tag{21}$$

The activity of the second component will be equal to $a_2 = \frac{x}{M_1 + x}$, whence

$$x = \frac{a_2 M_1}{1 - a_2};$$

$$N_2 = \frac{M_2}{M_1 + M_2};$$

$$N_1 = \frac{M_1}{M_1 + M_2}.$$

Substituting these expressions in equation (19), and after corresponding conversions, we obtain

$$a_2^2(1 + zN_1) + a_2(zN_1 - N_2 + \omega) - N_2\omega = 0. \tag{22}$$

However, in deducing the true activity from this equation by substituting equation (21) there results an insufficiently graphic equation with respect to $a_2^1 = f(N_2, z, \omega)$.

Let it be assumed that the atoms of the dissolved substance are to be

found preferentially in the interstitial solution, i.e. $x < M_2 < M_1$. Simplifying equation (19) we obtain in the first approximation

$$x_0 = \frac{M_1 M_2 \cdot \omega}{M_1 (z+\omega) - M_2} . \tag{23}$$

In the next approximation x will be equal to:

$$x = x_0 + \varepsilon . \tag{24}$$

Upon substitution of expression (24) in (19) we obtain the value of

$$\varepsilon = - \frac{x_0^2}{M_1 (z-\omega) - M_2 + 2x_0} . \tag{25}$$

Substituting (25) into (24) and converting accordingly, we have

$$x = \frac{M_1 M_2 \omega}{M_1 (z+\omega) - M_2} \cdot \left(1 - \frac{M_1 M_2 \omega}{[M_1 (z+\omega) - M_2]^2 + 2M_1 M_2 \omega}\right) . \tag{26}$$

As was shown above, $a_2 = \frac{x}{M_1}$, and the true activity $a_2^1 = a_2 \frac{z+\omega}{\omega}$. In taking also $N_2 = \frac{M_2}{M_1 + M_2}$ and $N_1 = \frac{M_1}{M_1 + M_2}$, we finally obtain

$$a_2^1 = \frac{N_2 (z+\omega)}{N_1 (z+\omega) - N_2} \times \times \left(1 - \frac{N_1 N_2 \omega}{[N_1 (z+\omega) - N_2]^2 + 2N_1 N_2 \omega}\right) . \tag{27}$$

For w = 0 and z = 0.25 equation (27) changes into the well known Temkin and Shvartsman equation (11)

$$a_2^1 = \frac{N_2}{1 - 5 N_2} . \tag{28}$$

As known, equation (28) for carbon solution in iron conforms satisfactorily only when the contents of carbon is below 3%. For higher carbon contents formula (28) gives overrated results for the values of carbon activity. In this case it is necessary to use equation (27). This may be explained by the fact that with the growing of the concentration of carbon, part of it passes from the interstitial solution into the substitutional solution. Equation (28) may be written in this form

$$\frac{1}{a_2^1} = \frac{N_1}{N_2} - \frac{1}{\varepsilon} . \tag{29}$$

Figure 5 shows the data of L. Darken (18), O. A. Yesin and L. K. Gavrilov (19), and D. Chipman and Marshall (20) processed in accordance with equation (29). Almost all the points, with the exception of the lower ones, fit satisfactorily on a straight line. The four lower points correspond precisely to the contents of carbon higher than 3%. With the exception of the four lower points, all experimental points were processed according to the method of the least squares, whereupon z equals 0.247, i.e. almost 0.25 as this was adopted by M. I. Temkin and L. A. Shvartsman. The dotted line in Figure 5 gives the shape of the curve according to equation (27), whereat $w_{av.} = 0.035$.

Figure 5. Relationship between $\frac{1}{a_C}$ and $\frac{N_{Fe}}{N_C}$ in the Fe-C system:
x - Chipman & Marshall data (20); • - Yesin and Gavrilov data (19); 0 - Darken data (18).

Figure 6. Relationship between $\frac{1}{\gamma_S^C(N_C+N_S)}$ and $\frac{N_{Fe}}{N_C+N_S}$ in the Fe-C-S system at 1600°.
————the authors' data 0 - data from study (6).

Figure 7. Relationship between $\frac{1}{\gamma_S^P(N_P+N_S)}$ and $\frac{N_{Fe}}{N_P+N_S}$ according to the authors' data at 1600°.

Applying the same reasoning to a ternary system, we obtain the following expression:

$$a_2^1 = \frac{N_2(z+\omega_2)}{N_1(z+\omega_2)-(N_2+N_3)} \cdot \left(1 - \frac{N_1 N_2 \omega_2}{[N_1(z+\omega_2)-(N_2+N_3)]^2 + 2N_1N_2\omega_2}\right). \quad (30)$$

where N_1 - molar fraction of the dissolvent;

N_2 and N_3 - molar fractions of the dissolved substances.

In this case it is assumed that the third component is to be found only in the interstitial solution. For $\omega = 0$, after conversion, we obtain the following equation:

$$\frac{N_2}{a_2(N_2+N_3)} = \frac{N_1}{N_2+N_3} - \frac{1}{z}. \quad (31)$$

which changes into A. M. Samarin's and L. A. Shvartzman's equation

$$\gamma_2 = \frac{1}{1-5(N_2+N_3)},$$

if $z = 0.25$.

Figures 6-7 show the data on the Fe-C-S and Fe-P-S systems.

The conclusion may be drawn that equation (31) conforms with the experimental data only up to a definite concentration of carbon in system Fe-C-S,

and of phosphorus in system Fe-P-S. If the concentration is higher, the experimental values of the activity of sulfur in systems Fe-C-S and Fe-P-S turn out to be lower than it follows from equation (31). Similarly to carbon in the Fe-C system, starting at a certain moment the sulfur passes from the interstitial solution to the substitutional solution, thus reducing its activity. This agrees with equation (30) in accordance with which the dotted line in Figures 6 and 7 indicates the shape of the curve; thereat in system Fe-C-S $z = 0.25$, $\omega_{cp} = 0.04$, and in system Fe-P-S $z = 0.3$, $\omega_{cp} = 0.06$.

Discussion of Results.

The derivation of the relationship of sulfur activity in system Fe-C-S to the carbon contents is given in literature (13) for the case when sulfur and carbon form an interstitial solution with iron. However, this formula agrees with the experimental data only when the percentage of carbon is up to 3%. Whenever the contents of carbon is higher than 3%, the results turn out to be overrated as compared to the experimental data. A theory of metalloid solutions in liquid metal is advanced by us on the basis of the fact that sulfur and carbon in the Fe-C-S system simultaneously form both an interstitial and a substitutional solution. The resulting equation agrees satisfactorily with the test data over a wide range of carbon concentrations.

As shown by the test data, the values of $\Delta \overline{H}$ for sulfur are high, and if not for a simultaneous growth of $\Delta \overline{S}$, the solubility of sulfur would have ceased. The reason for the growth of $\Delta \overline{H}$ may consist in that carbon, silicon, and phosphorus alter the energy of interaction of sulfur and iron, owing to the change in the short-range order. It is not excluded that in our experiment, as in the case of hydrogen dissolution in β-palladium (16), specific forces may be acting, which are associated with the metallic nature of the dissolvent. If one should proceed from the consideration that sulfur and iron form both an interstitial and substitutional solution, then the higher values of $\Delta \overline{H}$ may be ascribed to the fact that an increase in C, P, and Si concen-

trations leads to the passage of sulfur from the interstitial into the substitutional solution.

The experimental data (see Tables 5-7) show a very substantial growth of the partial molar entropy of sulfur during the transfer of a mole of sulfur from the Fe-S solution into a solution where, in addition to iron and sulfur, there still is another element: carbon, silicon, or phosphorus. According to Wagner (17) there are two types of entropies in a solution: the positional entropy and the vibrational entropy. The calculation presented herein indicates that a strong growth of partial molar entropy is related, apparently, not to the positional entropy but to the variation of vibrational entropy. The frequency of sulfur vibrations diminishes sharply owing to the distortion of the short-range order caused by the additions of carbon, silicon, or phosphorus.

CONCLUSIONS

1. On the basis of a newly developed procedure the thermodynamic activity of sulfur was determined in the Fe-S, Fe-C-S, Fe-Si-S, and Fe-P-S systems for different temperatures.

2. The thermodynamic characteristics: $\Delta \bar{H}$, $\Delta \bar{F}$, and $\Delta \bar{S}$ were computed on the basis of the test data.

3. A theory of metalloid solutions in liquid iron was formulated on the basis of the assumption that the dissolved substance forms with liquid iron both an interstitial and a substitutional solution.

4. The experimental data obtained in this work, as well as those obtained by other authors, are in accord with the theory.

REFERENCES

1. J. Chipman and Ta Li, Transactions of American Society for Metals, 1937 vol. 25, 435.

2. J. White and H. Skelly, Journal of Iron and Steel Institute, 1947, vol. 155, 201.

3. E. Maurer, G. Hammer und G. Mobius, Archiv für das Eisenhüttenwesen, 1942-1943, 16, 159.

4. I. A. Kitchener, J. Bockris and A. Liberman, Discussion of Faraday Society, 1948, 4, 39.

5. J. P. Morris and A. Williams, Transactions of American Society for Metals, 1949, vol. 41, 1421.

6. J. P. Morris and R. C. Buehl, Journal of Metals, 1950, 188, 317.

7. J. Chipman and C. W. Sherman, Revue de Metallurgie, 1951, 48, 613.

8. C. W. Sherman, H. J. Elvander and John Chipman, Journal of Metals, 1950, 183, 334.

9. C. W. Sherman and J. Chipman, Journal of Metals, June, 1952, 597.

10. V. A. Karasev and A. M. Samarin, Izvestiya AN SSSR /News of the Academy of Sciences of the USSR/, OTN, 1956, No. 3, 170.

11. M. I. Temkin and L. A. Shvartsman, Zhurnal fizicheskoy khimiyi /Journal of Physical Chemistry/ AN SSSR, 1949, v. 23, 755.

12. R. Smith, Journal American Chemical Society, 1946, 68, 1163.

13. A. M. Samarin, L. A. Shvartsman, Izvestiya AN SSSR /News of the Academy of Sciences of the USSR/, OTN, No. 3, 407, 1951.

14. O. A. Yesin, P. V. Gel'd Fizicheskaya khimiya pirometricheskikh protsessov /Physical Chemistry of Pyrometric Processes/, Metallurgizdat, part 2, p. 388, 1954.

15. V. K. Zhuravlev and A. A. Zhukhovitskiy, Sb. XXXIV, MIS. Primeneniye radioaktivnykh izotopov v metallurgiyi /Volume 34, Moscow Institute of Steel. Application of Radioisotopes in Metallurgy/ Metallurgizdat, p. 91, 1955.

16. A. N. Frumkin, V. S. Bagotskiy, Z. A. Iofa, B. N. Kabanov, Kinetika elektrodnykh protsessov /Kinetics of Electrode Processes/, p. 45,

17. Wagner, Thermodynamicsof Alloys, 1952.

18. L. Darken, Metals Technologie, 1163, 2, 1940.

19. O. A. Yesin and L. K. Gavrilov, Izvestiya AN SSSR /News of the Academy of Sciences of the USSR/, OTN, 1950, 7, 1040.

20. J. Chipman, S. Marshal, Trans. Am. Soc. Metals, 1942, 30.

Prof. Dr. of Tech. Sciences I. N. KIDIN.

Department of Metallography and Heat Treatment.

CONDITIONS OF CARBON TRANSITION INTO SOLID SOLUTIONS DURING INDUCTION HEATING OF CHROME STEEL

In view of the wide industrial application of the method of induction heating for heat treatment, there frequently arises a necessity to ascertain the possibility and the conditions of treatment of articles manufactured from chrome steel. It is, therefore, desirable to conduct a systematic study of the various chromium alloy compositions in an attempt to establish certain general principles to be used in the development of a concrete technology for heat treatment of objects produced from chromium steel. In this research the study of the mode of carbon transition into solid solution during heating is of the greatest importance for the purpose of establishing the optimum heating conditions.

The chemical compositions of the types of chrome steel investigated by us, which contained 0.6, 0.8, 1.0% C and 1.0, 2.5, 5.0, 10.0% Cr, and their critical points determined by the dilatometric method during slow heating are described in work (1).

All the chromium alloys investigated in this work preserve a γ-phase of some other magnitude and must, therefore, undergo phase transformations in the process of heat treatment.

Among these alloys there are hypoeutectoid alloys as well as alloys of the carbide class (at 10% Cr the proportion of carbon amounted to 0.4% and more, for 5% Cr to 0.6% and higher). Since the maximum contents of chromium in our alloys was 10%, and of carbon - 1%, there were no ledeburite steels among them. The type of carbides available in our alloys is determined by the data of Tofaute et al (2), as well as by those of I. L. Mirkin and M. M. Blatner (3).

None of the investigated alloys had the most stable cubic carbide $(Cr,Fe)_4C$. In the alloy with 1% C there were carbides only of the cementite type $(Cr,Fe)_3C$, while in alloys with 2.5 and 5% C trigonal carbide $(Cr,Fe)_7C_3$ was also to be found.

Only one type of carbide -- trigonal -- was present in alloys with 0.2 and 0.4% C at 5 and 10% Cr, and in alloys with 0.6 and 0.8% C at 10% Cr in the initial state. To pass a correct judgment on the rate of dissolution of carbides during heating and on the contents of carbon and chromium in the forming austenite it is important -- in addition to the knowledge of the initial carbide types -- to consider the temperature range of transformation. It is also important to determine the position of this temperature range in relation to the Curie point, upon which position depends the possibility of phase transformations taking place at various stages of heating.

The concentration state of austenite formed towards the end of heating was determined on the basis of martensite produced as a result of quenching.

Figure 1. Specimens for X-ray diffraction studies.

Carbon concentration in martensite was determined by the X-ray diffraction method from specimens (4) subjected to single induction heating and quenching (Fig. 1). The photographs were taken in a standard Debye chamber with iron radiation (λ_{Fe} = 1.934 Å). Reflections from the (110)-face were taken for purposes of determination. The angle of reflection was $28^{\circ}35'$.

The X-ray photos were photometered on a visual microphotometer. The blackening of the line was well within the limits of 0.3-0.8. Carbon contents were determined by the magnitude of the photometric curve area. The area was

Figure 2. Width of the line in the X-ray photograph (radiograph) as a function of carbon concentration in martensite.

measured planimetrically; the mean arithmetic value of three measurements was taken into account.

Using the relationship of the tetragonal lattice parameters a and c to the carbon contents (in weight %), as proposed by G. V. Kurdyumov (5)

$$a = 2{,}861 - 0{,}015\,p, \tag{1}$$

$$c = 2{,}861 + 0{,}118\,p, \tag{2}$$

we find their values for carbon concentrations 0.25, 0.50, 0.75, 1.0 and 1.2%.

Substituting the values of a and c in expression

$$\sin^2\vartheta = \frac{\lambda^2}{4a^2}\left(H^2 + K^2 + L^2\frac{a^2}{c^2}\right). \tag{3}$$

we obtain the magnitudes Sin $\vartheta_{(110)}$ and Sin $\vartheta_{(011)}$ and angles $\Theta_{(110)}$ and $\Theta_{(011)}$ for the above concentrations of carbon in solid solution.

Further, we determine for each of these concentrations the value

$$\Delta\vartheta = \vartheta_{(110)} - \vartheta_{(011)}. \tag{4}$$

For example, for a 0.25% carbon concentration

$$\Delta\vartheta = 28°35' - 28°25' = 0°10'.$$

Considering the irregularity of our chamber, we find

$$2L_{\Delta\theta=1^\circ} = \frac{D_{факт}}{D_{станд}} \cdot 2L_{станд} = \frac{57,5}{57,3} = 0,5020 \text{ mm.}$$

Thus, the broadening of the line at $\Delta\theta = 0^\circ 10'$ (i.e., in consequence of the presence of 0.25% C) will amount to

$$2L_{\Delta\theta=0^\circ 10'} = \frac{0,5020}{6} = 0,08 \text{ mm.}$$

Calculating in this manner the magnitude of broadening for carbon concentrations of 0.5, 0.75, 1.0 and 1.2% we plot a $\Delta\theta$ -% C, or X, mm-% C curve (Fig. 2).

The value of X, in mm, is deduced from the photometric curve while diagram 2 is used to determine the contents of carbon in martensite.

The determination of carbon contents in solid solution after high-frequency hardening of chromium and tungsten steels is sometimes made difficult owing to the presence of crystals with a carbon concentration exceeding the average concentration in steel. The photometric curves plotted from the X-ray pictures have, in this case, an unsymmetrical form. On the other hand, carbon determination on the basis of the area delineated by the photometric curve is not sufficiently exact. This inhomogeneity and the corresponding distortions of photometric curves are most distinctly manifested for steel with 1% of alloying element; in a smaller degree - at 5 and 10% contents of alloying element.

For purposes of obtaining uniform data, the carbon contents in solid solution was in this case calculated on the basis of one half of the area limited by the photometric curve from the side of the larger angles (4).

In those cases when -- in spite of the existing slight inhomogeneity -- a doublet appeared in the X-ray picture, the contents of carbon was determined by the doublet. The values of carbon concentrations in solid solution obtained in this case corresponded to the general regularity.

The contents of carbon in martensite after high-frequency hardening under

one or another conditions of heating was deduced from two X-ray photographs. In plotting the curves both values of carbon concentration in martensite were taken into account.

Reproduced in Figures 3-6 are the X-ray pictures and photometric curves illustrating the variation in width of line (110) depending on the conditions used in heating chrome steel with 0.8% C at 1 and 5% Cr. The X-ray photos show the changing width of 1% Cr steel line with rising temperature at a constant rate of heating v = 75° per second (Fig. 6-a, -b, -c), and for growing heating rate at an invariable quenching temperature of 960° (Figs. 3-d,-e,-f). A similar group of X-ray pictures is given for 5% Cr steel in Figure 4.

Data on the concentration of carbon in martensite are recorded in Figure 7 and the accompanying table.

Carbon Concentration in Martensite.

Quenching Temperature °C.	Carbon contents in steel, %											
	0.6				0.8				1.0			
	Rate of heating v, °C per second											
	40	75	130	200	40	75	130	200	40	75	130	200
	Carbon contents in martensite, %											

Steel with 1% Cr

A more complete transfer of carbon into the solid solution is to be observed in the 0.6% C and 1.0% Cr steel than in steel with 5 and 10% Cr. For

Figure 3. X-ray photographs of hardened chrome steel containing 0.8% C and 1% Cr.

Heating rate v = 75° per sec., quenched from 880°(a); 960°(b); and 1040°(g). Quenching temperature 960°; heating rate v = 40° per sec. (d); 130° per sec (e) and 200° per sec. (f).

example, in the first brand total transfer of carbon into the solid solution occurs at 960°, if the rate of heating is 40° per sec., and at 1040°, if the heating speed is 75% per sec. In steel with 5% Cr the concentration of carbon at 1040° amounts to 0.3%, when the rate of heating is 40° per sec., and 0.27%, when it is 75° per sec. More than one half of the amount of carbon remains in the carbides. In the 10% Cr steel the concentration of carbon in solid solution after hardening under the same heating conditions is even smaller. The greater part of carbon is retained by carbides.

The relationships for chrome steel with 0.8% C and the same concentra-

tion of chromium are of a similar character. The distinction between this steel and the 0.6% C brand consists in that there is a still greater proportion of trigonal carbides in the initial state at 5% Cr. Consequently, for the same heating conditions the concentration of carbon in the solid solution after quenching is still smaller. It is evident that a considerable increase in temperature over the normal is required to cause the trigonal-type carbides to dissolve during rapid heating.

Figure 4. X-ray photograph of hardened chrome steel containing 0.8% C and 5% Cr.
Heating rate v = 75° per sec., quenched from 880°(a); 960° (b) and 1040° (c). Quenching temperature 960°; heating rate v = 40° per sec. (d); 130° per sec. (e), and 200° per sec. (f).

The influence of quenching temperature at one or another rate of heating upon the concentration of carbon in solid solution of 1-, 5- and 10-% chromium steel with 1%C is shown in Figures 7-g,-h,-i. The proportion of carbon passing

Figure 5. Photometric curves for line (110) plotted from X-ray pictures reproduced in Figure 3.

into the solid solution during rapid induction heating of 1-, 5-, and 10-% chromium steels with 1% C in this case is even smaller than in the case of steels containing 0.6 and 0.8% C. The drop of carbon concentration in solid solution with increasing speed of heating to the same temperature is well reflected in all the curves. For example, 58% of the total amount of carbon contained in 1% C and 1% Cr steel passes into the solid solution after heating to 960° at a rate of 40° per second. An increase of the speed of heating to 75° per second reduces this proportion to 50%, and for a rate of 200° per second - to 37%.

The effect of the state of the carbide phase on the kinetics of carbon transfer into solid solution is shown in Figures 8-10. A sharp drop in carbon concentration in the solid solution is to be registered in changing over from steel with 1% Cr to that with 5% Cr. On the other hand, the decline of carbon concentration in the solid solution is negligible as a result of an

Figure 6. Photometric curves for line (110) plotted from X-ray pictures reproduced in Figure 4.

increase in chromium contents up to 10%.

The difficulty with which carbides dissolve in consequence of a growth of chromium contents in steel, is to be attributed to a rise in the stability of carbides and the narrowing of the transformation temperature range. In the initial state 1% C steel contains only the cementite-type carbides. In steel with 5% C the carbide phase consists mainly of trigonal carbides, and in 10% carbon steel the entire carbide phase is composed of the more stable and difficult of solution trigonal carbide. As the contents of chromium increase in steel, the transformation range begins to diminish and this reduces the possibility for the carbides to dissolve. For instance, the rise of critical temperature A_1 from 730 (for 1% Cr) to 790° (for 5% Cr) after quenching from

960° narrows the temperature range substantially. The difference between the quenching temperature and the critical point A_1 diminishes from 250° to 170° (Fig. 11).

Of great importance is also the influence of the isothermal stage of induction heating upon the development of the process of phase transformation. The higher the temperature of the isothermal stage (t_c) in relation to the lower critical point, the greater the role of this stage.

Let us consider the example of chrome steel with 0.6% C. When the rate of heating up to 1040° is 75° per second, the transfer of carbon into the solid solution is complete for steel containing 1% Cr. However, for steel with 5% Cr the same heating pattern assures the passage of only 42% of carbon into the solid solution, and this proportion drops to 33% for 10% Cr steel.

The heating of 1-, 5-, and 10% chrome steel to 960° under the same conditions causes 85, 33 and 28% of carbon, respectively, to pass into the solid solution. Heating up to 880° assures the relative proportion of carbon in solid solution to attain 54, 19 and 17%.

The data obtained permit important practical conclusions to be drawn on the most expedient conditions of induction heating of chrome steel to obtain one or another degree of carbide dissolution to satisfy the production requirements.

Figure 7. Carbon concentration in chrome steel martensite as a function of the quenching temperature at heating rates of 40, 75, and 200°.
a - 0.6% C and 1% Cr, A_1 - 725°, A_s - 600°; b - 0.6% C and 5% Cr, A_1 - 790, A_3 - 830; c - 0.6% C and 10% Cr, A_1 - 800, A_3 - 835°; d - 0.8% C and 1% Cr, A_1 - 730°, A_3 - 830°; e - 0.8% C and 5% Cr, A_1 - 730°, A_3 - 810°, f - 0.8% C and 10% Cr, A_1 - 825°, A_3 - 875°; g - 1% C and 1% Cr, A_1 - 730° and A_3 -775°; h - 1% C and 5% Cr, A_1 - 775°, A_3 - 830°; i - 1% C and 10% Cr, A_1 - 810°, A_3 - 860°.

Figure 8. Carbon concentration in martensite after high-frequency hardening as a function of the contents of chromium in steel with 0.6% C. Temperature of quenching: 880, 960 and 1040°.

Heating rate a - 40° per sec; b - 75° per sec; c - 200° per sec.

Figure 9. Carbon concentration in martensite after high-frequency hardening as a function of the contents of chromium in steel with 0.8% C. Temperature of quenching: 880, 960, and 1040°.

Heating rate: a - 40° per sec; b - 75° per sec; c - 130° per sec.

Figure 10. Carbon concentration in martensite after high-frequency hardening as a function of the contents of chromium in steel with 1% C. Temperature of quenching: 800, 960, and 1040°.

Heating rate: a - 40° per sec.; b - 75° per sec; c - 130° per sec.

Figure 11. Effect of chromium contents on the position of the isothermal stage (t_c) and critical point A_1.

REFERENCES

1. I. N. Kidin, Sb. Moskovskogo instituta stali "Obrabotka stali i splavov" [Symposium of the Moscow Institute of Steel "Treatment of Steel and Alloys"] v. 34, Metallurgizdat, 1957.

2. Tofaute, Küttner u. Büttighaus, Archiv f. d. Eisenhüttenwesen, 9, 1936.

3. N. L. Mirkin, M. Ye. Blatner, Metallurg [Metallurgist], 1940, No. 8.

4. I. N. Kidin, Izvestiya AN SSSR, OTN [News of the Academy of Sciences of the USSR, Division of Technical Sciences], 1956, No. 2.

5. G. V. Kurdyumov, Sb. dokladov sektsiyi metallovedeniya i termicheskoy obrabotki VNITOM [Symposium of Reports of the Section of Metallography and Thermal Treatment of the All-Union Scientific and Technical Society of Metallurgists], 1940.

Prof. Dr. of Tech. Sciences B. G. LIVSHITS and Candidate of Tech. Sciences N. N. KOSSAKOVSKAYA

Department of Metallography.

INVESTIGATION OF THE DECOMPOSITION KINETICS AND HEAT-RESISTANCE OF ALLOY KhN80T.

The KhN80T-type alloys belong to the class of structurally hardening (aging) alloys. Yet, in practice, it has been established that their heat-resistance properties become very low after normal hardening (high-temperature heating and drastic quenching in water) followed by tempering. If, on the other hand, cooling from homogeneous solid solution proceeds at a comparatively low rate, depending on the alloy composition, then the heat-resistance properties resulting after tempering turn out to be very high. It is obvious that the mechanism of precipitation hardening in type-KhN80T alloys is unusual.

A similar phenomenon was revealed during the investigation of magnetic alloys. In studies of high-coercivity alloys it was disclosed that considerably better magnetic properties may be produced as a result of uninterrupted cooling than after hardening and tempering (1).

Further research has shown that a large group of magnetic alloys (Fe-Ni-Al, Fe-Ni-Al-Co, Cu-Ni-Co, Cu-Ni-Fe, and others) are apt to produce this type of transformation. Two phases based on Fe and NiAl separate after the decomposition of the solid solution in the region of 800-900°. These phases differ by concentration from each other and from the original solid solution. The space lattices of the initial solid solution and the decomposition products are identical crystallographically and are close as to period. An assumption was made as to a successive disintegration of phases, i.e. decomposition at 800-900° and pre-disintegration at 600-700°, and the formation of a substructure (2, 3) in the high-coercivity state.

There are reports (4, 5) on the experimental confirmation of this hypothesis in Fe-Ni-Al alloys. More recently this was proven in studies (5, 6).

It was revealed that the type-KhN80T alloys acquire the best heat-resistance properties after cooling at a specified rate followed by tempering. It may, therefore, be assumed that the kinetics and the mechanism of solid solution decomposition in these alloys and in high-coercivity alloys are similar. The purpose of this work is to verify the above assumption. A study was made of a series of heat-treatment processes: hardening with subsequent tempering, cooling at different rates, and a stepped heat treatment. The latter process makes it possible to check the presence or the absence of successive aging.

The investigated alloy contained: 0.05% C, 0.43% Si, 0.24% Mn, 0.003% S, 0.005% P, 0.02% Ce, 20.55% Cr, 2.44% Ti, 0.79% Al, 0.04% Cu, 0.56% Fe, the balance being Ni. A special chemical analysis has shown that there were no harmful impurities (antimony and lead).

The alloy was forged into 20 x 20 mm rods, from which specimens were prepared for a study of the microstructure, hardness, and physical properties, and into rods with a diameter of 20 mm, from which 20-mm dia. samples were made for phase analysis and stress rupture tests. The Brinell hardness number of the alloy after forging was 298, its microstructure was fine-grained. Inclusions of titanium nitrides and carbides of yellow color were to be found in the alloy.

The KhN80T alloy was heat-treated under the following conditions:

1. The specimens were water quenched and tempered at different temperatures. After heating and 8-hour holding at 1080° the specimens were quenched in water and then tempered for 16 hours at 600, 700, 800, 900, and 1000° with subsequent cooling in the air.

2. Treatment with different rates of cooling ranging from 60° per sec. (water) to 20° per hour (furnace). To bring the solid solution into a homogeneous state, the specimens were heated in a Silit-resistor furnace up to 1080°, held at this temperature for 8 hours and cooled in various media: in water,

in oil, in air, and also with the furnace at 400, 200, 160, 120, 80 and 20° per hour.

The speed of 400° per hour could be attained only in cooling up to 900°. On further cooling the cooling rate of the furnace was half of that prescribed. After cooling the samples were tempered at 700° for 16 hours.

A special mechanism (developed and constructed by A. V. Panov) was used to control the furnace cooling rate. This mechanism served as an accessory to the contact galvanometer of the Silit-resistor furnace (Figure 1).

3. Hardening with furnace cooling. This procedure was utilized in an endeavor to clarify the processes developing as a direct result of controlled furnace cooling. After heating to 1080° and holding the specimens for 8 hours, they were cooled at a rate of 400, 160, and 40° per hour down to 900, 800, and 700° and were then water quenched from these temperatures.

4. Step treatment. This was carried out by means of protracted homogenizing heating of samples under normal conditions (1080° for 8 hours), their transfer into a furnace heated to 600, 700, 800, 900 and 1000°, holding at these temperatures for periods of 1, 2, 4, 8, and 16 hours, and final quenching in air. Thereafter, the specimens were allowed to age at 700° for 16 hours.

Metallographic analysis was carried out with the aid of transmitting-type microscopes MIM-6 and MIM-3 assuring a magnification of 400-1500 times, and by means of electron microscope EM-100 with magnification of 6000 times.

The microsections for microscopic study were mechanically, and in certain cases electrolytically, polished. The composition of the reagent used for etching was: 4 g $CuSO_4$, 20 cm^3 HCl, 20 cm^3 H_2O.

The microsections used for electron microscopic analysis were prepared by means of electrolytic polishing in concentrated nitric acid at current density of 1.5-2 A/cm^2 for a period of 40-60 sec. The Shapiro reagent was

Figure 1. Diagram of the mechanism for cooling rate control:
1 - clockwork; 2 - thermocontroller; 3 - electric motor (2 rpm); 4 - pulley; 5 - wire; 6 - setting handle.

used for microsection etching, with the current density being 0.5-0.6 A/cm^2 and the etching period of 5 sec. Quartz replicas produced by one-step technique were investigated. The quartz film was electrolytically separated from the specimen (7).

The hardness of all the heat treated specimens (3-5 specimens for each process and 3 tests for each specimen) was determined on a "Briviskop" (Briviscope) device with a 2.5 cm ball and a 187.5 kg load.

In addition many specimens were tested for microhardness. This operation was carried out for checking purposes.

Electric resistivity was measured on 5 x 5 x 50 mm specimens by means of a potentiometer of the UPN-$^3/_2$ type. The measuring accuracy was about 0.3%.

Stress rupture tests were performed on a YaB-1 machine. The temperature was checked with the aid of a thermocouple connected to the midsection of the sample and to a potentiometer. The temperature variations did not exceed $\pm 3^\circ$. The design length of the test specimens was 25 mm with the diameter of the working section being 5 mm. After the given temperature had been

attained the specimen was held without load for one hour. It was then subjected to measured tensile stress, and the time was noted at the beginning of the test. The test conditions were identical for all specimens and corresponded to the State standard requirement (700°, 36 kg/mm^2 stress). The specimen was held until failure.

In addition to these tests, a phase analysis of the electrolytically separated deposit was also carried out.

The deposit was studied analytically and by the X-ray diffraction method. X-ray photograms were taken in a cylindrical chamber with chromium radiation, with the film set in an upright position.

WATER QUENCHING AND TEMPER AT VARIOUS TEMPERATURES.

This type of treatment was applied to determine the processes which develop during normal quench aging, i.e. during tempering of a supercooled homogeneous solid solution. Heating at 1080° for a period of 8 hours caused the KhN80T alloy to assume the state of homogeneous solid solution which was fixed by quenching in water.

The hardness of the KhN80T alloy after quenching comprised 170 H_B units. Under microscopic examination the alloy appeared to have a single-phase structure with individual inclusions of titanium carbides and nitrides.

Investigation of the alloy after a 16-hour temper at 600-1000° showed that its hardness increases, attaining 300 H_B units, at 800° in consequence of tempering at 600, 700, and 800°. The hardness value drops considerably after heating up to 900° and at 1000° it approaches the hardness of quenched samples (Fig. 2). Changes in electric resistivity, in the main, correspond to the hardness variation. The sharpest drop is to be observed over the 600-750° temperature range, thereafter resistivity increases on heating to 1000°.

The data on hardness and resistivity variations indicate that tempering over the temperature range of 600-800° causes the solid solution to decompose

with precipitation of the second phase. This was already mentioned in earlier investigations (8). Noteworthy is the rise of electric resistivity as a result of tempering at temperatures up to 600°. The same anomaly was observed also in the case of Nichrome by Thomas (9) who ascribes this fact to the, so-called, K-state.

Microscopic study of the alloy showed that the change in structure after a 700-800° temper is evidenced by the etch figures and the striations, clearly discernible under visual examination, and indicating the beginning of dissociaton. The heterogeneity resulting after tempering at 700° is visible upon 6000-power magnification. A 900 to 1000° temper produces a single-phase structure similar to that of a hardened alloy.

Stress rupture tests were carried out after the samples have been processed under conditions assuring maximum hardness (See Fig. 2).

The results of tests carried out at 700° and under a stress of 36 kg/mm^2 are recorded in Table 1.

Figure 2. Hardness and resistivity variation as a function of the tempering temperature after quenching from 1080°:
0 - hardness, H_B; ● -electric resistivity, ρ
1) Hardness, H_B; 2) ρ, ohm.mm^2/m; 3) Water quench; 4) Temper temperature, °C.

The stress rupture test results have demonstrated low tensile properties of the alloy failing to meet the specified requirements.

COOLING AT DIFFERENT RATES AFTER HIGH-TEMPERATURE HEATING

Water Quenching Electronic microscope examination*) of the KhN80T alloy after water quenching showed that the alloy structure is slightly inhomogeneous and has a hardly noticeable submicroscopic relief. Considering that the precipitates of the second phase have already formed, it may be assumed that its crystals do not exceed 100 Å. Apparently, no total supercooling

Table 1

Results of Stress-rupture Tests of Samples at 700° at a 36 kg mm^2. Stress.

Heat Treatment	Time until rupture, h.-min.
Heating: 1080° - 8 h.; water quenching Aging: 650° - 16 h.	2-20
Same	7-45
Heating: 1080° - 8 h.; water quenching. Aging: 700° - 16 h.	35-00
Same	12-20
Heating: 1080° - 8 h.; water quenching. Aging: 750° - 16 h.	5-10
Same	17-00

of the solid solution results after water quenching. The α'-phase produced in this case evidently has a composition closely approaching that of the α-phase. The same phenomenon is to be observed in water quenching of other alloys, in particular, the high-coercivity type (7).

Subsequent aging at 700° for a period of 16 hrs. increases the hardness up to 295 H_B units. Electronic-microscope study of the alloy showed a two-phase structure after aging; the precipitates of the second phase, however, were still too finely dispersed, this size amounting to about 200-250 Å (Fig. 3).

*) The participation in electron microscopic analyses of Yu. A. Shakov, Assoc. Pr. Technical Sciences, is hereby acknowledged.

Oil Quenching. The results of oil quenching after heating at elevated temperatures were practically the same as in the case of water quenching. The hardness value was registered at 190 H_B units, the resistivity remained unchanged.

Subsequent aging at 700° for 16 hours contributes to a considerable growth of hardness - up to 295 H_B units. The structure of the alloys after aging as viewed through microscope is characterized by striation of the grains, with the grain boundaries developing more intensely under etching. Examination of the alloy by electronic microscope, after oil quenching and subsequent aging, revealed a two-phase, but very fine, structure (Fig. 4). The size of the second-phase particles varies between 200-250 Å.

Figure 3. Microstructure of alloy KhN80T after heating to 1080°, water quenching, and aging at 700°. X 6000.

Figure 4. Microstructure of alloy KhN80T after heating to 1080°, oil quenching, and tempering at 700°. X 6000.

Air Quenching. Cooling in the air immediately after prolonged high-temperature treatment yields only a minor increase in hardness as compared with water and oil quenching (up to 200 H_B).

The structure, as observed under microscope, is similar to that registered upon water and oil quenching. Aging at 700° for a period of 16 hours

Figure 5. Microstructure of alloy KhN80T after heating to 1080°, air quenching, and tempering at 700°. X 6000.

after air quenching results in a hardness rise to 300 H_B. Electronic microscope examination indicates that the alloy has a two-phase structure (Fig. 5). The precipitates of the second phase range from 300 - 400 Å in size. However, it is still difficult to define the shape of the particles.

Figure 6. Hardness and resistivity versus rate of cooling. 1) Hardness, H_B; 2) H_B without tempering; 3) Water; 4) Oil; 5) Air; 6) Asbestos; 7) Cooling rate, deg/h.

Controlled Rate Cooling in the Furnace. Investigation of cooling rates over the range of 200-20° per hour has shown that cooling at 160° per hour produces the maximum hardness both before and after tempering (Fig. 6).

The hardness of the alloy after cooling at 160° per hour attains 265 H_B, and after aging at 700° for 16 hours - 365 H_B. If the cooling rate is further reduced, the hardness drops both before and after aging (Fig. 6). The microstructure of an alloy cooled in the furnace at different rates differs from the microstructure of rapidly quenched specimens. Already at a cooling rate of 160° per hour, even before tempering (Fig. 7), a selective coloration of the grains, striation and broadening of their boundaries are to be registered upon etching.

Electronic microscope examination makes it possible not only to observe the evolved phase (black squares), but also to determine the size and shape of its crystals (Fig. 8). Annealing at 700° for 16 hours leads to a still greater decomposition; the precipitates of the second phase appear to be more concentrated at the grain boundary (Fig. 9).

With further reduction of the cooling rate the size of the crystals of the separated phase increases from 800 Å for the cooling rate of 160° per hour to 1300 Å for 80° per hour, and to 2000 Å for 20° per hour (Fig. 10). The number of crystals per 1 cm^2 of the photographed area decreases respectively from 150 to 65 and 25. The image of the crystals in all cases resembles a square (a certain rounding off of the square shape occurs owing to dissolution ensuing in the process of electrolytic etching and during the separation of the film). The crystals evidently have a cubic shape.

Chemical analysis of the precipitate electrolytically separated from the specimen cooled at 20° per hour showed that the α-phase contains 8.36% Cr, 68.7% Ni, 17.4% Ti, and 5.85% Al. The ratio Ni: (Ti + Al) = 2.96:1.

X-ray diffraction study of the deposits precipitated from the specimens, cooled at 160° per hour, and at 20° per hour, and then tempered at 700° for 16 hours showed that lines of the hexagonal phase appear in addition to those of an ordered face-centered structure. After cooling at a rate of 160° per hour weak lines (110) and (220) of the hexagonal phase, with interplanar

spacing of 2.54 and 1.26, may be discerned. Upon cooling at 20° per hour there appear, in additon to the above, also lines (101), (103), (200), (004), and (203) with interplanar spacings corresponding to the published data. The (110) lines of the hexagonal lattice are superimposed on the (110) line of the face-centered lattice.

HARDENING WITH FURNACE COOLING.

Of greatest interest is the cooling of specimens with the furnace at a rate of 160° per hour. It is assumed that the separation of the α'-phase occurs in the process of cooling.

The specimens were heated to 1080°, held for 8 hours at this temperature and cooled at a rate of 160° per hour to 900, 800, 700, and 600° with subsequent quench in water. As a result of this investigation it became evident that after furnace cooling to 900° and subsequent quenching in water the hardness of the alloy remains low - at 160 H_B (Fig. 11), and its structure approaches that of an alloy quenched after heating at elevated temperatures.

Figure 7. Microstructure of alloy KhN80T after heating to 1080° and cooling at a rate of 160° per hour. X 1500.

After furnace cooling to 800° the hardness increases to 217 H_B. Investigation with the transmitting-type and electron microscopes makes it possible to observe clearly the two-phase structure (Fig. 12). The crystals of the separated α'-phase structurally approach the cubic shape. The linear size of these crystals averages 1000 Å. The quantity of the separated α'-phase averages 60 crystals per cm^2 of the photographed area. A large number of light

Figure 8. Microstructure of alloy KhN80T after heating to 1080° and cooling at a rate of 160° per hour. X 6000.

Figure 9. Microstructure of alloy KhN80T after heating to 1080° and cooling at a rate of 160° per hour, and tempering at 700°. X 6000

formations and but a few black crystals of the second phase may be observed in Figure 12. This is to be attributed to the fact that the crystals of the second phase α' are solidly bound to the matrix at the first stage of evolution, and disengage only with difficulty during electrolytic separation of the film. The chemical composition of the deposit precipitated after furnace cooling to 800° evidences that the α' -phase contains 8.16% Cr, 63% Ni, 16% Ti, and 8% Al. The ratio Ni:(Ti + Al) = 2.91 : 1.

After furnace cooling to 700° and subsequent cooling in water the separation of the "strengthening" α' -phase occurs with greater intensity. This is evidenced by a growth of hardness up to 260 H_B and also by phase analysis. Chemical analysis of the deposit shows that the α' -phase contains 5.98% Cr, 66.85% Ni, 15.74% Ti, and 6.53% Al. The ratio Ni : (Ti + Al) = 3.16: 1.

Microscopic investigation confirms the two-phase state of the alloy. A large number of crystals of the second phase was revealed; they are of cubic shape and their size equals 800-900 Å (Fig. 13).

Figure 10. Microstructure of alloy KhN80T after heating to 1080°, cooling at a rate of 20° per hour, and tempering at 700°. X 6000.

After furnace cooling to 600° the hardness value exhibits no changes, as compared with that obtained in furnace cooling to 700°, and remains equal to 260 H_B units. In this case the chemical analysis of the precipitate showed that the α'-phase contained 2.7% Cr, 63.6% Ni, 16.3% Ti and 8.16% Al. The ratio Ni : (Ti + Al) = 3.31 : 1.

Figure 11. Hardness variation after hardening with furnace cooling to 900°.
1 - without tempering; 2 - with tempering.
a) Hardness, H_B; b) cooling rate, deg/h.

Tempering at 700° for 16 hours after cooling to 600° at a rate of 160° per hour hardly affects the alloy structure. The shape of the deposit still remains cubic, the linear size of the crystals amounting to 800 Å. The results of stress rupture tests of samples at 700° and a 36 kg/mm^2 stress are listed in Table 2.

The stepped treatment was carried out by prolonged heating at 1080° with subsequent transfer of the samples into a furnace with a lower temperature (600-1000°). On comparing the hardness obtained after step-treatment and tempering at 700° for a period of 16 hours with the hardness registered upon

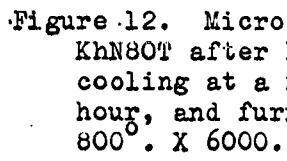

Figure 12. Microstructure of alloy KhN80T after heating to 1080°, cooling at a rate of 160° per hour, and furnace cooling to 800°. X 6000.

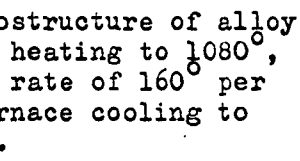

Figure 13. Microstructure of alloy KhN80T after heating to 1080° cooling at a rate of 160° per hour, and furnace cooling to 700° X 6000.

water quenching and tempering at corresponding temperatures (Fig. 14) one comes to the conclusion that hardness after stepped treatment and tempering is higher than after quenching and tempering . The least difference is to be registered at 800° temperature.

Thus, the samples subjected to stepped treatment at temperatures lower and higher than 800° have a greater capacity for additional aging at 700°. At 800° the highest degree of separation is to be observed. At higher temperatures the α'-phase begins to dissolve in accordance with phase equilibrium, and this leads to additional aging. This also takes place in the case of incomplete separation at temperatures below 800°.

RESULTS OF THE RESEARCH

The results of the study of water quenching with subsequent tempering at different temperatures show that at temperatures higher than 700° normal "dispersion" hardening (aging) takes place in the KhN80T alloy (see Figure 2.)

Table 2.

Results of Stress Rupture Tests of Samples at 700°.

Heat Treatment	Stress rupture test time hours-minutes.	
	Sample No. 1	Sample No. 2
Heating to 1080°, holding time 8 hours, cooling at a rate of 160° per hour to 900°; water quench; 16-hour temper at 700°.	59-00	87-50
Heating to 1080°, holding time 8 hours, cooling at a rate of 160° per hour to 800°; water quench; 16-hour temper at 700°.	122-45	133-15
Heating to 1080°, holding time 8 hours, cooling at a rate of 160° per hour to 700°; water quench; 16-hour temper at 700°.	198-20	190-00
Heating to 1080°, holding time 8 hours, cooling rate of 160° per hour to 600°, 16-hour temper at 700°.	228-20	261-00
Heating to 1080°, holding time 8 hours, cooling rate of 80° per hour to 600°, 16-hour temper at 700°.	154-30	114-00

It may be assumed that up to 700° the anomalous rise in resistivity in alloy KhN80T is to be associated with the intercrystalline segregation (K-state). Judging by the resistivity in case of tempering at temperatures above 700°, the solid solution undergoes a process of normal decomposition. Then, with rising temperature, a coagulation of the separated phase and the subsequent formation of a homogeneous solid solution is to be observed. This process terminates when the temperature reaches approximately 1000°. Additional evidence thereto is to be found in the change of hardness.

An impression is created that the intercrystalline segregation (the K-state) is not a process ushering in precipitation hardening. The formation of the K-structure and its resorption occur at temperatures below 700°. Precipitation hardening takes place at elevated temperatures. It is possible that these processes overlap in the temperature region near to 700°.

Figure 14. Effect of the tempering temperature, after water quenching and stepped treatment upon the hardness of alloy KhN80T:

● - after quenching; 0 - after stepped treatment. 1) Hardness, H_B; 2) Quenched in water; 3) Temperature, °C.

As for the results of uninterrupted cooling from a high temperature (see Fig. 6), an anomalous aging is to be observed in the KhN80T-type alloys along with quench aging. This anomalous aging was first revealed in Fe-Ni-Al magnetic alloys (1). In the investigated alloys maximum hardness, just as the coercive force in magnetic alloys, appears at a definite critical rate of cooling. This hardness rises after additional tempering at 700° for a period of 16 hours. The maximum hardness, both before the temper and after it, corresponds to the cooling rate of 160° per hour. It is at this rate of cooling that the greatest strengthening takes place.

When cooling from 1080° is slowed down, the linear dimensions of the deposited particles of the "hardening" phase increase from 200 Å (water) to 2000 Å (20° per hour). Although all the investigated samples were tempered at the same temperature (700°) and for the same period of time (16 hours), the magnitude of the precipitated α'-phase crystals varied over a wide range depending on the rate of cooling during the preceding treatement (Table 3).

One should assume that the formation of the visible microstructure terminates at comparatively high temperatures, most probably in the region of

Table 3.

Variation of the Size of Crystals and of Their Number Depending on the Type of Heat Treatment.

Heat Treatment	Size of α'-phase crystals	Number of α'-phase crystals per 1 cm^2 of the photograph.
Heating to 1080°; water quench.	100 Å	-
Heating to 1080° for 8 hours; water quench and 16-h temper at 700°	200-250 Å	-
Heating to 1080° for 8 h. Oil quench; 16-h temper at 700°	200-250 Å	-
Heating to 1080° for 8 h. Air quench; 16-h temper at 700°.	300-400 Å	-
Heating to 1080° for 8 h. Furnace cooling at 160° per h.; 16-h. temper at 700°.	700-800 Å	150
Heating to 1080° for 8 h. Furnace cooling at 80° per hour; 16-hour temper at 700°.	1300 Å	65
Heating to 1080° for 8 h. Furnace cooling at 20° per h; 16-h temper at 700°.	2000 Å	25

800°. On the other hand, during tempering at 700° there develops a process of K-state formation within the α'-phase, with the hardness increasing in the process. Apparently, the predominant process at 700° is not precipitation hardening but intercrystalline segregation without precipitation. This hypothesis, to a certain extent, represents a reiteration of the assumption made in the study of the high-coercivity alloys (10).

In its essence this hypothesis boils down to the following. On cooling at a critical rate, the solid solution, in the upper intervals of temperatures, separates into two phases, which at a lower temperature undergo so called "final aging" (diffusion hardening) and hardness attains its highest value. Tempering at 700° for 16 hours is required to complete "final aging" which has not reached culmination in the cooling process. The difference between the high-coercivity Fe-Ni-Al alloys and the KhN80T alloy consist, in our opinion,

in the following. In magnetic alloys "final aging" is achieved, as it was proven in studies (5, 6), by final separation, i.e. by additional precipitation at 600-700° of the Fe-phase in the NiAl-phase, and of the NiAl-phase in the Fe-phase, i.e. in the phases which appeared at 800-900° in the process of cooling. At the same time it was shown that at 800-900° the composition fails to reach equilibrium. In the case of KhN80T alloy separation into α- and α' -phases takes place at 800-900°, but at a low temperature "final aging" occurs (presumably) through the mechanism of K-state formation in the α - phase without additional precipitation.

Supplemental hardening ensues after cooling at any given rate, from 60° per second (water) to 20° per second (furnace), (see Fig. 6). The number of the separated crystals diminishes as they grow with the decreasing rate of cooling from 160° per hour to 20° per hour (see Table 3). A rough planimetric determination of the quantity of the separated phase shows that it grows, as was to be expected, with decelerating rate of cooling.

An explanation is required for the variation of hardness as a function of cooling rate before tempering (Fig. 6). When the cooling rates are high (water, oil, air), the hardness is low even though the structure -- as observed through the electron microscope -- is highly dispersed. This may be explained by the fact that the decomposition phases by their chemical composition differ little one from another and from the initial solid solution. Coagulation of the evolved phase -- which decreases hardness -- proceeds to a considerable extent at low rates of cooling (40° per hour, 20° per hour). The optimum combination of factor which leads to the greatest hardness is to be observed at medium cooling rates (160° per hour), at sufficiently complete chemical isolation of the phases, and not overly high coagulation.

Consequently the maximum hardness obtainable as a result of industrial heat treatment (160° per hour with a 16-hour temper at 700°) coincides with the highest heat resistance.

However, it does not follow therefrom that heat resistance is a single-valued function of hardness at room temperature. Hardness is but an indication of the phase transformations and structural changes which occur at anomalous hardening of an alloy of the KhN80T type.

Cooling of a high-temperature solid solution at a definite controlled rate leads to an increase in hardness as a result of a reduction of the furnace cooling temperature from which water quenching was effected. This rise in hardness evidences the fact that dispersion hardening takes place in the process of cooling. It is to be assumed that this involves mainly the high temperatures, above 700°; predominant at lower temperatures is the K-state.

The hardness obtained on cooling to 700 and 600° is identical. This is partially confirmed by electron-microscopic investigation. A marked growth of the α'-phase crystals is to be observed at a change-over from 900 to 800°. At a lower temperature the size of the α'-crystals remains practically unchanged. The microstructure discernible by electron microscope examination is virtually determined by the exposure of the alloy to 800° temperature. In this case the resulting phase is always ordered.

Additional tempering at 700° after heat treatment with furnace cooling (curve 2 in Fig. 11) produces an increase in hardness. This is connected with the "final aging" phenomenon at 700° attributable mainly to the formation of the K-state (without precipitation). Supplementary hardening is the lower, the lower the temperature (in the region of 900-700°), to which the alloy was cooled at the given rate. This regularity is disrupted in case of precooling to 600° at a rate of 160° per hour. Cooling to this temperature entails a considerable additional hardening after tempering at 700° for a period of 16 hours. Therefore cooling to 700-600° - notwithstanding the fact that the final stage in industrial heat treatment practice is tempering at 700° - is of great importance. Tensile strength properties rise continuously with a reduction in furnace cooling temperature (Table 2). Of considerable interest

is the investigation of furnace cooling to temperatures below 600°. At the present time we may only surmise that the intracrystalline process in the 700-600° range affects "final aging" at 700°.

CONCLUSIONS

1. Quench aging and aging at controlled cooling of the KhN80T alloy was investigated in this work.

2. In studying the effect of the cooling rate on the hardness over a wide range of cooling rates from 60° per second to 20° per hour it was found that the greatest hardness value is to be registered at the rate of cooling of 160° per hour, which coincides with the rate recommended by the "Electrostal'". Works for the production of the KhN80T alloy with the highest heat resistance.

3. It was demonstrated by electron-microscopic examination that the precipitation of the "hardening" α' -phase and its coagulation occur with considerably greater intensity as a result of uninterrupted cooling from an elevated temperature, than after tempering of a supercooled solid solution.

4. It has been established that the size of the α' -phase particles is greatly dependent on the rate of cooling. For the investigated range of cooling rates it varies from 200 Å for 60° per second to 2000 Å for 20° per hour.

5. To obtain the highest hardness at room temperature and the highest degree of heat resistance at 700° it is expedient to effect cooling at a controlled rate to 600° and, perhaps, even to lower temperatures.

6. It has been established by X-ray diffraction structural analysis that after very slow cooling and prolonged tempering a hexagonal phase appears along with the α' -phase.

7. A hypothesis was advanced as to successive hardening in the process of continuous cooling. Dispersion hardening with precipitation of the α' -

phase takes place at high temperatures (900-700°), while diffusion hardening, the so-called "final aging" of the phases produced at elevated temperatures, occurs at low temperatures (700° and lower).

8. "Final aging" may occur as a result of the formation of the K-state or in consequence of final decomposition.

REFERENCES

1. A. S. Zaymovskiy & B. G. Livshits, Kachestvennaya stal' [Quality Steel] 5-6, 1933.

2. B. G. Livshits, Izvestiya AN SSSR, sektor fiziko-khimicheskogo analiza [News of the USSR Academy of Sciences, Sector of the Physicochemical Analysis], V. 16, No. 2, 1941.

3. B. G. Livshits, Vysokokoertsitivyye splavy [High-Coercivity Alloys] Metallurgizdat, 1945.

4. N. I. Buynov, R. M. Lerinman, DAN SSSR [Reports of the USSR Academy of Sciences,] 1, 1951.

5. B. G. Livshits and V. S. L'vov, Tekhnologicheskiye protsessy obrabotki stali i splavov [The Technolcgical Processes of Steel and Alloy Treatment], Metallurgizdat, 1955.

6. B. G. Livshits and V. V. L'vov, Fizika metallov i metallovedeniye [Physical Metallurgy and Metallography,] v. 1, No. 3, 455, 1955.

7. L. M. Utevskiy, Zavodskaya laboratoriya [Plant Laboratory], 1952, 6.

8. I. L. Mirkin, M. Ya. L'vovskiy, & M. I. Gavrilyuk, Byulleten' tsentral'nogo instituta informatsiyi [Bulletin of the Central Information Institute] 1947, 14, 82.

9. H. Thomas, Zeitschrift für Physik, 1951, Bd. 129.

10. B. G. Livshits, Zhurnal tekhnicheskoy fiziki [Journal of Technical Physics], 1940, No. 10, p. 1981.

Engineer G. M. ASHKARIN, Prof. Dr. of Physical and Mathematical Sciences B. N. FINKEL'SHTEYN
Department of Physics

ELASTIC PROPERTIES OF IRON-VANADIUM ALLOYS.

Elucidation of the effect of alloying additives on the electric properties of alloys, as characterized by the Young modulus and the modulus of rigidity (shear modulus), presents a considerable interest for metallography. The strength of a solid solution is characterized by the binding forces, of which the Debye characteristic temperature ϑ is considered to be one of the criteria, as well as the moduli of elasticity which depend on the interaction of atoms in the crystal lattice.

The question of the factors which determine the relationship between the elastic properties and the Debye characteristic temperature Θ of alloys and their composition cannot be considered solved as yet. For the Ag-Al system (1), in which the atoms of the components have closely approaching diameters, it has been shown that the self-diffusion activation energy and the modulus of rigidity diminish as the aluminum contents increases. This indicates that the binding energies decrease in the alloy with growing concentration of conduction electrons.

In alloys of transition metals the picture, apparently, becomes even more complex owing to the participation of d-electrons in the bond. For example, the lattice parameter in Fe-Cr alloys grows with rising Cr contents with a simultaneous increase of the elasticity moduli E and G (2). The relationship of the elasticity modulus to concentration does not always appear to be uniform. In the Fe-Co system the E modulus reaches the maximum at 20% Co (3, 4), but it drops by more than 20% as the contents of Co continues to increase in α -solid solution.

A comparison of the experimental data pertaining to Young's modulus, as recorded by a number of authors, reveals not only quantitative but also qualitative divergences. This may be attributed to the fact that measurements

were taken by different methods, that the materials differed in the degree of purity and chemical composition, and that the samples might have been subjected to varying machining and heat treatments.

The data on the concentration dependence of the rigidity modulus of alloys are very scarce.

The effect of various alloying additions on the elastic properties of α -solid solution of iron is still insufficiently studied.

The present work was confined to the study of the effect of vanadium on the elastic properties of ferrite. At room temperature the system Fe-V over the investigated range of concentrations (0.3 - 25% /atomic/ V) represents a single-phase solid solution with body-centered cubic lattice.

Measurements were taken by the electroacoustic method with the equipment of the Physical Department of the Moscow Steel Institute (5). The advantage of this method consists in that the Young modulus and the modulus of rigidity are determined from one and the same sample. This assures a sufficiently high accuracy of the experimental results.

The essence of the method consists in the following. The natural frequency of the fundamental tone f_l of longitudinal elastic oscillations and the natural frequency of transverse oscillations f_t are determined from a 240-mm long cylindrical specimen with a diameter of 5 mm. A determination is made of the density of the investigated specimen, and then the values of Young's modulus and the modulus of rigidity are calculated from the respective formulas:

$$E = \frac{4L^3 f_l^2 D^3}{981 \cdot 10^5} \text{ kg/mm}^2; \qquad (1)$$

$$G = \frac{4L^3 f_t^2 D^3}{981 \cdot 10^5} \text{ kg/mm}^2, \qquad (2)$$

where L - length of the specimen, cm;

f_l - natural frequency of the longitudinal oscillations;

f_t - natural frequency of the transverse oscillations;

D - density of the alloy, g/cm^3.

The Poisson ratio is calculated by formula

$$\mu = \frac{1}{2}\left(\frac{f_l}{f_t}\right)^2 - 1. \qquad (3)$$

Using the experimental values of f_l, f_t and D, we may compute (6) the Debye temperature

$$\theta = \frac{h}{K}\left(\frac{3N_A}{4\pi A}\right)^{\frac{1}{3}} \cdot 2Lf_t \left\{ \frac{3D}{2 + \left[\frac{3 - \left(\frac{f_l}{f_t}\right)^2}{4 - \left(\frac{f_l}{f_t}\right)^2} \right]^3} \right\}^{\frac{1}{3}} \qquad (4)$$

where h - Planck's constant;

K - Boltzmann's constant;

N_A - Avogadro number;

A - atomic weight of the alloy calculated from its chemical composition.

The specimen is clamped in the middle. In determining the natural frequency of the longitudinal oscillations an electromagnetic vibration exciter, actuated by audio-frequency oscillator ZG-2, is set opposite one end of the specimen. Installed against the other end of the specimen is an induction receiver, constructed along the same lines as the exciter and converting the mechanical oscillations into alternating electric current. Ths signals from the receiver are amplified and delivered to an electron-beam oscilloscope. By changing the oscillator tuning the maximum amplitude corresponding to the resonance is found on the oscilloscope screen, and the natural frequency of the longitudinal oscillations is determined.

The system described in study (5) was used to excite torsional oscillations. The conversion of the sample's mechanical torsional oscillations into electric current is achieved by means of a receiver similar to the exciter.

The procedure for determining the natural frequency of the specimen's torsional oscillations is the same as that used for longitudinal oscillations.

Density was determined by the pycnometric method on an analytical balance. The lattice parameters were measured by taking X-ray photograms with the aid of a RKU-type camera, 86.95 mm in diameter, in chromium radiation.

The relative error in measurements of the elasticity moduli comprised ± 0.33%. The accuracy of the determinations of Poisson's ratio ranged from ± 0.5 to ± 1.0%.

Table 1.

Chemical Composition of the Fe-V Alloys, % (by weight).

V	C	N	Mn	Si	Al

The alloys were fused in an induction furnace and cast into ingots weighing 5 kg each (Table 1). Armco-iron and ferrovanadium (75% V, 0.12% C) served as starting materials. For purposes of homogenizing the ingots were subjected to pre-annealing for 2 hours at 1200° and then forged into 8-mm diam. bars over a temperature interval of 1200-900°. The bars were then turned into rods 240 mm long and 5 mm in diameter.

Measurements were taken for the initial state prior to heat treatment and after annealing. Determinations were made of the longitudinal and transverse oscillations and the density of each specimen. Altogether 3-8 samples were taken from each alloy after each type of heat-treatment. The average frequency and density values for each series of samples were substituted in formulas (1), (2), and (4) to calculate Young's modulus E, modulus of rigidity

G, and Debye temperature θ. After the introduction of the first vanadium additions Young's modulus drops from $21.60 \cdot 10^3$ to $20 \cdot 10^3$ kg/mm^2 and remains at this level until the contents of vanadium reaches 12% (Fig. 1). Thereafter, Young's modulus grows with rising percentages of vanadium, approaching the value of Young's modulus for pure iron. The modulus of rigidity depends little on the concentration of vanadium in the alloy. Its maximum value attains $8.85 \cdot 10^3$ kg/mm^2 at 2% V. The variation of Poisson's ratio as a result of vanadium additions to iron is quite substantial, ranging from 0.3 at 1% V to 0.15 at 2% V. After further additions of vanadium the Poisson ratio of the alloy approaches the value of 0.3.

It should be noted that the results obtained for samples in the initial state cannot serve as a characteristic of alloys in the state of equilibrium. For this reason the specimens were annealed (heated to 1200°, held at this temperature for 2 hours, and then cooled with the furnace). Young's modulus in the annealed alloys drops sharply in the interval of vanadium concentrations from 1 to 4.7%, and reaches the maximum value of $19.24 \cdot 10^3$ kg/mm^2, when the contents of vanadium attain the 4.7% mark (Fig. 2). This value is 11% smaller than that of Young's modulus for ferrite. After a further increase of vanadium contents the E modulus begins to grow and for 25% V it attains the value of E modulus for pure iron.

The modulus of rigidity G remains almost unchanged after fusion of ferrite and vanadium. The poisson ratio changes depending on the contents of vanadium with its minimum value showing 0.16 at 4.7% V.

Table 2 gives the values of the Debye characteristic temperature.

Debye characteristic temperature Θ also assumes its lowest value (457°K), when the vanadium contents is at this level (4.7%). The growth of vanadium contents is accompanied by a rise in Θ, and at 25% V it attains 484°.

In order to provide a basis for comparison of our data with the results

Figure 1. Variation of E (1) and G (2) moduli and Poisson's ratio as a function of growing vanadium concentration in α -iron. Specimens were not annealed after forging. a) G x 10^{-3} mg/mm^2, E x 10^{-3} kg/mm^2; b) Contents of V, % (atomic).

Figure 2. Variation of E (1) and G (2) moduli, Poisson's ratio μ (3), and Debye temperature Θ (4) with growing concentration of vanadium in α -iron. 2 hour anneal at 1200°.

obtained by other investigators (4, 7, 8) the forged specimens were annealed in vacuo at lower temperatures. It turned out that a variation of the annealing temperature within the limits of 700-900°, with specimens held for 2 hours, failed to produce any changes in the investigated characteristics of the alloys.

Shown in Figure 3 is the concentration dependence of E and G after a 2-hour anneal at 900°. The variation of these values as a function of vanadium contents resembles the concentration dependence registered for unstabilized specimens. The same results were obtained after four-and six-hour holding periods for this temperature range.

Table 2.

Values of Debye Characteristic Temperature

Vanadium contents, % (atomic)	Debye Characteristic temperature °K.

It may be deduced from this that a 700-900° anneal is insufficient to produce equilibrium iron-vanadium alloys.

Figure 3. Variation of E (1) and G (2) moduli with growing vanadium concentration in ∝ -iron. 900° anneal for 2 hours.
a) Contents of V, % (atomic).

Figure 4 illustrates the concentration dependence of the lattice parameters for the investigated alloys. At 4.7% V the lattice constant (parameter) constitutes a linear function of vanadium contents. Thereafter the linear

shape of the curve is impaired, and there appears a flexure at 20% V. Measurements of the lattice constant in the Fe-V system are also recorded in papers (9, 10). But in these studies alloys with less than 13% V were not investigated.

Our data on the concentration dependence of Young's modulus may be compared with the results of Nishijama (4), who has studied alloys with less than 7% vanadium (the composition is given by the charge). The author has found that vanadium causes the E modulus to drop to $20.9 \cdot 10^{3}$ kg/mm^2. For the same type of treatment we have registered (see Fig. 3) a greater drop in Young's modulus ($20.25 \cdot 10^{-3}$ kg/mm^2 at 8.7% V). Qualitatively the agreement is good, but quantitatively the comparison is made difficult because Nishijama has used the statical method in measuring Young's modulus.

Figure 4. Variation of the ferrite lattice parameter as a function of vanadium concentration.
1) Lattice parameter, Å ; 2) Contents of V, % (atomic).

A comparison of the concentration dependence of Young's modulus for different annealing temperatures indicates that this relationship experiences a qualitative change as the annealing temperature rises from 900 to 1200°. This difference may, apparently, be explained by the uneven distribution of vanadium atoms in solid solution during low-temperature anneal. The same is also evidenced by the higher microhardness values at the periphery of the grain as against its central section.

The variation of vanadium contents in iron affect the values of modulus G in a far lesser degree thanthose of Young's modulus E. The annealing temperature also produces but a minor effect on the character of the concentration dependence of modulus G. The Poisson's ratio depends little on the type of heat treatment.

A drop in the characteristic temperature Θ accompanies the growth of vanadium concentration to 4.7%. Qualitatively this is in good accord with the data recorded by V. A. Il'yina and V. K. Krivitskaya (7) who have found that an addition of 2% V lowers the characteristic temperature of α -iron. However, a concentration of vanadium exceeding 4.7% leads to an increase in the characteristic temperature of the alloys. According to Yu. V. Piguzov's data (2) obtained by the same method, Θ for α -Fe amounts to 467°. As it may be seen from our data (see Table 2), the characteristic temperature of the alloy, containing more than 8% vanadium, is higher than the characteristic temperature of unalloyed ferrite. Thus, an increase in the interatomic bond strength is to be registered at these percentages of vanadium.

Noteworthy is the resemblance of the concentration curves of Young's modulus and the Debye temperature Θ . Should this resemblance be revealed also in other systems then -- inasmuch as the latter quantity is universally accepted as a characteristic of the strength of the interatomic bonds -- the concentration curve of Young's modulus could serve, along with the characteristic temperature Θ , as a criterion for evaluation of the effect of alloying on the bond strength in the crystal lattice.

As was shown in work (8), determination of the temperature dependence of the modulus of rigidity G by the method of low-amplitude torsional oscillations simplifies the study of the effect of alloying upon the process of temperature softening (temperature-induced reduction in strength).

The concentration and temperature dependence of the modulus of rigidity of binary alloys was theoretically studied in work (11). The following

formula was derived:

$$\frac{d \ln G}{dC} = \frac{4}{N_0 K} \left(\frac{\delta R}{R}\right)^2 \frac{dG}{dT}. \qquad (5)$$

where C - concentration;

N_o - number of atoms per unit volume;

R - radius of the solvent atom;

δR - difference between the atomic radii of the alloy components;

K - Boltzmann's constant.

In deriving this formula account was taken only of the geometrical factor -- the different sizes of the alloy component atoms -- and of the variation of the crystal lattice elastic spectrum, determined by this factor.

Thus, formula (5) is applicable only to such alloys where no redistribution of electrons occurs among the atoms of the alloy components, or there is no variation of the electron concentration in the conductivity zone (as, for instance, in the Ag-Al system [17].

Consequently, this formula is inapplicable to alloys of transition metals in which the chemical factor must play a predominant role in comparison with the geometric factor.

In this aspect the Fe-V system investigated by us presents a considerable interest, since both components here belong to the category of transition metals and the difference in atomic radii attains 6%. Thus, both factors referred to above are represented here.

The experimental value of the left-hand member of equation (5) according to our data $\left(\frac{1}{G} \cdot \frac{dG}{dC}\right)$ amounts to 0.33. A substitution of the values of the temperature coefficient of the modulus of rigidity $\left(\frac{dG}{dT}\right)$ resulting from our experiments in the right-hand side of the equation produces 2.5.

This discrepancy indicates that another factor which acts in the opposite direction is superposed upon the geometric factor.

The effect of this second factor -- designated by us as the chemical

factor -- may overshadow the influence of the geometric factor. From this point of view the Fe-Cr system presents a great interest. The difference in the atomic radii of Fe and Cr amounts to about 1%.

Since a rise in temperature is always accompanied by a drop in the modulus of rigidity ($\frac{dG}{dT} < 0$), then following Zener's theory (11) it appears that with increasing concentration the modulus of rigidity should decrease to ($\frac{dG}{dC} < 0$). Yet, as demonstrated by measurements carried out by Yu. V. Pigyzov (2) and Nishijama (4) the modulus of rigidity exhibits a rise when the contents of chromium increases in the solid solution.

Using the experimental data obtained by Yu. V. Piguzov, we have a positive value of 0.41 for $\frac{1}{G} \cdot \frac{dG}{dC}$. On the other hand, a substitution of the experimental data for the temperature coefficient of the modulus of rigidity in the right-hand side of formula (5) results in the value of $0.6 \cdot 10^{-4}$.

The data given in this paper indicate that the question of the concentration and temperature dependence of the moduli of rigidity of alloys, which characterize the strength of bonds in the crystal lattice, demand a further study to obtain more dependable experimental data, and in order to develop a theory based on modern ideas concerning the structure of metals and alloys.

REFERENCES

1. B. N. Finkel'shteyn & A. I. Yamshchikova, DAN SSSR /Reports of the USSR Academy of Sciences/, 1954, 98, No. 5.
2. Yu. V. Piguzov, Sb. 36 Moskovskogo instituta stali /Vol. 36 of the Symposium of the Moscow Institute of Steel/ Metallurgizdat, 1957.
3. Köster, Archiv. f. d. Eisenhüt., 1940, 14, No. 6.
4. Nishijama, Sci. Rep. Tohoku Univ., 1929, 18, 359.
5. V. I. Korotkov, Fizika metallov i metallovedeniye /Physical Metallurgy and Metallography/, 1956, 2, No. 1, 160.
6. V. I. Korotkov, B. N. Finkel'shteyn, DAN SSSR, 1956, 108, No. 5, 846.
7. V. A. Il'yina, V. K. Kritskaya, Problemy metallovedeniya i fiziki metallov /Problems of Metallography and Physical Metallurgy/, 1955, p. 412.

8. N. S. Rysina & B. N. Finkel'shteyn, Ibid, 1955.

9. Osawa, Oja. Sci. Rep. Tohôku Univ., 1929, 18, 727.

10. F. Wever, W. Jellinghaus, Mitt. Keis-Wilh. Inst. Bd. 12, 1930, 317.

11. G. Zener, Acta Cryst, 1949, 2, 163.

Engineer G. M. Ashmarin.
Department of Physics.

INTERNAL FRICTION FEATURES IN IRON-VANADIUM ALLOYS

The temperature - internal friction relationship for commercially pure iron is sufficiently well known. As to the effect of alloying additives on the internal friction of alpha-iron, it is, with the exception of very small concentrations, an almost unexplored field. An inquiry into the effect of alloying additions on the internal friction of solid solutions, particularly ferrite, may yield a number of valuable data for the study of the problem of alloying.

In this work a study was made of the influence exerted by vanadium on the temperature curve of internal friction in iron. All the alloys examined, with the exception of that with 25% (atomic) V, are single-phase solutions, within the investigated temperature range, as indicated by the equilibrium phase diagram (2).

The alloys were melted in a 5-kg capacity induction furnace, annealed prior to forging, at 1200° for 2 hours, and forged into bars 10 mm in diameter. The bars were rough-turned to remove surface defects and drawn down to 0.7 mm diameter with one intermediate tempering. Alloys with 20 and 25% (atomic) V were drawn in a heated state (300-500° depending on the composition) down to 1.8 mm, and then again at room temperature to 0.7 mm in diameter, with two intermediate temperings.

The chemical composition of the alloys is given in paper (3). Investigated were alloys containing 1, 2, 4, 7, 8, 10, 12, 20 and 25% (atomic) V.

Internal friction was measured by means of a RKF-MIS-2 device of the torsion pendulum type with a free oscillation frequency of about 1 cps. Wires 0.7 mm in diameter and 300 mm long served as samples. Quantity Q^{-1}, the logarithmic decrement of free oscillation damping divided by π, was

taken as unit measure of internal friction.

To reduce the background of damping and avoid oxidation of samples all measurements were taken in vacuo. Temperature adjustment was by means of a thermocontroller whose hookup was that of a four-arm resistance bridge with a photoelectron relay, and a Chromel-Alumel thermocouple used for measurement. The error in internal friction determination did not exceed ± 0.5% at room temperature and attained 2% at 500-600°.

A vacuum extension designed by Yu. V. Piguzov was used for determinations of the activation energy. This device made it possible to vary the natural oscillations of the sample by varying the torsion rod, without affecting the vacuum.

The frequency could be varied within the limits of 0.35 to 1.5 cps

The activation energy of the respective relaxation process was computed by formula:

$$H = \frac{R \ln\left(\frac{f_2}{f_1}\right)}{\frac{1}{T_1} - \frac{1}{T_2}}, \qquad (1)$$

where f_1 - oscillation frequency for the larger moment of inertia of the torsion rod;

f_2 - oscillation frequency for the smaller moment of inertia;

T_1 - absolute temperature corresponding to the peak position for frequency f_1;

T_2 - absolute temperature corresponding to the peak position for frequency f_2;

R - universal gas constant.

The relative error in determining H comprised ± 10%.

EFFECT OF VANADIUM ON THE INTERNAL FLOW OF FERRITE IN ANNEALED STATE.

All alloys after deformation, were annealed at 900° and cooled with the furnace. Their grain size was of the same order, and approaching the diameter of the sample. Up to 400° the temperature dependence of internal friction for

all alloys represents a straight line running parallel to the temperature axis (Fig. 1). A sharp growth of internal friction begins to be manifested after 400°, i.e., the relaxation processes commence to develop. The grain size being the same, the level of internal friction at temperatures above 400° depends on the amount of vanadium contained in the solid solution. This level rises as the contents of vanadium in the solid solution drops. The strongest effect is produced by the initial additions of vanadium.

A flexure on the curve for the annealed alloy with 12% (atomic) V was revealed in the region of 630°; for the 25% V alloy this flexure turns into a maximum. This phenomenon will be dealt with in greater detail further in the discussion.

Figure 1. Internal friction of alloys with different contents of vanadium after 2-hour annealing at 900°; 1 - alloy with 0.88% (atomic) V; 2 - 2.1%; 3 - 4.27%, 4 - 9.7%; 5 - 11.95%.

a) Internal friction $Q^{-1} \cdot 10^4$; b) Temperature, °C.

Alloy with 2% (atomic) V.

It is interesting to clarify the effect of hardening on high-temperature internal friction, since this may help to reveal the nature of this type of internal friction. Singled out for study was the 2% V alloy which retains a single-phase structure (4) over the entire range of temperatures, as confirmed by the results of dilatometric analysis.

The samples were hardened in stainless steel capillaries, and also in quartz capillaries, heated in a vertical tubular furnace. In all these tests the heating time in the hardening cycle amounted to 15 min. The specimens were quenched in water containing NaCl. They were subjected to annealing prior to quenching.

Figure 2. Internal friction in samples of alloy with 2.11% (atomic) V; - one of them annealed and two quenched from different temperatures:
1 - annealed at 900° for 2 hours; 2 - quenched from 1200°; 3 - quenched from 1300°.
a) Internal friction; b) Temperature, °C.

Figure 2 shows the temperature curves of internal friction of three samples of 2% V alloy: one-annealed, and two-quenched from different tempera-

tures. High-temperature internal friction (B) appears in the annealed sample at a lower temperature than in the quenched samples. Internal friction B diminishes, when the temperature of heating for hardening is increased. Thus, if a test temperature of 550° is adopted, then Q^{-1} for annealing will amount to $152 \cdot 10^{-4}$, and for quenching from 1300° - only to $11 \cdot 10^{-4}$.

A carbon peak was obtained in the region of room temperature, when quenching from 1300°. Evidently, this temperature for the given holding time is sufficient to cause the carbides to dissociate and carbon to dissolve in the alloy.

Alloy with 25% (atomic) V.

After annealing of cold-worked alloys containing vanadium in amounts exceeding 12% (atomic), a flexure on the temperature curve of internal friction appears in the region of 600°. For 25% (atomic) V this flexure changes into a pronounced maximum.

Let us examine the behavior of this peak obtained in the annealed samples. We designate the section of the internal friction curve in the region approaching to the peak by A (Fig. 3), the section of the curve in the region of the peak itself - by Б , and use B to denote high-temperature internal friction. A hysteresis in the sample for sections Б and B, but not for section A is to be registered. During heating, at a frequency of 0.8 cps, the peak corresponds to the temperature of 620°, after which the Q^{-1}-t° curve shows a drop, and then a steep rise (section B). During cooling section B shifts in the direction of low temperatures; the value of Q^{-1} for the same temperature increases. Internal friction in the region of the peak Б augments during cooling. The internal friction hysteresis increases in the Б region, if the specimen is held at a certain temperature, say, at 700° for 1 hour, before cooling (Fig. 4). However, for the sample annealed at 900° for a period of 12 hours a similar hysteresis is to be registered, as for the specimen annealed for 2 hours, but section A is shifted towards a higher temperature;

the maximum corresponds to the temperature of 620°.

It is interesting to consider the internal friction of a sample, subjected to a 2-hour anneal at 1200° in a quartz ampoule in a compartment furnace, and cooled with it (Fig. 5). Sections A and B shift into the region of higher temperatures. The temperature position of the peak remains the same. The height of the peak increases considerably. Such shape of the internal friction curve may be explained, if, on the basis of the principle of superposition, one is to assume that -- in the absence of the process of relaxation which accounts for section Б -- branch A smoothly passes into branch B of the temperature curve of internal friction. It may well be that A and B result from the same processes. Then the temperature function for internal friction in section Б may be determined by subtraction.

From Figure 6, plotted by this method, it may be seen that the height of peak Б is greater for the sample annealed at 1200°. For such a sample

Figure 3. Internal friction in alloy containing 25% (atomic)$_o$V subjected to 2-hour anneal at 900°. Measurements were taken during heating (1) and during cooling (2).

1) Internal friction, $Q^{-1} \cdot 10^4$;
2) Temperature, °C.

Figure 4. Internal friction in alloy containing 25% (atomic)$_o$V subjected to 2-hour anneal at 900°; heating, holding time - 1 hour at 700°, cooling.

1) Internal friction, $Q^{-1} \cdot 10^4$;
2) Temperature, °C.

Figure 5. Internal friction in alloy containing 25% (atomic) V subjected to 2-hour anneal at 1200°.
1) Internal friction, $Q^{-1} \cdot 10^4$;
2) Temperature, °C.

Figure 6. Internal friction (peak Б determined by subtraction; alloy with 25% (atomic) V;
1 - annealed at 900°; 2 h;
2 - annealed at 900°, 12 h;
3 - annealed at 1200°, 2 h.
1) Internal friction $Q^{-1} \cdot 10^4$;
2) Temperature, °C.

the internal friction comprises $80 \cdot 10^{-4}$, and for a sample annealed at 900° - $60 \cdot 10^{-4}$. As a result of an increase in the annealing time (900° - 2 hours and 12 hours) the peak moves slightly towards higher temperatures. The difference in the peak heights lies within the limits of the error. The stronger effect on peak Б is produced by a rise in the annealing temperature (900°- 2 hours and 1200° -2 hours). Although the peaks in Figures 3 and 5 correspond to the same temperature, it appears to be more correct to consider the position determined by subtraction as the temperature position of the peak. For the 900° anneal the peak positions in Figures 3 and 6, determined by subtraction, do not coincide, because a considerable contribution to internal friction is made by the process of relaxation which is responsible for branch B.

The effect of the temperature of quenching on the peak was also studied in this work (Fig. 7). The samples were annealed at 900° and quenched from

900, 1050 and 1200°. The temperature curve of internal friction for the sample quenched from 900° differs little from the curve of internal friction for the annealed sample, during heating. The distinction is in the position of branch B (at corresponding temperatures). A further increase of the temperature of quenching lowers branch A and, particularly, branch B. The higher the quenching temperature, the more does the internal friction branch B move towards the higher temperatures. This phenomenon is analogous to the one described for the alloy with 2% (atomic) V.

After quenching from 900° peak Б differs neither by height nor by position from peak Б obtained for samples annealed at 900° for 2 hours. However, a further rise in the temperature of quenching causes peak Б to shift slightly in the direction of higher temperature and somewhat reduces its height.

The hardened samples were tempered at 760° for a period of 1 hour. It was established that the hysteresis of internal friction is highly dependent on the quenching temperature and attains the highest value for samples quenched from 1350°. Isothermal internal friction was measured on a sample quenched from 1350° and tempered at 760°. In the process of holding during tempering the internal friction manifested a linear growth. Isothermal internal friction increased, ultimately approaching the value of internal friction of a tempered specimen. After tempering peak Б shifted in the direction of lower temperatures, while its height increased for samples quenched from 1200°. Thus, in samples quenched from 1200° the internal friction amounted to $48 \cdot 10^{-4}$ as a result of heating, while after tempering it showed a value of $60 \cdot 10^{-4}$.

As the tempering temperature increases, the sample quenched from 1200° reverts to the state which existed before quenching (Fig. 8). However, even after one hour of tempering at 850°, Q^{-1} in region B is lower than for an annealed sample.

During frequency measurement the activation energy of the relaxation

Figure 7. Internal friction of alloy containing 25% (atomic) V quenched from different temperatures:
1 - Quenched from 900°; 2 - quenched from 1050°;
3 - Quenched from 1200°.

1) Internal friction $Q^{-1} \cdot 10^4$; Temperature, °C.

Figure 8. Internal friction of alloy containing 25% (atomic) V quenched from 1200° and tempered at different temperatures:
1 - quenched from 1200°; 2 - tempered at 800°, 1 h;
3 - tempered at 850°, 1 h.

1) Internal friction $Q^{-1} \cdot 10^4$; 2) Temperature, °C.

process, responsible for peak Б , was determined on the basis of the peak's displacement. Measurements were made on one and the same sample, thus reducing

error. The activation energy of the process, causing the appearance of peak Б , amounts to 97 Kcal/mol.

The amplitude curve of internal friction was determined over the range of peak Б temperatures for a fivefold change of the deformation amplitude (not exceeding the 10^{-5} values). Internal friction within the limits of the test error does not depend on the amplitude for a given interval of temperatures.

Alloys with 20 and 12% V.

Similar tests were carried out with an alloy containing 20% (atomic) V. For all types of treatment there appears a more or less explicit maximum on the temperature curve of internal friction in the region of 620°. With growing temperature of quenching the height of peak Б , derived by the method of subtraction, diminishes. In the case of this alloy internal friction is also marked by a strong hysteresis at temperatures above 600°. After an increase in the time and temperature of annealing peak Б shifts to higher temperatures (Fig. 9). An increase of the quenching temperature also displaces peak Б in the direction of higher temperature, as this was registered in the case of the alloy with 25% (atomic) V. An increase of the quenching temperature entails a shift of the internal friction branch B towards a higher temperature.

The alloy with 12% (atomic) V yields no maximum no matter what type of heat treatment is applied (Fig. 10). A bend is revealed on the temperature curve of internal friction in the region of 630°. The maximum appearing for 1 cps frequency around 630° may be defined by the method of subtraction. The height of this peak diminishes after quenching and with increasing temperature, as compared with the maximum for the annealed state. Quenching is accompanied by a growth of hysteresis. A rise in the temperature of quenching involves a lowering of branch A and a sharp decline of branch B. Branches A and B show a rise as a result of tempering, but the height of peak Б varied

insignificantly in our tests.

* ** *

The high-temperature branch of internal friction, i. e., the region where internal friction increases sharply with the test temperature, presents an interesting object of study. Information on the effect of cold working on internal friction at elevated temperatures is available in the literature. The tests described were carried out on pure metals. There are practically no data on the effect of either solid solution concentrations or various heat treatments on internal friction at high temperatures.

Figure 9. Internal friction of alloy with 20.8% (atomic) V: 1 - annealed at 900° for 12 hours; 2 - quenched from 1050°; 3 - quenched from 1200°.
a) Internal friction.

Figure 10. Internal friction of alloy with 12% (atomic) V: 1 - annealed at 900° for 12 hours; 2 - quenched from 1300°.
a) Internal friction; b) Temperature, °C.

It is well known that an increase in grain size causes the high-temperature internal friction branch (in our case the branch designated by B) to shift into the region of more elevated temperatures.

This type of internal friction cannot be ascribed only to the influence of the grain boundaries, since branch B exists also in monocrystals.

In our work the samples of alloys with various contents of vanadium at approximately the same proportion of other admixtures had grains of equal size. In the annealed state branch B moves towards higher temperatures as the contents of vanadium increases (see Fig. 1). This effect of vanadium is less conspicuous in alloys containing more than 12% (at.) V. This is, possibly, due to the fact that the $Б$ section of the curve somewhat obscures the general picture. However, upon subtraction of peak $Б$, a certain shift of the B branch becomes noticeable, when the proportion of vanadium increases in the alloy.

An increase in the quenching temperature produces an effect on branch B similar to that exerted by a rising vanadium percentage (see Fig. 2). Prior to quenching all samples of each alloy were annealed under identical conditions and had the same grain size. The pre-quench heating time was insufficient to cause an appreciable growth of grain. Thus, here as well, the shift of branch B in the direction of higher temperatures cannot be explained by a change in grain size. Furthermore, after a quenched sample had been tempered, branch B moves towards lower temperatures. The higher the tempering temperature, the closer it approaches to the curve of a sample, subjected to the same anneal as was given to the specimen in question prior to quenching.

It is possible that branch B is produced as a result of at least two processes. One is subject to the influence of grain size, and the other - affected by the contents of alien atoms in the solid solution, i.e. in the case of alloying - by vanadium atoms, in the case of quenching - by the atoms of impurities.

The effect of the grain size may be observed on alloy samples with 25% (atomic) V, after they have been subjected to 2 hours of annealing at different temperatures (see Figs. 3 and 5.) Branch B lies in the region of higher temperature for a sample with coarser grain which was subjected to 1200° anneal.

The other process is, probably, related to the presence of defects in the lattice, and to the interaction of dissolved atoms with these defects. The specimens which have undergone annealing at 1200° have fewer defects, and this is the reason why branch B appears at a higher temperature. The admixtures dissolved in the process of hardening, and this also leads to a shift of branch B in the direction of a higher temperature. The internal friction hysteresis may be associated with the dissolution and separation of impurities, present in commercially pure alloys, and also with the existence of the second phase. In tests of annealed samples hysteresis may be connected with a certain amount of dissolution and precipitation occurring in the process of the test, since hysteresis increases during a high-temperature hold (see Figs. 3 and 4) prior to cooling. Ke Ting Sui, who has studied cold-worked iron (1), attributes high-temperature relaxation to the imperfections arising in the course of cold working which fail to disappear after recrystallization.

Let us consider peak Б . As it may be seen from the drawings, it appears, when the vanadium contents in the alloy exceed 12% (atomic). A further increase of vanadium concentration up to 25% causes the flexure on the temperature curve to turn into a peak. If the alloys have been given the same treatment, the peak for the alloy with 12% V will be found in the region of a somewhat higher temperature, than in the case of the 25% V alloy.

During quenching the peak becomes more sharply expressed owing to the fact that branch B, which is superposed on this process, shifts to a higher temperature. The peak hysteresis may be explained by the hysteresis of the relaxation process, producing the branch B condition, since the height of the peak,

obtained by subtraction, is the same for annealed samples during heating and cooling.

The difference in the atomic diameters of vanadium and iron amounts to 6%, and the concentrations of the alloying element are sufficiently high. It could, therefore, be assumed that peak Б comes as a result of a stress field reorientation in a substitutional solid solution. This type of relaxation was studied for alloys of non-transition metals (5, 6). It was shown that the temperature position of the peak and its height are greatly dependent on the composition. No such clearcut relationship was to be observed in the case of Fe-V alloys. Moreover, with an increase in the annealing temperature the peak shifts towards higher temperatures (see Fig. 6). The maximum diminishes somewhat in the process of quenching.

Had this peak resulted from the above discussed relaxation process in the solid solution, its temperature position should have been greatly dependent on the contents of vanadium. There is no marked difference in the temperature position of peak Б for alloys with 12% (atomic) V and for those with twice as great a concentration: 25% (atomic) V. Nor does this peak resemble the grain-boundary maximum of a solid solution, since the grain in our samples is commensurate with the diameter of the specimen, i. e. the samples may be considered as "monocrystalline".

No grain-boundary peaks were registered in our tests, because industrial materials were used for the melts, and the inclusions at their grain boundaries were difficult of solution. This may have led to the disappearance of this type of peak (7).

It is possible that the appearance of peak Б is related to the formation of the second phase, and to the presence of interfaces between it and the crystallites of the mother liquor.

The second phase is probably precipitated in the form of crystals of almost similar size. This is confirmed by the fact that the width of the peak,

obtained by the method of subtraction, corresponds to a narrow relaxation time interval. With an increase in the holding time for annealing the quantity of the second phase increases, and the height of the peak augments. A certain displacement of the peak in the direction of a higher temperature, following an increase in the annealing temperature, may be attributed to the enlargement of the second-phase particles.

In the process of quenching the peak diminishes slightly in height, since the 15 minutes of pre-quench heating is sufficient for a certain proportion of the second phase to get dissolved. The height of the peak increases after tempering.

The height of the peak grows with a rising content of vanadium. This may be associated with an increase in quantity of the second phase. The existence of the second phase in our alloys is conjectural. No second-phase lines appear on the X-ray pictures. No precipitation was found in examinations with a metallographic microscope at regular rates of magnification. However, the fact that the alloy with 25% (atomic) V was located in the two-phase region (2), suggests the presence of a second phase. The σ-phase may constitute such second-phase. The possibility of σ-phase formation, when the contents of the alloying element is rather low, was discussed in paper (8). Moreover, the formation of σ-phase may also be influenced by the fluctuations of the solid solution concentration. This is indicated by the inhomogeneity of the solid solution with respect to microhardness. The high sensitivity of the internal friction method makes it possible to reveal small quantities of precipitates which fail to produce visible lines in the X-ray photograms (radiograms).

On the other hand, it cannot be conjectured that peak B is caused by carbides or nitrides, since carbon is also contained in vanadium-treated alloys, and no such peak is to be observed for these alloys. In alloys with 8.7% (atomic) V the contents of carbon is somewhat higher than in the other

alloys, yet no peak Б could be observed. Nitrogen is contained in all these alloys in quantities not exceeding 0.007%. The highest percentage of nitrogen is to be found in alloys with 8.7 and 12% V. Yet the highest peak Б is to be observed not in these alloys, but in alloys with a higher percentage of vanadium.

CONCLUSIONS

1. An increase of vanadium contents in a solid solution causes the high-temperature branch of internal friction to shift to the region of higher temperatures.

2. Quenching shifts the high-temperature branch of internal friction to higher temperature zones.

The shift of this branch grows with an increase in quenching temperature.

3. A peak appears on the internal friction curve in the region of 600°, when the contents of vanadium exceed 12%.

4. In alloys with 1 and 2% (atomic) V, being quenched from temperatures higher than 1300°, a peak was revealed in the room temperature region.

REFERENCES

1. Ke, Ting-Sui, Met. Techn. 1948, 15, No. 8.
2. Rostoker, Jamamoto, Transact ASM, 1954, 46, 1136.
3. G. M. Ashmarin, B. N. Finkel'shteyn. See this volume.
4. Lukas, Fischel, Transact. ASM, 1954, 46, 247.
5. Nowick, Phys. Rev., 1952, 88, 925.
6. Childs, Le Claire, Acta Met. 1954, 2, No. 5.
7. Ke Ting-Sui, J. Appl. Phys. 1950, 21, 414.
8. A. G. Lesnik, Voprosy fiziki metalov i metallovedeniya [Problems of Physical Metallurgy and Metallography], 1954, 5.

Assistant I. N. Chernikova and Professor, Doctor of Physical and Mathematical Sciences B. N. Finkel'shteyn.

Department of Physics

EFFECT OF TEMPERING ON THE MODULUS OF RIGIDITY AND THE INTERNAL FRICTION OF HARDENED CARBON STEEL

The modulus of rigidity (shear) and the internal friction of carbon steel samples with 0.015 to 0.58% C (Table 1) were tested over the 20-650° temperature range.

Table 1

Chemical Composition of Samples, % (by weight)

Conditional designation of samples	C	Si	Mn	Ni	S	P	Al	N

Steel was melted in a 35-kg capacity high-frequency induction furnace at the experimental plant of the Central Scientific-Research Institute of Ferrous Metals (TsNIIChM). Ingots weighing 7 kg were forged into rods 9-mm in diameter. Samples for measurement of the temperature dependence of the modulus of rigidity and internal friction were produced by drawing the rods into 0.7-mm wire with intermediate anneals at 800-850°. For measurements of the modulus of rigidity the rods were turned to a 3.5 mm diameter.

Martensitic hardening was carried out after a three-minute hold of the samples in the furnace in a ten-percent solution of NaCl.

Tempering was effected with one-hour holding in vacuum at temperatures ranging from 100 to 600° with intervals of 100°.

Under this type of treatment decarburization of samples could proceed

from the surface. An additional microstructural analysis revealed that the thickness of the decarburized layer did not exceed a few hundred angstroms.

The temperature curve of the modulus of rigidity and internal friction was studied by the method of low-amplitude torsional oscillations using a RKF-1 unit ("relaxator" of the Department of Physics of the Moscow Institute of Steel, model 1), at an oscillation frequency of about 1 cps. The modulus of rigidity G is known to be related to the frequency of free torsional oscillations by ratio:

$$G = \frac{8\pi ILf^2}{\mu^4}, \qquad (1)$$

where L - length of the specimen;

μ - radius of the specimen's cross-section

I - moment of inertia of a system producing torsional oscillations;

f - oscillation frequency of the specimens.

Ignoring the temperature function of quantities I, L, and μ, one may identify the shape of the temperature curves of G and f^2.

Figures 1-4 show the temperature curves of the modulus of rigidity of steel with different contents of carbon as a function of heat treatment. As a rule, the hardened samples possess the lowest values of the modulus of rigidity practically over the entire investigated range of temperatures. Only steel containing 0.015% C presents an exception. It is possible that this disruption of the regular relationship, as observed in all the other samples, is due to insufficient hardening for so low a percentage of carbon. With a rise in the tempering temperature the modulus-of-rigidity values gradually increase. This regularity is also observed in the case of steel with 0.015% C.

The almost rectilinear decline of the modulus of rigidity with temperature swerves into a steeper drop in the region of 400-440°, for temperatures higher than 500° the curves for the same steel, which correspond to different types of treatment, begin to intersect.

Listed in Table 2 are the values of the temperature coefficient for the modulus of rigidity of steel after three heat treatments (hardening, 200 and 600° temper).

The modulus of rigidity G of plastically deformed and annealed samples was also measured at room temperature by the electroacoustic method in a unit designed by V. I. Korotkov (1). The results of these measurements are given in Table 3.

In annealed steel the modulus of rigidity grows uniformly with increasing carbon percentage at room temperature. In plastically deformed samples an increase in carbon contents leads to a decline of the modulus of rigidity.

Figure 1. Temperature curves of modulus G as a function of heat treatment (0.015% C steel):
1 - tempered at 200°; 2 - 300°; 3 - 400°; 4 - 500°; 5 - 600°
6 - after hardening.
a) The squares of the oscillation frequency of the samples, f^2; b) Temperature, °C.

It is natural to associate such variation of the modulus of rigidity with distortions of the crystal lattice: the growth of distortions as the carbon content increases, and their diminution after annealing.

Measurements of internal friction also lead to a similar conclusion.

Figure 2. Temperature curves of modulus G as a function of heat treatment (0.35% C steel):
1 - tempered at 100°; 2 - 200°; 3 - 300°; 4 - 500°;
5 - 600°; 6 - after hardening; 7 - after annealing.
a) The square of the oscillation frequency of the samples, f^2; b) Temperature, °C.

Figure 3. Temperature curves of modulus G as a function of heat treatment (0.46% C steel):
1 - tempered at 100°; 2 - 200°; 3 - 300°; 4 - 500°;
5 - 600°; 6 - after hardening; 7 - after annealing.
a - The square of the oscillation frequency of the samples, f^2; b) Temperature, °C.

Figure 4. Temperature curves of modulus G as a function of heat treatment (0.58% C steel):
1 - tempered at 100°; 2 - 200°; 3 - 300°; 4 - 500°;
5 - 600°; 6 - after hardening; 7 - after annealing.
a) The square of the oscillation frequency of the samples, f^2; b) Temperature, °C.

Figure 5 shows the shapes of the temperature curve of internal friction for hardened samples with varying contents of carbon. In the region of 200° the height of the internal friction peak grows regularly with rising contents of carbon. If one is to consider (2) that this peak for ferrite is caused by the interaction of carbon atoms with the defects in the crystal lattice, then this behavior would seem to be quite regular. From this point of view it is also possible to explain the reduction of the peak's height after tempering, this reduction increasing the higher the temperature of tempering (Fig. 6). From the data referred to above it follows that after tempering, accompanied by a decrease in the crystal lattice distortions, there should be a growth in the activation energy of the relaxation process responsible for this internal friction peak. Indeed, this was substantiated by a determination of

Table 2.

Temperature Coefficient ($\gamma \cdot 10^{-4}$) of the Modulus of Rigidity G

Temperature Range °C	0.58 C steel			0.46% C steel			0.35% C steel			0.015% C steel		
	Hardened	Tempered		Hardened	Tempered		Hardened	Tempered		Hardened	Tempered	
		200°	600°		200°	700°		200°	600°		200°	600°

Figure 5. Internal friction temperature curve in hardened steel:
1 - 0.015% C; 2 - 0.35% C; 3 - 0.46% C; 4 - 0.58% C.
a) Internal friction, Q^{-1}; b) Temperature, °C.

activation energy H made by means of measuring the shift of the peak's position on the temperature scale, in transition to another oscillation frequency, and by using the well known formula (3):

$$H = \frac{RT_1T_2 \ln\left(\frac{f_2}{f_1}\right)}{T_2 - T_1},$$

where f_1 and f_2 - frequencies of torsional oscillations;
T_1 and T_2 - temperatures (°K) correspond to these frequencies and at which the internal friction peak appears.
R - universal gas constant,

Table 3.

Absolute Values of the Modulus of Rigidity G at Room Temperature kg/mm^2

Conditional designations of samples.	Strain-hardened samples	Annealed samples.

Figure 6. Effect of the tempering temperature on the position of the internal friction maximum for hardened steels:
1 - 0.58% C; 2 - 0.46% C; 3 - 0.35% C; 4 - 0.28% C.
a) Internal friction, Q^{-1}; b) Temperature, °C.

This determination has shown that one-hour temper at 250° leads to an increase of the activation energy from 28 to 58 Kcal/g-atom, for steel with 0.58% C. Similar is the behavior of steel with 0.35% C.

REFERENCES

1. V. I. Korotkov, Fizika metallov i metallovedeniye [Physical Metallurgy and Metallography], 1956, 2, No. 1.

2. W. Koestler, L. Banget, & P. Hahn, Archive fuer das Eisenhuettenwesen, 1954, 25, 11/12.

3. Ke Ting-Sui, Sb. Uprugost' i ne uprugost' metallov [Elasticity and Non-Elasticity of Metals, Symposium], IL., 1954.

Assistant M. A. VEDENEYEVA, Professor N. D. TOMASHOV
Department of Metal Corrosion.

VARIATION OF INTERNAL FRICTION AND NATURAL OSCILLATION FREQUENCY OF TYPE Kh18N9 STEEL SAMPLES DURING INTERCRYSTALLINE CORROSION.

Intercrystalline corrosion results in a change of certain physical properties of steel samples. Due to intercrystalline decay there is an increase in resistivity which thus can be utilized for a quantitative evaluation of intercrystalline corrosion (1-3). There are data which indicate that intercrystalline corrosion strongly affects the damping capacity (which is determined by internal friction) of cylindrical samples (4) and the modulus of elasticity (5).

The purpose of this work was to determine the possibility of evaluating intercrystalline corrosion by measurement of internal friction.

The following grades of steel were subjected to investigation: OKh18N9, 1Kh18N9, IKh18N9T, 2Kh18N9 and Kh23N23M3D3 brands of chrome-nickel, and type Kh18N9 low carbon steel. The samples used in the tests were 80 x 5 x 0.4-mm plates. In addition, the 1Kh18N9 and 2Kh18N9 steels were tested on samples in the form of wire 310 mm long and 0.7 and 0.9 mm in diameter. The data on carbon and titanium contents are listed in Table 1.

Before the tests the samples were quenched from 1080-1100° and tempered at 650° for a period of two hours. A part of the 1Kh18N9 steel samples was tested after hardening without subsequent tempering.

Intercrystalline corrosion was produced by holding samples in a boiling solution containing 110 g $CuSO_4 \cdot 5H_2O$ and 55 cm^3 H_2SO_4 (specific gravity 1.84) in a liter of water. For the evaluation of intercrystalline decay before and after holding in the corrosive medium, measurements were taken of resistivity, internal friction, and tensile strength. Two methods were used for measuring internal friction: plotting the resonance curve during excitation of transverse

oscillations in the samples, and damping the amplitude of free torsional oscillations. In applying the method of induced oscillations internal friction was measured by means of a unit (6) consisting of a 20-200 cps oscillator and a vibrator (Fig. 1). The vibrator includes an electromagnet with core 6, actuated by the oscillator. The electromagnet excites oscillations in strip-holder 2 in which sample 5 is fastened. The amplitude of the sample oscillations was measured by means of a cathetometer.

T a b l e 1.

Carbon and Titanium Contents in the Test Specimens.

Grade of Steel	Contents, %	
	C	TI
	Plate Samples	
OKh18N9	0.08	-
1Kh18N9	0.12	-
1Kh18N9T	0.10	0.65
2Kh18N9T	0.16	
Kh23N23M3D3	0.04	0.09
Kh18N9 low-carbon		
1	0.015	-
2	0.018	-
	Wire Samples	
IKh18N9	0.13	-
2Kh18N9	0.23	-

Figure 1. Equipment for the fastening of samples:
1 - support with bracket; 2 - strip-holder; 3 - armature; 4 - clamp; 5 - sample; 6 - electromagnet; 7 - guides; 8 - micrometric screw; 9 - terminals.

The quantity which characterizes internal friction Q^{-1} was calculated by formula:

$$Q^{-1} = \frac{\Delta\omega}{\omega_p \sqrt{3}}, \qquad (1)$$

where ω_p - resonance frequency of the sample oscillations;

$\Delta\omega$ - width of the resonance curve at one half of the maximum amplitude (7).

Determination of internal friction consisted in the measurement of the amplitude of oscillations for the resonance frequency and frequencies close to it. All measurements were made for the same value of maximum amplitude equal to 3 mm. During measurements of internal frequency a simultaneous registration was made of the resonance oscillation frequency. On the basis of the resonance frequencies before and after corrosion the Young modulus E was computed from formula

$$\frac{\Delta E}{E} = \frac{\Delta\omega^2}{\omega^2}, \qquad (2)$$

where $\Delta\omega^2 = \omega^2 - \omega_1^2$ (ω_1 - resonance frequency of the sample oscillations after the corrosion test);

ω - resonance frequency of the sample oscillations before corrosion.

The wire samples were used in internal friction measurements by the method of damping of free torsional oscillations for frequencies of the order of 1 cps. The RKF-MIS apparatus was used for this purpose (8). The logarithmic decrement of damping was taken as a quantitative characteristic of internal friction. Calculations were carried out on the basis of formula

$$Q^{-1} = \frac{\ln n}{\pi N}, \qquad (3)$$

where $n = \frac{a_1}{N}$

a_1 - initial amplitude of oscillations;

a_N - amplitude after N oscillations;

N - number of oscillations required to change the amplitude by n times.

Ratio $\frac{a_1}{a_N}$ was preset and adopted as equal to 1.5 and 2.0. The measurements consisted in the counting of the number of oscillations N required to change the amplitude by a given value.

Taken as corrosion indices were the changes in all the measured sample characteristics, resulting from corrosion, expressed in percentages of the respective values before corrosion. Thus, the rise in resistivity was expressed by ratio

$$K_R = \frac{\Delta R}{R} \cdot 100, \qquad (4)$$

where $\Delta R = R_1 - R$ (R_1 - resistivity of the sample after the corrosion test;

R - resistivity of the sample before the test).

The other indices were calculated in a similar way. The test results are recorded in Table 2 and Figure 2.

The measurements have shown that in the process of intercrystalline corrosion internal friction rises, the resonance oscillation frequency decreases, the modulus of elasticity, calculated from the resonance frequencies, diminishes as well. The changes in resistivity, resonance frequency, and hardness are close to each other. The growth of internal friction is several times higher than the changes affecting the other characteristics. For example, after a 20-min. hold in boiling $CuSO_4 + H_2SO_4$ solution the internal friction of tempered 1Kh18N9 steel samples increased five times, while electric resistivity rose only by a factor of 1.5.

Internal friction and resonance oscillation frequency measurements revealed that the susceptibility of steel to intercrystalline corrosion increases with growing carbon contents (low-carbon steel, 0Kh18N9, 1Kh18N9, 2Kh18N9). Introduction of titanium (steel 1Kh18N9T) increases the resistance of steel to intercrystalline breakdown. Quenching of steel 1Kh18N9 from 1080-1100° does not provoke a tendency towards development of intercrystalline corrosion,

Figure 2. Variation of internal friction (1), electric resistivity (2), and resonance oscillation frequency (3), in percentages, as a function of the time during which the samples were held in boiling $CuSO_4 + H_2SO_4$ solution

(heat treatment of steel: hardening and temper at 650°): a - steel 2Kh18N9; b - 1Kh18N9; c - 0Kh18N9; d - low-carbon steel with 0.018% C; e - Kh23N23M3D3.
1) Variation of the corrosion indices.

Table 2.

Changes in the Various Corrosion Indices of Plate-samples of Chrome-Nickel Steels after Tests in Boiling $CuSO_4 + H_2SO_4$ Solution.

Grade of Steel	Heat Treatment	Corrosion time, hrs.	Growth of internal friction %	Frequency decrease %	Growth of Resistivity, %	Reduction in strength, %	Decrease of the modulus of elasticity, %
Low carbon 1	Hardening and tempering at 650°						
Low carbon 2	Same						
	"						
	"						
	"						
	"						
	Hardening						

whereas a 2-hour temper followed by corrosive treatment at 650° causes intergranular decay. These results were confirmed by measurements of resistivity and strength (see Table 2 and Fig. 2) and correspond to the published data on the effects of studied factors upon intercrystalline corrosion. The corrosion resistance of steel Kh23N23M3D3 is higher than that of steel 0Kh18N9, but lower than the resistance of low-carbon steel.

Analogous tests were carried out with wire samples of steels 1Kh18N9 and 2Kh18N9. Corrosion resistance of steel was evaluated on the basis of internal friction variation, measured by the damping of free torsional oscillations, and on the basis of natural oscillation frequency and electric resistivity changes after corrosive treatment in boiling $CuSO_4 + H_2SO_4$ solution. The results of these determinations are given in Table 3 and Figure 3.

Table 3.

Variation of Internal Friction, Free Oscillation Frequency, and Resistivity of Wire Samples as a Result of Corrosion in a Boiling $CuSO_4 + H_2SO_4$ solution.

Grade of Steel	Heat Treatment	Corrosion time, h.	Growth of Internal Friction %	Frequency decrease, %	Growth of electric resistivity, %
1Kh18N9	Hardening				
1Kh18N9	Hardening and tempering at 650°				
2Kh18N9	Same				

The test results show that tempering is conducive to intercrystalline breakdown in 1Kh18N9 and 2Kh18N9 steels. Increased carbon contents augments intercrystalline corrosion. As in the case of tests with plate-samples, the variation of internal friction exceeds the change in the frequency of free oscillations and electric resistivity.

On the basis of the results obtained a conclusion may be drawn to the effect that, regardless of the method of measurement, internal friction and the

frequency of natural oscillations of the samples (the resonance frequency of induced oscillations and the frequency of free oscillations) as well as electric resistivity provide a quantitative characteristic of intercrystalline corrosion.

Of all the investigated characteristics of corrosion, internal friction is the most sensitive and may be especially useful in revealing minor intergranular decay. Of the two utilized methods of internal friction measurement in steel, for purposes of detecting intercrystalline corrosion, the more convenient is the method of induced oscillations which make it possible to use smaller samples and to take measurements of both plate and wire specimens.

Figure 3. Variation of different corrosion indices (%) of wire samples of steel 2Kh18N9 (a) and 1Kh18N9 (b) as a function of the holding time in boiling $CuSO_4 + H_2SO_4$ solution (heat treatment of steel: hardening and tempering at 650°):
1 - internal friction variation;
2 - electric resistivity variation;
3 - variation of the frequency of free oscillations.
a) Variation of corrosion indices, %.

To explore the possibilities of new procedures for intercrystalline corrosion determination, in additon to tests in sulfuric acid solution $CuSO_4$, corrosion resistance of tempered 1Kh18N9 steel (plate samples) was tested in nitric acid liquors, capable of promoting intercrystalline corrosion. Tests were carried out in boiling 55% solution of HNO_3, in 20% HNO_3 solution containing 1% NaF, and in a 5% HNO_3 solution containing 1.5% $FeCl_3$, at 19-21° temperatures. Corrosion resistance of steel was determined on the basis of the changes in internal friction (measured by the method of induced oscillations) in the resonance frequency of oscillations, and in electric resistivity, resulting after corrosion. Moreover, the losses of samples in weight were also determined. The test results are given in Table 4 and Figure 4.

In the case of tempered 1Kh18N9 steel the changes in electric resistivity and the resonance frequency of oscillations after treatment in all the above solutions showed close values (Table 4, Fig. 4).

An increase in the duration of the corrosion tests results in greater changes of these characteristics. The growth of internal friction, resulting from steel corrosion in solutions with HNO_3, constitutes a more complex function of the corrosion time. The curves of internal friction variation display a maximum. Such character of the curves should be attributed to the fact that the corrosion of steel in solutions containing HNO_3 is accompanied by losses in weight (see Table 4). Internal friction undergoes practically no change in the process of general corrosion, but increases as a result of intercrystalline corrosion. In view of this, the curves of internal friction

Table 4.

Variation of Corrosion Characteristics after Holding of Steel 1Kh18N9 Samples in Different Corrosive Media

Corrosive Medium	Time of corrosion h.-min.	Losses in Weight %	Growth of Internal friction %	Frequency decrease %	Growth of electric resistivity, %
Boiling $CuSO_4$ + H_2SO_4 solution					
20% HNO_3 & 1% NAF, 20°					
Boiling 5% HNO_3 solution					
5% HNO_3 & 1.5% $FeCl_3$, 20°					

variation in the process of both types of corrosion, depending on the velocity ratio, may have different shapes as schematically represented in Figure 5. Curve а-б (Fig. 5) represents the variation of internal friction in the absence of general corrosion, or in the case of an insignificant rate in comparison with the rate of intercrystalline corrosion. Such nature of the curves is to be observed in connection with steel corrosion in sulfuric acid solution $CuSO_4$ (see Fig. 4, curve 1-а). If the rate of intercrystalline corrosion exceeds that of general corrosion, but the latter manifests an increase with time, the internal friction variation will be characterized by curve а-в. The rates of both types of corrosion are equal at point в. If their equality is maintained past point в, the pattern of internal friction variation will follow the straight line в-г. If the rate of general corrosion

Figure 4. Variation of internal friction (1), electric resistivity (2), and resonance oscillation frequency (3) of 1Kh18N9 steel samples as a function of the time they were held in different corrosive media (heat treatment of steel: hardening and tempering at 650°).
а - boiling $CuSO_4 + H_2SO_4$ solution; б- 20% HNO_3 + 1% NaF, 20°; в - boiling 55% HNO_3; г - 5% HNO_3 + 1.5% $FeCl_3$, 20°.
1) Variation of corrosion indices, %; 2) 2 h. 3 min.

exceeds the speed of intercrystalline corrosion, internal friction variation will proceed along curve в-д. Point д characterizes the absence of intergranular decay (intercrystalline breakdown). In the case of corrosion in solutions containing HNO_3 (see Fig. 4, curves 1-б, 1-в, 1-г), internal friction changes in accordance with curve а-в-д (see Fig. 5). A study of

the corrosion resistance of 1Kh18N9 steel in different solutions showed that the increase of internal friction is brought about by intercrystalline corrosion, whereas the variation of resonance oscillation frequency and electric resistivity occurs as a result of both the intercrystalline and general corrosions.

Figure 5. Variation of internal friction during simultaneous development of general and intercrystalline corrosions:
а - б - rate of general corrosion is insignificant; а-в - the rate of intercrystalline corrosion (K_M) is greater than the depth index of general corrosion (K_0); в - г - $K_M = K_0$; в - д - $K_M < K_0$; д - absence of destruction along the grain boundaries.
1) Variation of internal friction;
2) Time of corrosion.

Measurement of internal friction permitted us to establish the difference in the nature of intercrystalline corrosion in sulfuric acid solution $CuSO_4$ and in solutions containing HNO_3. Photomicrographs (Fig. 6) and the exterior of the samples of several grades of steel (of the Kh18N9-type) confirm the different mechanism of corrosion in the solutions used in the tests. In $CuSO_4 + H_2SO_4$ solution corrosion proceeds along the weakest boundaries of the metal, and the most active, narrow boundary zone is attacked by it. In boiling HNO_3 and in 20% solution of HNO_3, containing 1% NaF corrosion, begins along the grain boundaries and then attacks the less weakened sections of the grain within the boundaries. This is attributable to the "slit effect" - a decline in the oxidizing power of the solution in the intergranular zone, due to partial consumption of acid in the process of boundary metal dissolution, and the difficulty with which mixing proceeds in the narrow intergranular slit; normally the mixing process would have contributed to the restoration of the solution. The metal grain located on the surface, evidently, constitutes a microcell.

Its cathode is formed by the outer side of the crystal, contiguous to the initial solution of 55% or 20% HNO_3 and 1% NaF, while the inner side, which is in contact with the solution contained in the intergranular slit, constitutes its anode. In view of the intensified corrosion along the grain boundaries a part of the crystals dissolves and a part of them breaks up. Thus the weight losses of the samples are made up of dissolved grains (mostly from the inner side) and those chipped off.

The curves of internal friction variation for solutions, which cause the metal to suffer losses in weight, have a maximum (see Fig. 4); in view of this, the time of corrosion tests conducted in these solutions should be limited, if internal friction is to be used as a criterion of intercrystalline corrosion.

Measurements and comparisons of internal friction resonance frequency of oscillations, and resistivity, were used to test the method [recommended in literature (9)] of accelerated testing of steel for intercrystalline corrosion in a boiling solution of $CuSO_4$ and H_2SO_4, while the sample is in contact with copper shavings. Determinations of corrosion resistance of 1Kh18N9 steel after a 2-hour temper at 700° were made in the following two ways: in boiling $CuSO_4$ + H_2SO_4 solution of standard concentration (110 g $CuSO_4 \cdot 5H_2O$ and 55 cm^3 concentrated H_2SO_4) while keeping the samples in contact with copper shavings placed in the solution, and in the same solution without shavings. A change in all characteristics (Fig. 7) showed that contact with copper shavings reduces by 3-4 times the test time required for intercrystalline breakdown in 1Kh18N9 steel to set in. The shape of the internal friction curves in both cases is the same. As in all other tests, the growth of internal friction exceeded the changes involving all other characteristics.

CONCLUSIONS

1. Internal friction and the frequency of natural oscillations constitute quantitative characteristics of intergranular breakdown. Internal friction is a more sensitive indicator of intercrystalline corrosion than the other

Figure 6. Photomicrographs of unetched microsections after testing in $CuSO_4 + H_2SO_4$ solution(c), in 20% HNO_3 + 1% NaF (a) and in boiling 55% HNO_3(b). X 188.

Figure 7. Variation of internal friction (1) and resistivity (2) after tests of 1Kh18N9 steel in $CuSO_4 + H_2SO_4$ solution with copper shavings (a) and without them (b). Heat treatment of steel: hardening and tempering at 700°C. 1)Variation of internal friction $\frac{\Delta Q^{-1}}{Q^{-1}} \cdot 100$ and resistivity $\frac{\Delta R}{R} \cdot 100$, %

known corrosion characteristics.

2. Utilization of internal friction as a criterion of intercrystalline corrosion enables the time of corrosion tests to be shortened. It is particularly useful for determining minor intergranular destruction and also in the cases, when it is impossible to apply other methods to reveal intercrystalline corrosion.

3. Internal friction variation characterizes only intercrystalline corrosion, while the variations of electric resistivity and of the natural oscillation frequency reflect the total effect of the general and intercrystalline corrosions.

4. Of the two utilized methods of measuring internal friction in steel with a view to revealing intercrystalline corrosion, the more convenient is the method of induced oscillations. Smaller samples, both in the form of plates and wire, may be used in such tests.

5. It was established that the mechanism of intercrystalline breakdown of steel is different in boiling $CuSO_4 + H_2SO_4$ solution and in solutions containing HNO_3 (boiling 55% HNO_3 and 20% HNO_3 + 1% NaF). It is the narrow intercrystalline zone of the weakest boundaries that corrodes in $CuSO_4 + H_2SO_4$. In solutions with HNO_3, on the other hand, it is the grain in the intercrystalline region that is subjected to an intensified attack which leads to the chipping and dissolution of the metal grains.

REFERENCES

1. J. J. Rutherford, R. Aborn, Transactions of the American Institute of Mining and Metallurgical Engineering, 1939, 100, 293.

2. I. A. Levin, A. A. Babakov, Z. V. Lyutova, Vestnik inzhenerov i tekhnikov [Herald of Engineers and Technicians], 1950, No. 2, 66.

3. V. Sh. Shekhtman, M. A. Vedeneyev, N. P. Zhuk, ZhFKh [Journal of Physical Chemistry], 1954, 28, 2199.

4. R. Förster, W. Köster, Zeitschrift für Metallkunde, 1937, 29, 116.

5. Masio A. Ferry, Ref. Journal of the Iron and Steel Institute, 1952, 172, 459.

6. M. A. Vedeneyeva, A. V. Panov, N. D. Tomashov, Zavodskaya laboratoriya [Plant Laboratory], 1957, No. 1.

7. K. Zener, Sb. Uprugost' i neuprugost' metallov [Elasticity and Non-Elasticity of Metals], IL, 1954.

8. V. S. Postnikov, Yu. V. Piguzov, Pribor typa RKF-MIS dlya opredeleniya modulya sdviga i vnutrennego treniya provolochnykh obraztsov,

/Apparatus of the RFD-MIS-type for Determination of the Modulus of Rigidity and Internal Friction of Wire Samples/, ITEIN AN SSSR, No. P8, 55-448, Moscow, 1955.

9. E. Brauns, G. Pier, Stahl und Eisen, 1955, No. 9, 579.

Academician N. T. GUDTSOV, Engineer R. I. TRUBETSKOVA,
Candidate of Technical Sciences M. L. BERNSHTEYN.
Department of Metallography and Heat Treatment.

EFFECT OF SMALL ADDITIONS OF BORON, CALCIUM, NIOBIUM, ZIRCONIUM, AND CERIUM ON THE STRUCTURE AND PROPERTIES OF A HIGH-NICKEL HEAT-RESISTANT ALLOY

The development and use of heat-resistant alloys based on nickel, as well as of high-nickel austenitic steels, involves considerable difficulties, arising during deformation processing of these steels. In order to improve the deformability of alloys it was proposed (1-4) to add alkali- and rare-earth elements to them. Defined also was the contents of the additions to be introduced into these alloys depending on the percentage of nickel contained in the latter. At the present time it has become a well established practice in metallurgy abroad to add alkali- and rare-earth elements to improve the processes of hot mechanical working of heat-resistant alloys, including the 18-8 type steels.

No sufficiently conclusive substantiation of the effect produced by small additions on the improvement of deformability of high-nickel heat-resistant steel and alloys can be found in the literature. Yet, on the basis of studies (5, 6) it is possible to associate the influence of additions with a reduction of the harmful effects of impurities such as sulfur, antimony, arsenic, and lead, for example. It has been established that the presence of even negligible amounts of sulfur, antimony, and arsenic results in an appreciable reduction of heat resistance, as well as in a sharp deterioration of the deformability of high-nickel steels and alloys. This impairment of properties is related to the formation of readily fusible boundary films and particles which represent compounds of nickel with sulfur, lead, arsenic, and antimony. The melting and softening of these films and the disengagement of the grains, which, evidently take place in the process of heating, bring about a sharp deterioration of deformability and heat resistance.

Additions of alkali- and rare-earth elements evidently exert an influence

on the compounding of nickel with the harmful admixtures referred to above. This is indirectly evidenced by the relationship existing between the contents of nickel and the quantity of the added element which tends to improve the heat resistance and deformability of alloys. It should also be borne in mind that by virtue of their character alkali- and rare-earth elements are surface-active. Consequently, in settling themselves in high-nickel alloys and steel at the grain boundaries, these additions affect both the characteristics of the boundaries and the nature of the boundary phases.

However, the mechanism of the influence exerted by minor additions upon the properties of high-nickel steels and alloys is not, apparently, confined only to their refining action (reduction of the harmful effect of sulfur, arsenic, antimony, and lead). It is possible that there also occurs a change in the conditions of crystallization from the liquid state, a change in the boundary energy, the formation of specific phases or boundary solid solutions, and many other phenomena attributable to the presence of small additions in a high-nickel alloy.

In view of the fact that these aspects have so far been insufficiently studied, and because high-nickel steels and alloys acquire an ever growing significance in industry, an investigation was carried out to define the effect of minor additions on the structure and properties of a deformable high-nickel austenitic alloy.

A chromium-nickel austenitic alloy of the 36KhTYu type was selected as the object of this investigation. A study was made of the effect of additions of boron (0.005%), calcium (0.1%), niobium (0.5%), zirconium (0.2%), and cerium (0.01%). The alloys were melted in a high-frequency induction furnace of 55 kg capacity. Small quantities of boron, calcium, zirconium, and cerium were added by introducing correspondingly calculated amounts of ferroboron, metallic calcium, zirconium-silicon, and ferrocerium after final deoxidation of the metal by calcium-silicon. Niobium was introduced into the heat by

feeding ferroniobium, after ferrochromium, into the charge under the slag.

The metal was top-poured into ten-kilogram cast iron molds without feeder heads. Metal from each heat was teemed into six molds. To cause the ingots to solidify at varying rates, the metal was poured under different conditions: two ingots were cast in preheated molds set in hot sand; two molds were filled in ordinary shop conditions; and, finally, the remaining two ingots were cast in molds cooled by water. The consumption of cooling water was so controlled as to assure that the temperature of the outflowing water should not exceed 20°.

Thus, each heat yielded three pairs of ingots with the metal of each pair cooled at a different rate while solidifying in the molds: slowed-down, normal, and accelerated rates. The hotter metal, at the beginning of pouring, was teemed into the preheated molds embedded in hot sand. The cooler metal, at the end of tapping, was used to fill the water-cooled molds.

The temperature of the liquid metal both in the ladle and in the molds was measured by means of tungsten-molybdenum thermocouples of the TsNIIChM-1 type (Central Scientific-Research Institute of Ferrous Metallurgy). A number of ingots of the test heats were cut along the axis, and macrosections were subsequently prepared on the longitudinal templates. The macrosections were treated by etchant consisting of 1 liter distilled water, 1 liter muriatic acid, 50 grams potassium bichromate, and 0.1 liter nitric acid. After the template has been etched for 20 min. at a temperature of 60-70°, the section was washed by acid solution (50 g potassium bichromate and 0.1 liter sulfuric acid per 1 liter distilled water) and then by hot water, whereupon it was thoroughly dried.

The remaining ingots were forged into 12, 16, and 18-mm dia. rods, from which samples were prepared for creep tests and for a study of the aging process by the method of hardness and electric resistivity measurements.

The resistivity of alloys was measured during heating to 1200° and during

cooling by the compensation method on a potentiometric unit. The heating and cooling rates amounted to 3 degrees per minute. Resistivity measurements were taken for every 25° from samples previously water-quenched from 1200°.

The macrostructure of the longitudinal templates of a number of ingots is shown in Figures 1-6.

The different rates of crystallization were determined by the variation of the temperature of teeming and by the degree of the mold cooling in the process of metal solidification. A reduction in the temperature of the liquid metal, prior to teeming, from 1550 to 1410° coupled with a simultaneous intensification of the mold cooling (by water) leads to a more pronounced drop in the temperature of the solidifying metal (Fig. 7). Qualitatively, a confirmation of such growth of the crystallization rate is provided by the macrostructure of the ingots.

An increase in the crystallization rate of an alloy, containing no minor additives, is conducive to a shrinkage of the zone of acicular crystals and to a general diminution (refinement) of the crystallites, in particular, their equiaxial variety in the central part of the ingot (see Fig. 1).

An addition of boron entails a considerable fragmentation of the crystallites at all cooling rates during the solidification of metal. The effect of boron is particularly pronounced at high crystallization rates (see Fig. 2-c).

The effect of calcium on the fragmentation of primary crystallites is not as potent as that of boron (see Fig. 3). No difference at all was to be observed between the structure in question and that of an alloy without any additions (Fig. 1-a) in the case of pouring into hot molds. It can be confidently stated that the fragmentation of the crystallites under the influence of calcium takes place only when crystallization proceeds at a very high rate (see Figs. 1-c and 3-c).

A substantial change is to be registered in the macrostructure of ingots after additions of niobium (0.5%) and zirconium (0.2%) - Figures 4 and 5. The

Figure 1. Macrostructure of the longitudinal ingot sections of an alloy without additions:
a - ingot cast in a preheated mold embedded in hot sand;
b - ingot cast in a mold under normal shop conditions;
c - ingot cast in a water-cooled mold.

effect of crystallization rates is somewhat leveled down as a result of the considerable fragmentation of crystallites in all ingots.

The greatest influence on the diminution of the size of crystallites was produced by cerium (see Fig. 6), particularly so in the case of a high rate of crystallization (Fig. 6-b).

The kinetics of the aging process were studied on disks prepared from the forged rods, after they were quenched from 1200°, held for 1 hour, and cooled in water. The curves of hardness variation as a function of holding time at aging temperature are shown in Figure 8.

Aging at 700° (Fig. 8-a) caused the hardness to increase in all investigated alloys. The tendency to age turned out to be independent from the rate

Figure 2. Macrostructure of the longitudinal ingot sections of alloy with an addition of 0.005% of boron: a - ingot cast in a preheated mold embedded in hot sand; b - ingot cast in a mold under normal shop conditions; c - ingot cast in a watercooled mold.

of crystallization: the curves are located approximately within the same interval of hardness values both for the case of metal poured into a hot, sand-protected, mold, and for the case of normal teeming. A similar result is to be registered in consequence of pouring into a water-cooled mold. It should be noted that alloys which contain small additions manifest a greater rise in hardness after aging than the initial alloy which was free from such additions. A particularly high degree of hardening was observed in the alloy with 0.5% Nb. Moreover, if a certain decline in hardness is to be registered in the initial alloy after prolonged holds (100 hours), then small additions, particularly those of niobium and boron, cause the alloy to maintain its hardness at the same value during prolonged heating at 700°.

The favorable effect of minor additions on the hardening of type N36KhTYu

Figure 3. Macrostructure of the longitudinal ingot sections of alloy with an addition of 0.1% Ca:
a - ingot cast in a preheated mold embedded in hot sand;
b - ingot cast in a mold under normal shop conditions;
c - ingot cast in a water-cooled mold.

alloys in the process of aging was equally well displayed at a temperature of 750° (see Fig. 8-b). In this case, too, particularly noticeable is the high hardness value of the niobium-containing alloy. An increased hardness value was also displayed in heats containing 0.005% B and 0.2% Zr. The alloy without additions in all cases was conspicuous for having the lowest hardness values. In considering the shapes of the curves reflecting aging at 750°, one should note a certain stabilization of the hardness values after as much as one hour of holding, and a noticeable decline in hardness after a holding time of 25 hours. These curves have a considerably different shape than those for 700° aging which reflect an almost steady growth of hardness. A certain amount of softening observable in the alloys under review after 25-hour holding

Figure 4. Macrostructure of the longitudinal ingot sections of alloy with an addition of 0.5% Nb:

a - ingot cast in a preheated mold embedded in hot sand;
b - ingot cast in a mold under normal shop conditions;
c - ingot cast in a water-cooled mold.

(at 750°) is mostly inherent to the alloy without any additions, and least of all characteristic for the niobium-containing alloy.

Characteristic for aging at 800° (see Fig. 8-c) is the rapid growth of hardness which attains the maximum after a holding time of but one hour. Thereafter the alloy begins to soften. A steady decline in hardness is to be subsequently observed, until after a hold of 100 hours a value is reached approaching that of quenched samples. One might say that at this temperature the alloy is insufficiently heat-resistant. Small additions of niobium, boron, calcium, zirconium, and cerium do not affect the general trend of the curves and they run sufficiently close to each other, especially when the holding

Figure 5. Macrostructure of the longitudinal ingot sections of alloy with an addition of 0.2% Zr:

a - ingot cast in a preheated mold embedded in hot sand;
b - ingot cast in a mold under normal shop conditions;
c - ingot cast in a water-cooled mold.

time is short. The beneficial influence of small additions on the resistance to hardness drops in the process of reheating is manifested during very long periods of holding (50-100 hours).

Represented in Figure 8-d are the aging curves for 850°. It is obvious that this temperature is too high to bring the alloy into a hardened state as a result of reheating after hardening. Even after an exposure for one hour the high values of hardness, as obtained in aging at 700-800°, cannot be attained. The curves for 850° reveal the fact that the positive effect of small additions -- which impart an increased hardness to the alloy for any length of holding in the process of heating to 850° -- is particularly clearly

Figure 6. Macrostructure of the longitudinal ingot sections of alloy with an addition of 0.01% Ce:
a - ingot cast in a preheated mold embedded in hot sand;
b - ingot cast in a mold under normal shop conditions;
c - ingot cast in a water-cooled mold.

Figure 7. Curves of metal cooling in molds:
a - metal poured at 1550° into a preheated mold embedded in hot sand; b - metal poured into a mold under normal shop conditions;
c - metal poured at 1410° into a water-cooled mold.
1) Temperature, °C; 2) Time, sec.

manifested in the softened state. And in this case, too, the highest resistance to a decline in hardness is exhibited by the alloy containing an addition of niobium, and also of boron, and zirconium.

Alloys which contain small additions, particularly those of niobium,

boron and zirconium, disclose a higher tendency to hardening during aging and a higher resistance to softening in the process of prolonged exposure to the aging temperature, than the alloy without additions (Fig. 9). Moreover, an increase in the aging time involves a shifting of the hardness peak towards lower temperatures. However, the position of the curves characterizing the hardening influence of the small additions remains unchanged.

The results of resistivity measurements of the alloys are recorded in Figures 10 and 11. Measurements were taken during continuous heating at a rate of 3 degrees per minute from 400 to 1200°. The shape of the curves reflects the progress of the aging process in the investigated alloys. Thus, a slow down in resistivity growth is to be observed about 600° temperature, and an almost horizontal "plateau" forms thereafter extending approximately to 900°. Beyond this temperature resistivity again resumes its normal growth under the influence of rising temperature. The "plateau" which is to be observed in the curves is to be ascribed to a simultaneous development of two processes in the alloy during heating: a) a drop of electric resistivity caused by disintegration of the solid solution and separation of the hardening phase particles within the temperature range 600-900°, and b) a growth of resistivity due to a positive temperature coefficient. The combination of these two processes is actually responsible for the formation of an almost horizontal "plateau".

The separation of the particles of the hardening phase practically comes to an end at 850-900°. As heating continues to a higher temperature, when the phase begins to coagulate and dissolve, a growth of resistivity is to be registered again. This branch of the curve shows a steeper trend than the original section up to the "plateau". This is attributable to an enrichment of the solid solution by alloying elements in consequence of the dissociation of the hardening phases.

Figure 8. Hardness of hardened alloys after aging at different temperatures as a function of holding time:

a - aging temperature 700°; b - 750°, c - 800°, d - 850°.

1) Hardness, H_V; 2) Initial; 3) Without additions; 4) Time lg τ, hours.

Figure 9. Hardness of hardened alloys after reheating up to 700-850°.

a - heating for 1 hour; b - for 5 hours; c - for 15 hours; d - for 100 hours.

1) Temperature, °C.

Figure 10. Resistivity curves for alloys without additions (a) and with additions of 0.005% B (b), 0.5% Nb (c), 0.01% Ce (d).

1) Variation of resistivity $\frac{R_t - R_o}{R_o}$ 100%

2) Cooling; 3) Heating; 4) Temperature, °C.

Figure 11. Resistivity curves for alloys without additions (a) and with additions of 0.1% Ca (b), and 0.2% Zr (c).

1) Variation of resistivity $\frac{R_t - R_o}{R_o}$ 100%

2) Cooling; 3) Heating; 4) Temperature °C.

At the beginning of the cooling process a smooth decline in electric resistivity is to be observed, and then, in the 800-750° range, a jump (kink) appears on the curve. Further cooling is accompanied by a drop of resistivity. Yet this branch manifests a steeper descent than the one reflecting the initial period of cooling. The appearance of a kink (jump) at 800-750° on the curve of resistivity variation may be explained by the precipitation of the hardening phase particles. As shown by dilatometric analysis, this process is accompanied by a considerable volume effect and, consequently, also by the development of internal stresses with the formation of the hardening phase particles in the solid solution. The stresses actually cause the appearance of the resistivity jump, while the additional precipitation of the hardening phase particles, which continues in the process of further cooling, leads to a drop of resistivity (the steeper branch of the curve) more intensive than that which characterized the cooling of the solid solution (the curve branch covering the temperatures above the kink).

In comparing the resistivity variation curves, the following may be observed: a) the resistivity of alloys with minor additions is always slightly higher than that of the unadulterated alloy; b) the "plateau" and the "kinks", which characterize the process of precipitation of the dispersed hardening phase, are more sharply defined on the curves of the alloys with additions; c) the plateau on the heating curves for alloys with additions has a somewhat larger stretch and is shifted in the direction of higher temperatures than in the case of unadulterated alloys without additions. This fact is directly connected with greater stability and a lesser tendency towards coagulation of the hardening phase in alloys with additions. This is also confirmed by the data referred to above on the variation of hardness.

Figure 12 shows the curves of resistivity variation for the alloy of initial composition (without additions) during heating of samples made from rods, which were forged from ingots subjected to different cooling conditions

in the process of crystallization. It might have been assumed that hot mechanical working should have leveled out any difference in the macrostructure of alloys crystallized in molds cooled by water, in the air, or in sand. However, a coincidence of the curves is to be noted only in the case of cooling in air and in sand, while the results of water cooling are characterized by a higher position of the curve. The samples forged from ingots crystallized at an increased rate are distinguished by a particularly fine-grained structure. It is obviously in them, therefore, that the processes of aging -- which proceed mainly along the grain boundaries -- develop more intensively; in this connection, it is understood that quenching from 1200° must have brought about a total saturation of the solid solution by the alloying elements, without affecting thereby the relatively finer grain.

Figure 12. Variation of resistivity for the unadulterated alloy during continuous heating and cooling:
a - ingot cast in preheated mold embedded in hot sand; b - ingot cast in a mold under normal shop conditions; c - ingot cast in a water-cooled mold.
1) Variation of resistivity; 2) Cooling; 3) Heating; 4) Temperature, °C.

The results of creep tests are given in Figure 13. These tests are still being continued. In particular, experiments are conducted with samples of the alloy containing niobium. It may be concluded that small additions entail an increase in creep resistance, especially at the initial stage.

Figure 13. Creep curves for alloys containing small additions.
1) Alloy without additions; 2) Deformation, mm;
3) Time, hours.

The mutual arrangement of the elements according to their hardening action justifies the assumption that the main reason for the growth of creep resistance is the refining effect produced by the small additions, particularly the refining of the grain boundaries which play an important role in resisting creep at the initial stage. Obviously, it is from this point of view -- of the greater or lesser manifestation of the horophility of the small additions -- that one should consider the influence of the cooling rates during crystalllization upon creep resistance (Fig. 14). A definite size of the grain and a cooling rate, corresponding to the concrete conditions of crystallization, are evidently related to the optimum distribution of the small

additions along the grain boundaries and to their most favorable refining effect, both of which lead to an increase in creep resistance at the initial stage.

Figure 14. Creep versus crystallization rate curves for the alloys:
(a) and (a') - ingots of alloys without and with boron addition, respectively, cast in heated molds embedded in hot sand; (b) and (b') - ingots of alloys without and with boron addition, respectively, cast in a mold under normal shop conditions; (c) and (c') - ingots of alloys without and with boron addition, respectively, cast in a water-cooled mold.
1) Deformation, mm; 2) Time, hours.

CONCLUSIONS

1. A study was made of the effect of small additions of boron (0.005%), calcium (0.1%), niobium (0.5%), zirconium (0.2%), and cerium (0.01%) on the microstructure of cast chrome-nickel heat-resistant austenitic alloys of the N36KhTYu type.

It was established that under all conditions of crystallization (molds were cooled by water, in the air, and in sand) small additions of the above elements lead to a considerable fragmentation of the crystallites in the cast metal and to a shrinkage of the zone of acicular crystals. The highest effect in producing such a change in the macrostructure is exerted by cerium, then by zirconium, boron, niobium, and calcium.

2. The kinetics of aging at 700-850° after previous quenching from 1200° in water was studied on forged samples. Aging at 700° leads to a steady growth of hardness in all the investigated alloys, with those containing small additions revealing a greater degree of hardening in the process of aging than the initial unadulterated alloy.

The usual curves with a maximum were registered for aging at 750°, indicating that during relatively prolonged holdings there develops a process of softening, which is mainly associated with the coagulation of the particles of the hardening phase. However, in this case as well, the beneficial effect of small additions on the hardening of the type N36KhTYu alloy is clearly manifested; the alloys with additions turn out to be more resistant to softening than the initial alloy.

The kinetics of the hardness changes in the process of aging at 800 and 850° demonstrate that these temperatures prove to be too high to cause the formation of a hardened state during reheating after quenching. Although the investigated alloys are in general insufficiently heat-resistant at these temperatures, the favorable influence of small additions on the resistance to loss of hardness during protracted aging is, nevertheless, particularly strongly manifested in the softened state.

At all investigated temperatures and for all aging periods the highest hardness values were to be registered in alloys containing additions of niobium, and of boron and zirconium.

3. A study of electric resistivity variation during continuous heating up to 1200° confirmed the fact that the alloys with small additions reveal an increased tendency to aging, and that the particles of the hardening phase precipitated in these alloys are less prone to coagulate than in the case of the unadulterated initial alloy.

4. The results of creep tests (for the initial stage of creep) have shown that small additions result in a growth of heat resistance. The main reason for the increase of creep resistance is evidently the refining effect of the small additions, particularly, the refining of the grain boundaries which play an important role in creep resistance at the initial stage.

REFERENCES

1. Iron Age, 1955, v. 176, No. 23, p. 139-142.
2. Journal of Metals, 1950, v. 188, No. 9, p. 1139-1143.
3. L'Industrie Chimique, 1955, v. 42, No. 433, p. 139.
4. Schweizerische Technische Zeitschrift, 1952, Bd. 49, No. 47, S. 652.
5. M. V. Pridantsev and G. V. Estulin, Stal' [Steel], 1957, No. 5.
6. F. F. Khimushin et al., Struktura i svoystva splava E1437 [Structure and Properties of Alloy E1437], Oborongiz, 1955.

Cand. of Tech. Sc. M. L. BERNSTEYN, Eng. Z. V. SVISTUNOVA.
Department of Metallography and Heat Treatment.

EFFECT OF COLD WORKING ON THE STRUCTURE AND PROPERTIES OF NICKEL-CHROME HEAT-RESISTANT ALLOY EI437

Paper submitted by Professor Doctor of Techn. Sciences I. N. Kidin.

Strain hardening -- involving an accumulation of part of the strain energy in the worked body -- results in a change of the structure and properties of metals and alloys in the metastable state. As shown by research in recent years (1, 2, 3), cold working involves the development not only of non-diffusional transformations, but also of those based on the diffusion migration of atoms.

The accelerating effect of cold working on the aging of austenitic heat-resistant iron-based alloys was studied in detail on alloys of the 18-8 type (4, 5) and 16-25-6 type (6, 7).

During the last decade heat-resistant alloys based on nickel found wide use in industry. Yet, the influence of cold working on the structure and properties of these alloys is still insufficiently explored. The available limited studies (8) pertain to minor degrees of volume (three-dimensional) deformations, not exceeding 10-15%. Moreover, the principal attention was devoted to surface peening.

As shown in our research (9), stresses produce a substantial effect on the processes developing in the nickel-chrome heat-resistant alloy of the EI437 type.

We have made a study of the effect of cold working with 5, 25, 50, and 75% reduction on the processes of internal transformations and the properties of nickel-chrome EI437 alloy of following composition: 0.075% C, 0.22% Mn, 0.47% Si, 0.0047% S, 0.009% P, 20.52% Cr, 0.04% Ce, 2.62% Ti, 0.56% Al, 0.02% Cu, 0.01% Fe. Strain hardening was produced by two forms of cold working:

rolling and drawing.

After heating to 1080° and holding at this temperature for a period of 8 hours, the samples were cooled by three methods: in water, in air, and with the furnace at a rate of 125° per hour in the 1080-700° temperature range, and then to 500° at a rate of 40-50° per hour. After hardening the stock was subjected to cold working.

The comparatively small degrees of reduction (5 and 25%) made it possible to study the general character of the cold work effect on the change of structure and properties of the alloy. The higher degree of reduction (50 and 75%) involved the formation of a texture, and this presented a special interest mainly at a later stage of the inquiry into the properties of the alloy. It was demonstrated (10) that a definite relationship exists between the nature of the stressed condition during testing (or use) of an alloy and its texture. This relationship, naturally, stems from the mutual orientation of the maximum tangential stresses and the eased slip planes.

A uniform direction of the eased slip planes may be created by "texturizing", as a result of which a polycrystalline body may be likened to a pseudo-monocrystal differing in the first approximation from a normal monocrystal by the presence of boundaries between similarly oriented grains. It is evident that, depending on the character of the given stress, such orientation of the sample (or part) should be selected as would assure the largest possible angle between the direction of the maximum tangential stresses and the planes of the readiest slip. A rise in resistance to plastic deformation will naturally take place in this case.

Depending on the type of cold working, different textures (axial or perfect and limited), as well as a different orientation of planes in the body-centered cubic lattice, may be produced. In view of this, in our experiments cycles of rolling and drawing were individually tested for obtaining textures at 50 and 75% reduction. The investigation was also designed to show whether

it is advisable to use two types of cold working to "texturize" metals with a cubic lattice, considering their high symmetry and the large number of planes and directions of the easiest glide.

Studied in this work was the variation of "hot hardness" and electric resistivity of samples in the process of heating to 500, 600, 700 and 800°, the holding times for each temperature being 5, 50, 500, 5000, and 50,000 minutes. These samples were previously subjected to hardening and reduction by 5, 50 and 75% by cold rolling and drawing. Measurements of "hot" hardness were carried out in a VIM-1M unit during heating of the hardened and cold-worked samples in vacuo ($\sim 10^{-5}$ mm Hg) to the above aging temperatures.

Electric resistivity was measured in the process of heating by the potentiometer compensation method based on the balancing of the measured e.m.f. against the known potential drop on a standard resistor.

Figure 1 shows the variation of "hot" hardness (measured in vacuo) and electric resistivity of undeformed samples as a function of holding time at the temperature of reheating (aging) and of the quenching rates.

The process of aging is practically untraceable at 500° in samples of metal cooled in furnace from hardening temperature. Aging at 600° leads but to a slight increase in hardness of samples quenched in air and in water.

At 700° a steady rise of "hot" hardness is to be observed in air- and water-cooled samples, and no decline of hardness is to be registered for holds up to 30,000 min. Holding for 30,000 minutes at 700° leads to an equalization of the hardness values in all samples cooled in air, water, and in the furnace; besides, aging at 700° results in greater hardening than at 500° and 600°. A certain stabilization of hardness after a rise during the initial 50 minutes is characteristic for heating at 800°. After the initial rise the value of hardness remains practically constant throughout a hold even as long as 30,000 minutes.

At 500° an anomalous increase in resistivity is to be registered.

Figure 1. Variation of hardness and electric resistivity of alloy EI437 samples - quenched with cooling in water (1), in air (2), and with the furnace (3) as a function of holding time at the temperature of aging.

a - 500°; b - 600°; c - 700°; d - 800° (---- ρ ; ——— H_V).

1) Electric resistivity ρ , microhm·cm; 2) Hardness, H_V; 3) lg of the annealing time, min.

As disclosed by many investigations (11, etc.), this is connected with the formation of atomic segregations (the so-called, K-state) in the solid solution. The intensity of resistivity growth is determined by the degree of supersaturation of the solid solution. This can be easily visualized, bearing in mind the high probability of the formation of atomic segregations of the type of Guinier-Preston zones (K-state) in a solid solution with a large number of dissolved "foreign" atoms. Consequently, a considerable growth of resistivity (by 8 microhm·cm) is to be observed in the water-quenched samples, a lesser growth in samples quenched in air (5 microhm·cm),

and a negligible growth in samples cooled with the furnace (2.8 microhm·cm).

If a comparison is to be made of the specific electric resistance of undeformed samples measured at room temperature, after hardening and after aging at 500° for a period of 5000 minutes (cooling from 500° in water), then the difference between the initial and final values would be found within the same limits as for heating with 5-min and 5000-min holds (Table 1).

A comparison of the results, used for plotting of resistivity curves, with the data on hardness shows that resistivity variation constitutes a more sensitive characteristic.

Aging at 600° reveals approximately the same regularities as those prevailing at 500°. However, all the processes associated with the formation of the K-state proceed less intensively at 600°. No variation of resistivity at all is to be observed in a solid solution impoverished (after cooling with the furnace) as far as the alloying elements are concerned.

Comparison of the data on resistivity for the cold state with resistivity data during heating (Table 2) exhibits a good coincidence of the difference in the initial and final values.

There exists a single-valued relationship between the resistivity variation and the formative processes of atomic segregation (K-state) during heating up to 500° and 600°. In the process of drastic cooling from these temperatures no additional phenomena leading to any structural changes were observed. As to the difference in the absolute values of resistivity, this is, naturally, related to the effect of the temperature coefficient.

At 700° the variation in the resistivity of samples quenched in water and in air manifests a similar character: at the beginning there is a certain stabilization, and then a drop in resistivity typical, for example, for the process of disintegration after aging. In samples cooled with the furnace, resistivity remains practically unchanged at up to 5000 minutes of holding.

Table 1

Resistivity of differently treated samples of EI437 alloy at aging temperature of 500°, microhm·cm.

Type of cold work	Degree of reduction	Water quenched from 1080°						Air quenched from 1080°		Hardened by furnace cooling from 1080°	
		Measured at 20°			Measured at 500°			Measured at 20°	Measured at 500°	Measured at 20°	Measured at 500°
		Before heating ρ_1	After 5000 min. ρ_2	After 10000 min. $\rho_2 - \rho_1$	After 5 min. ρ_1	After 5000 min. ρ_2	$\rho_2 - \rho_1$				
Unde-formed									[etc.]		
Rolled											
Drawn											

Table 2

Resistivity of differently treated samples of EI437 alloy at aging temperature of 600°, microohm·cm.

/Headings for table are same as for Table 1, except for substitution of "600°" for "500°" in the headings reading "Measured at 500°"/

Table 3

Resistivity of differently treated samples of EI437 alloy at aging temperature of 700°, microhm·cm.

/Headings for table are same as for Table 1, except for substitution of "700°" for "500°" in the headings reading "Measured at 500°"/

A comparison of these results with the data on "hot" hardness variation shows that a superposition of the processes of solid solution decomposition and formation of atomic segregations (K-state) takes place at 700°. Prolonged holdings lead to a prevalence of the decomposition processes. Consequently, the resistivity remains constant in the beginning. This corresponds to a simultaneous development of both processes, when the drop caused by the solid solution decomposition is compensated by a rise resulting from the formation of the K-state. Thereafter, resistivity begins to decrease with further progress of the solid-solution-decomposition process and the formation of the hardening phase. In samples quenched after furnace cooling, which reveal a lesser tendency to age (in view of the depletion of the solid solution after gradual cooling from the temperature of hardening), stabilization continues up to 5000 min. and only then does hardening begin, followed by a drop in resistivity in connection with the development of aging.

From a comparison of the results of resistivity measurements for the cold state (after quenching, and after quenching with 5000-min. aging at 700°) with the results of resistivity measurements during heating (Table 3), it becomes evident that no coincidence of the differences between the initial and final values is to be registered in this case. It is obvious, that even when quenching from 700° is drastic, and the 600-500° temperature interval is rapidly passed, there still occurs a partial formation of the K-state. In view of this, resistivity exhibits a certain growth, and the difference between the values of this characteristic, determined in tests at room temperature, will be smaller than the difference between the respective values obtained in high-temperature tests.

Heating to 800° results in characteristic changes in resistivity and hardness associated with the progress of solid-solution decomposition and the formation of the hardening phase. The decomposition is so intensive that it may be assumed to take place during holdings even shorter than 5 min. It should

be noted that due to this circumstance no comparison can be made of the data on resistivity measurements in the cold state (after hardening and after 5000-min holding with subsequent drastic cooling) with the results of resistivity measurements made during heating with 5 and 5000-min holding periods.

In determining the differently quenched samples for hardness variations, depending on the reheating temperature, it should be noted that hardening during the formation of K-state is far smaller than that resulting from the processes of high-temperature aging and hardening-phase formation. This explains the reciprocal disposition of the hardness curves of samples cooled in water, air, and furnace, if one should take into account the progress of aging in the process of different cooling from the temperature of hardening. The subsequent aging of hardened samples during reheating leads to a regular change in the relative position of the hardness curves, depending on the varying tendency of the solid solutions -- which were differently impoverished in the process of quenching -- to decompose.

In considering the influence of deformation on transformations in the EI437 alloy, the following should be taken into account. It is in the process of cooling at different rates from the hardening temperature that some measure of decomposition begins to take place together with the formation of the hardening phase. This is accompanied by the emergence of the K-state.

In all cases cold work increases hardness, the more so, the higher the degree of deformation (Table 4). It may be assumed that the hardening which results from cold working is connected with the supplementary decomposition of the solid solution and the formation of zones with finely dispersed phases, and also with the fragmentation of blocks and growth of stresses. For one and the same degree of deformation, drawing accounts for an appreciably higher rise in hardness than rolling. Apart from a possible specific influence produced by the different types of textures, this effect of the method of cold working is, apparently, attributable to the following: as a result of drawing,

Table 4.

Variations of Resistivity and Hardness of EI437 Alloy Samples. Tests Conducted at Room Temperature.

Type of cold Working	Degree of Deformation	Water-quenched from 1080°		Air-quenched from 1080°		Cooled from 1080° with furnace	
		microhm cm	kg/mm^2	microhm cm	kg/mm^2	microhm cm	kg/mm^2
Undeformed							
Rolled							
Drawn							

when the stress affects a greater volume, a greater amount of strain-hardening (for the same percentage of reduction) is produced and, accordingly, a greater degree of solid solution decomposition, or a greater change in the alloy's fine structure takes place.

Somewhat different is the effect produced by cold work on variation of resistivity. So long as the degree of reduction is low, amounting to but 5%, a normal rise in resistivity is to be observed in all cases. This means that not only do minor reductions fail to stimulate aging, associated with the formation of the phase, but there is even a lack of energy to destroy the K-state. After high degrees of reduction (50% and 75%) there occurs a considerable drop of resistivity, indicating the destruction of K-state and a change in the size of blocks, or the formation of dispersed hardening phases in the solid solution during cold working.

The variation of resistivity and hardness for heating to 500° of differently hardened and worked samples is illustrated in Figure 2. A minor reduction is conducive to a more intensive growth of resistivity in the process of holding at 500° than is the case for undeformed specimens. Apparently, the strain energy accumulated in the samples -- while insufficient to bring about

Figure 2. Variations in hardness and resistivity of hardened and deformed samples of EI437 alloy as a function of holding time at the aging temperature of 500°.

a - reduction by 5%; b - by 50%; c - by 75%; 1 - without straining; 2 - rolling; 3 - drawing; (----- ρ; ——— H_V).

1) Quenched from the hardening temperature in water; 2) Quenched from the hardening temperature in air; 3) Furnace-cooled from the hardening temperature; 4) Resistivity ρ, microhm·cm; 5) lg of the annealing time, min.; 6) Hardness H_V.

the destruction at room temperature of the K-state formed in the hardening process -- contributes at the same time to a still greater separation of the solid solution, and to a more intensive formation of atomic segregations in the process of heating at 500°. Along with the intensifying effect of minor strain hardening on the formation of the K-state, one should also note the influence exerted by the method of reduction to a preset degree. In all instances

the rolled samples display a higher resistivity than those drawn. This phenomenon may be explained in comparing the resistivity data with the results of hardness measurements. An inverse relationship is thereby revealed: the hardness of drawn specimens is higher than that of rolled specimens. It appears that greater microstresses arise as a result of drawing than of rolling. Hence, either the process affecting the size of the blocks, or that affecting solid-solution decomposition, develops to a larger extent in drawing. The one or the other is responsible for a lesser growth of the K-state in the process of subsequent heating to 500°. In rolled samples, where the decomposition of solid solution or the diminution of the blocks occur less intensively during deformation (and the growth of hardness is, consequently, less pronounced), the formation of atomic segregations (K-state), on the contrary, develops with greater ease. High r.m.s. stresses arise in the process of rolling.

Just as in the case of undeformed specimens, the highest resistivity variation is to be observed in samples reduced by 5% and quenched in water (the highest supersaturation of the solid solution), and the least resistivity variation - in samples cooled with the furnace (the least supersaturation of the solid solution).

Finally, a comparison of the values of resistivity measured at room temperature after hardening and after 5000-min holding at 500° (water-quench from 500°) with the values of resistivity measured during heating to 500° after 5 and 5000-min. holds (Table 1) reveals no coincidence of the difference in final and initial values, as in the case of undeformed specimens. At, say, a 5% reduction the intensity of K-state formation is so high that even after a 5-min. hold there occurs a rapid growth of resistivity which makes any comparison of the data in question impossible.

Noteworthy are the tests demonstrating that a 5% reduction applied in cold working yields a substantial increase in hardness, and what is most important creates conditions as a result of which hardness remains invariable

even after holding periods up to 30,000 min. Particularly marked is the growth of hardness and its stability in furnace-cooled samples. Drawing, as mentioned before, yields greater hardening than rolling.

Further research must show which of the processes capable of development during cold working -- decomposition of supersaturated solid solution, or the change in block size with stresses setting in, or both of them -- determine the growth of hardness referred to above.

It is true that intensive deformation (by 50 and 75%) actually leads to the destruction at room temperature of the K-state formed as a result of a different rate of cooling from the hardening temperature. Yet, an intensive growth of resistivity is to be registered after reheating to 500°, attesting to the restoration of the K-state.

If one compares the values of resistivity measured at room temperature prior to heating (i. e., after hardening and deformation) and after heating to 500° for a period of 5000 min (water quench from 500°), it will become clear that the difference between these initial and final values grows with the degree of prior deformation. Yet, the maximum final values to which resistivity may grow in the process of prolonged heating are approximately the same for all samples (varying within the limits of 132-134 microhm•cm). Then the effect of growing deformation on the growth of the difference between the initial and final resistivity values registered at room temperature is related to the sharp difference in the initial values (after deformation). This difference may be attributed to the varying intensity of the process of K-state destruction and solid-solution decomposition determined by different degrees of cold working. If one is to bear in mind that there is no inverse dissolution of the particles of the phase precipitated in the process of heating to 500°, then it may be concluded that the greater the amount of strain energy accumulated in metal after cold working, the more intensive the formation of the K-state during subsequent heating to 500°.

"Texture" forms in samples, when they are reduced by 50 and 75%. The effect produced by the method of cold working on resistivity values must, therefore, be considered with due allowance for the resulting grain orientation. After 5% reduction the degree of deformation was found to be related to a greater or lesser impoverishment of the solid solution in the process of working by drawing or rolling. Different relationships characterize the "textured" samples. Thus, in the case of a 50% reduction the resistivity variation curves for rolled and drawn specimens appear to be drawing closer together. In certain cases a more intensive variation is to be registered in the drawn samples. The intensive growth of resistivity is manifested particularly clearly in samples rolled with 75% reduction.

Texture resulting from drawing is responsible for greater hot hardness of samples, in the process of prolonged heating than that obtained by rolling. The stability of hardness, the high values of which are maintained throughout heating periods up to 30,000 min., should be noted. This phenomenon has an important practical significance, since in many cases it is required to produce parts or tools for operation in conditions of excessive heat or in aggressive media. Only in one instance (drawing with 75% reduction) a slight drop in hardness was registered after 5000-min. heating. However, in samples reduced to the same degree by rolling not only is there no decline of hardness, but, on the contrary, even a certain growth of it is observed. The above discussion, as well as the data on resistivity at room temperature after 500° heating for 1000 min., show that hardness changes cannot be explained by the development of a process involving a considerable decomposition of the solid solution.

It is difficult to believe that such a process could have progressed to a considerable extent in alloy EI437 at 500° temperature. Moreover, although a drop in resistivity is to be observed in both rolled and drawn specimens, hardness increases in certain cases, but in other cases it declines. It is

rather the stresses and a change in the size of blocks that produce a decisive effect on the magnitude and variation of hardness at 500°. These same characteristics vary differently as a result of prolonged heating, depending on the type of texture.

The variation of hardness and resistivity of differently hardened and deformed specimens depending on the length of heating at 600° (Fig. 3) is similar to the variation pattern observed in 500° heating cycles. Noteworthy is the somewhat smaller intensity of the K-state formation processes at 600° manifested specifically in a stabilization of the resistivity values, particularly, for long holding times (exceeding 5000 min.).

However, just as in the case of aging at 500°, the strain energy accumulated in the metal leads to a more considerable growth of resistivity during heating (to a more intensive formation of K-state), than is evidenced in heating of undeformed samples. This also holds for the case when the energy of deformation is small ($\sim$ 5%) and insufficient to bring about the destruction of the K-state, and for the case of considerable deformation (50 and 75%), when the K-state does not exist in the initial specimens. The intensifying effect of an increased degree of deformation on the growth of resistivity in the process of 600° heating may be illustrated by the data listed in Table 4. A comparison is made therein of the difference in resistivity values (determined at room temperature) of the initial samples and the specimens heated at 600° for 5000 min. (water-quenched from 600°). The influence of the texture on resistivity variation is of the same nature as that registered for 500°. As for hardness variation, no appreciable difference is to be observed here for rolled or drawn samples. Particularly close values of hardness were noted for samples subjected to different types of cold working with 50 and 75% reduction.

Unlike the case of 500° aging, prolonged heating (for more than 5000-10000 min.) at 600° involves the appearance of a tendency towards reduced hardness, which is especially strongly displayed for high degrees of reduction

Figure 3. Variation of hardness and resistivity in hardened and cold-worked samples of EI437 alloy as a function of holding time at the aging temperature of 600°

a - reduced by 5%; b - by 50%; c - by 75%; 1 - undeformed; 2 - rolled; 3 - drawn (----- ρ; ——— H_V).

1) Water-cooled from hardening temperature;
2) Air-cooled from hardening temperature;
3) Furnace-cooled from hardening temperature;
4) Resistivity ρ, microhm·cm;
5) lg of the tempering time, min.;
6) Hardness, H_V.

(50 and 75%). The question is, whether these changes are caused by a well advanced stage of solid solution decomposition, or by a redistribution of stresses and a change in the size of blocks. The answer to this question may be provided in the course of further research.

Let us compare the bends on the hardness variation curves (see Fig. 3) with the data on resistivity after prolonged heating (10000 min.)recorded in Table 2. This comparison reveals that in the case of drawing the drop in

hardness is accompanied by a decline in resistivity, whereas in the case of rolling resistivity is constant (or even displays a general tendency to grow) while the hardness values diminish. This remarkable fact justifies the belief that the decrease in hardness, observed in a number of samples as a result of prolonged heating at 600°, is related to the development of such processes the progress of which to a certain degree depends on the type of texture. Most probably these processes are represented by redistribution of stresses and the change of size and density of blocks.

A 700° aging of deformed samples (Fig. 4) leads to approximately the same changes in hardness and resistivity as those observed in the process of aging of undeformed specimens. Let it be recalled here that during 700° heating of EI437 alloy a simultaneous progress of two processes was observed: formation of atomic segregations and decomposition of the solid solution. In comparing the shapes of the curves for the deformed and undeformed samples the following features associated with the effect of cold-working may be noted.

1) The hardness and resistivity values of cold-worked samples for all investigated periods of heating (up to 30000 min.) turn out to be higher than the same values for undeformed specimens.

2) At the first stages of aging at 700° and for heating periods up to 5000 min. a stabilization of resistivity values with simultaneous growth of hot hardness was observed in undeformed samples. This was attributed to a superposition of the processes of K-state formation and solid solution decomposition (or the removal of stresses). In the deformed samples, however, such stabilization was but hardly noticeable. With increasing degree of deformation, a pronounced tendency towards a steady change (drop) of resistivity is to be observed. This is attributable to an intensive development in the cold-worked alloy at 700° of either of the following processes: stress relief or solid solution decomposition with formation of a hardening phase.

Figure 4. Variation of hardness and resistivity in hardened and cold-worked samples of EI437 alloy as a function of holding time at the aging temperature of 700°:

a - reduced by 5%; b - by 50%; c - by 75%; 1 - undeformed; 2 - rolled; 3 - drawn; (----- ρ ; ——— H_V).

1) Water-cooled from the hardening temperature;
2) Air-cooled from the hardening temperature;
3) Furnace-cooled from the hardening temperature;
4) Resistivity ρ, microhm·cm;
5) lg of the tempering time, min.;
6) Hardness, H_V.

3. Even though the question as to the nature of the transformations which occur during 700° heating is yet to be clarified in the course of further research, a number of assumptions may be made now, based on the comparison of resistivity values determined at room temperature: after hardening and deformation; after heating at 700° for 5000 min.; and after heating at 700° for 10000 min. A difference in the character of resistivity variation is noticeable between the samples cold-worked for a small-scale reduction and

the "texturized" specimens (50 and 75% reduced). After heating of 5% reduced samples, the usual drop of resistivity occurs, while texturized specimens heated for 5000 and 10000 minutes have a higher resistivity than the respective value of the initial (hardened and cold-worked) samples. It cannot be assumed that this phenomenon is connected with the dissolution (when heated) of the finely-dispersed particles of the hardening phase which precipitate in the process of cold working; or that it is associated, for example, with an intensive restoration of the K-state in cold-worked specimens in the very first minutes of heating. An analysis of the curves (see Fig. 4) shows a steady drop of resistivity during holding at 700°. In all probability it is the specific effect of the texture that is operative here. It may be assumed that a simultaneous development of the processes of solid solution decomposition and stress redistribution, coupled with a change in the mosaic structure, leads to the formation of hardening phases in the texturized samples, such as may determine the high values of electric resistivity.

4) Important is the major stability of the high hardness values of samples reduced by 5 and 50% which is demonstrated in the process of prolonged heating (up to 30,000 min.) at 700°. Cold working involving 75% reduction leads to instability of structure characterized, in particular, by a steady resistivity and hardness drop. Evidently, considerable strain-hardening is associated with an appreciable depletion of the solid solution due to its decomposition in the process of deformation, and also with the instability of the alloy resulting from the high values of strain energy accumulated in it. Subsequent heating involves an intensification of the processes which bring the alloy into a stable state, and this is, in fact, reflected in the decline of hardness and resistivity. As for the effect of the method of cold working on the absolute values of hardness and resistivity, it may be noted that very close (practically coinciding) resistivity values are produced in cases of 5% and 50% reductions by rolling and drawing. For 75% reduction resistivity turns

out to be higher in rolled than in drawn samples. The hardness of specimens reduced by drawing is, as a rule, higher than of those rolled.

At heatings up to 800° (Fig. 5) resistivity and hardness, on the whole, follow the variation pattern registered for 700°. It may be noted that the lower absolute values of resistivity characteristic for 800° heating, and the correspondingly small variation of these values in the process of prolonged holding, attest to the intensity of the processes of solid solution decomposition and the removal of cold-work-induced stresses; these (processes) occur even during short holds at this temperature. It is in connection with such kinetics of these processes that an explanation may be found for the close values of resistivity in samples differently cooled from the temperature of hardening, and for the absence of a visible difference between the rolled and the drawn specimens.

The hardness curves show an intensive softening of the cold-worked samples at the aging temperature of 800°. As a result of heating for periods from 10,000 to 30,000 min. the hardness of the deformed (cold-worked) specimens becomes the same as in those undeformed. The intensity of the softening processes at 800° may be related to the intensive precipitation and coagulation of the hardening phase particles, and also (and mainly) to the removal of stresses and the change in the size and density of the blocks in undeformed specimens during 800° heating (recrystallization). Consequently, as representing the processes, which develop at this temperature, the curves of hardness variation have a greater significance than those reflecting the variation of resistivity.

Figure 5. Variation of hardness and resistivity in hardened and cold-worked samples of EI437 alloy as a function of holding time at the aging temperature of 800°.

a - reduced by 5%; b - 50%; c - by 75%; 1 - undeformed; 2 - rolled; 3 - drawn; (----- ρ ; ——— H_V).

1) Water-cooled from the hardening temperature;
2) Air-cooled from the hardening temperature;
3) Furnace-cooled from the hardening temperature;
4) Resistivity ρ, microhm • cm;
5) lg of the annealing time, min.
6) Hardness, H_V.

REFERENCES

1. F. F. Khimushin, Nerzhaveyushciye, kislotoupornyye i zharoupornyye stali [Stainless Acid-proof, and Heat-Resistant Steels], Metallurgizdat, 1945.

2. M. L. Bernshteyn, Stali i splavy dlya raboty pri vysokikh temperaturakh [Steels and Alloys for Use at High Temperatures], Metallurgizdat, 1956.

3. V. N. Krivobok, R. A. Lincoln, Trans. Amer. Soc. f. Metals, 1937, v. 3, p. 637.

4. F. F. Khimushin, S. I. Ratner, Z. V. Rudbakh, Stal' [Steel], 1939, No. 8.

5. W. L. Sutton, Metal Progress, 1937, v. 31, p. 49-52.

6. M. L. Bernshteyn, G. V. Estulin, L. K. Gumennyy, Vestnik inzhenerov i tekhnikov [Engineers' and Technicians' Herald], 1948, No. 5.

7. Clark, Teploustoychiviye i zharoprochniye splavy [Thermally Stable and Heat-Resistant Alloys], Transl. from English under the editorship of M. L. Bernshteyn, Metallurgizdat, 1957.

8. S. T. Kishkin, A. M. Sulima, V. P. Stroganov, Issledovaniye vliyaniya naklyopa na mekhanicheskiye svoystva istrukturu splava EI437A. [Investigation of the Effect of Cold Working on the Mechanical Properties and Structure of Alloy EI437A], Oborongiz, 1956.

9. N. T. Gudtsov & M. L. Bernshteyn, Trudy nauchno-teknicheskoy sessiyi po zharoprochnym metallam i splavam [Proceedings of the Scientific Technical Conference on Heat-Resistant Metals and Alloys], USSR Academy of Sciences, 1953.

10. M. L. Bernshteyn & M. L. Grinberg, Sb. "Metallovedeniye i termicheskaya obrabotka" ["Metallography and Heat Treatment", symposium], supplement to magazine "Stal'", Metallurgizdat, 1957.

11. H. Thomas, Z. f. Physik, 129, 219, 1951.

Associate Professor and Candidate of Technical Sciences S. S. GORELIK and Engineer M. B. GUTERMAN.
Department of Metallography and Roentgenography.

ON THE PROBLEM OF THE RECRYSTALLIZATION MECHANISM AT CRITICAL STRAIN

It is well known that recrystallization of metals and alloys strained to the critical degree is characterized by the formation of a structure with unusually large grain size.

This condition is made particular use of when it is required to produce a coarse-grained structure and obtain monocrystals. In other cases, however, when coarse grain is undesirable, the use of small-scale deformation must be avoided. Low-degree deformation, but slightly larger than critical, under certain definite conditions leads to a consertal structure detrimentally affecting the mechanical properties. Structural changes arising in the process of creep, in certain cases, also appear to be similar to the recrystallization process initiated by low-degree straining.

In view of this, a clarification of the mechanism of recrystallization following deformation to the critical degree is highly interesting both from the standpoint of theory and practice.

However, notwithstanding the fact that a great deal of studies had been devoted to the problem of recrystallization, there are many questions which have as yet received no universally accepted interpretation.

According to the opinion of one group of researchers, recrystallization resulting from critical degree straining occurs by way of normal nucleation and growth. Coarse grain is formed owing to a small number of these nuclei (1, 2, 3).

Another school believes that direct "collective" recrystallization takes place, i. e. that some initial grains grow at the expense of the others (4, 5, 6). A number of authors (5, 6 and others) ascribe the reason therefor to small-scale deformations which are characterized by non-uniform straining of

various grains owing to their different orientation with respect to the strain forces. As a result a part of the grains experience relatively high deformations and resulting fragmentation, whereas the other grains suffer but slight distortions. In the process of heating these latter grains acquire a capacity of growing at the expense of those more deformed or crushed.

Ya. R. Rauzin and A. R. Zheleznyakova (5) maintain that at minor (pre-critical) degrees of deformation the initial grains migrate with respect to each other as one whole. In so doing some of the adjacent grains acquire a close crystallographic orientation and as a result their merger becomes possible during heating.

A substantial drawback in the investigations of this problem is that they were carried out by the method of statistical determination of grain size and not by way of direct study of the structural changes occurring in one and the same zone in the process of recrystallization.

Attempts at direct observation of the structure are known in the literature (7, 8), but they were all confined to the study of the grain growth mechanism, i.e. of the far advanced stage of collective recrystallization. Moreover, they were devoted to the relatively low-melting metals: tin (7) and zinc (8).

The purpose of this investigation was to ascertain the structural changes by means of direct observations in the process of recrystallization of high purity armco-iron after its subjection to critical strain.

The investigation was carried out in a vacuum unit of the VIM-1M type. The basic diagram of the unit is given in paper (9). However, a full use of this equipment for the study of the recrystallization mechanism in the deformed specimen turned out to be impossible for the following reasons.

Usually during vacuum heating the microstructure is revealed as a result of different intensity of metal evaporation within the grain and at its boundaries. This method is applicable only at temperatures exceeding

$0.5\ T^{\circ}_{melting}$. Yet, recrystallization commences at a temperature lower than $0.35\ T^{\circ}_{melting}$.

Evaporation in iron proceeds exceedingly slowly even at temperatures of 820-850°. The grain boundaries begin to emerge only upon heating for a period of 5 to 10 minutes. However, a special check has shown that recrystallization after critical strain terminates, on the whole, in the course of the first minute. Consequently, this method may be used only for studies of the far advanced stages of collective recrystallization, i.e. the growth of grains.

Other methods of structural examination of a heated specimen -- alternating oxidation (or etching) and reduction, preliminary etching, and so on -- also failed to produce the desired results.

The method which was finally applied consisted in the following: the initial specimen was electrolytically etched and the polished section area, on which the structural changes were studied, was marked off by means of imprints made with a diamond pyramid. The sample was then placed into a chamber and after a sufficient degree of evacuation had been attained ($1 \cdot 10^{-4}$ to $1 \cdot 10^{-5}$ mm Hg) it was heated to the required temperature, held at this temperature for a period of several seconds and cooled (in vacuo). Thereafter, the sample was withdrawn from the chamber, etched in the same electrolyte, whereupon the structure was photographed at the same place at which the picture of the initial structure was taken. After this the specimen was again returned into the chamber, and the whole operation was repeated.

By a special check it was disclosed that successive etching offered a correct picture of the recrystallized structure. Etching was very weak. The grain boundaries revealed after subsequent heating and fresh etching differed clearly from the previously exposed boundaries. To ascertain that these boundaries actually represented the boundaries of the recrystallized grains, the following check operation was carried out: after each heating, subsequent

etching, and photographing of the structure, the section was polished and re-etched. The structure revealed by polishing always coincided with the one observed before polishing (Figs. 1-c and -d).

Deformation was carried out by extension (stretching). As compared with other types of straining (compression, rolling, and so on) extension produces a more uniform distribution of strain across the section, and the strain magnitude, determined by elongation at a given stretch of the sample, approaches most closely to the true strain. Critical strain was determined on a flat sample with narrowing cross-section (with a taper of 2.5%). On being stretched such a specimen experiences an uneven deformation along its length. The magnitude of strain was determined by the changing distances between the transverse gauge-lines marked at 2-mm intervals. After annealing (recrystallization) and macro-etching a zone with very coarse grains, corresponding to critical, strain was clearly visible on this sample. The critical strain for armco-iron deformed by extension turned out to be equal to 7.5-8%.

The annealed plates of 200 x 10 x 35 mm armco-iron were reduced by extension by 7.5-8%, using a 5-ton tension machine. Samples 55-60 mm in length were cut from the mid-section of the stretched plates for the basic investigation. On one plane of the sample a section was prepared and electrolytically etched to reveal the microstructure. Used as electrolyte was a solution of the following composition: 10 ml. of concentrated HCl per 100 ml. methyl alcohol. The density of current was 1.5 A/cm^2. This type of etching revealed only the grain boundaries. The grains themselves were practically unetched. Then the zone to be investigated was selected and marks were made on it by the diamond pyramid of a PMT-3 instrument, whereupon the sample was introduced into the vacuum apparatus for heating.

The sample was heated by the contact method. The leads were water-cooled whereby the ends of the sample remained cold, while the temperature over its length varied attaining a maximum at the middle of the plate. Figure 2 shows

the structure on the plate surface after 1 hour of heating up to 820°. Although the strain along the entire length of the sample was the same, nevertheless, as a result of the above mentioned temperature distribution, recrystallization developed in different ways, and the largest grains formed in the zone which had been heated to the maximum temperature.

Figure 1. Variation of the armco-iron structure in the process of heating at 820° after straining to critical degree. X 100:

a - initial structure prior to heating; b - structure after holding for 5 seconds; c - 15 sec.; d - 15 sec. after section polishing.

Considering this condition the junction of the recording thermocouple was spot-welded to the reverse side of the sample opposite the zone in which the structural changes were to be examined. The measurements of the Pt, Pt-Rh thermocouple were registered by an indicating millivoltmeter, as well as by an automatic electronic potentiometer, which served for the recording and control of temperature.

Figure 2. Structure of the sample surface (the sample was predeformed by 8%) after electric heating for a period of 1 min. The structure reflects the uneven distribution of temperature over the sample's length. X 2.5.

RESULTS OF THE INVESTIGATION OF STRUCTURAL CHANGES

Analysis of photomicrographs, taken at different stages of recrystallization following deformation to critical degree, substantiated the statement that no signs of nucleation of new grains were revealed in any of the examined cases. The recrystallization nuclei (if they can be so termed) which develop into large grains, were in all cases some of the initial grains of the deformed structure.

Thus, it may be asserted that recrystallization resulting from deformation to critical degree has a purely "collective" character.

It was also possible to establish on the basis of microstructural analysis that this collective recrystallization may develop in two ways: by fusion of two or several adjacent grains (by means of what is known as coalescence) and by way of the growth of some of the initial grains, or a group of merged grains, at the expense of other grains through shifting the boundaries (migration). In this development the principal at the very early stages (in the first seconds of heating) is the first named process, in the later stages - the second.

We shall illustrate this conclusion by examples.

When several grains unite into one, the contour of the new grain boundary

must fit within the contour of the peripheral boundaries of the old grains, the merger of which had produced the new grain. If, on the other hand, the new large grain forms as a result of shifting the old grain boundaries, then -- provided the structure is fixed at very short heating time intervals -- the front of the shifting boundaries must be found passing across the body of the initial grains during the intermediate stages.

In our case for the early stages of recrystallization, with the anneal periods ranging from 5 to 15 seconds, the merger process turned out to be prevalent.

Figure 3. Variation of armco-iron structure in the process of holding at 820° after deformation to critical degree (8%). X 200.

a - initial structure before heating; b - structure after holding time of 5 sec.; c - 15 sec.; d - 60 sec.

Thus, picture 3-a shows three grains (A, B, C), the fusion of which begins in the course of the first five seconds (Fig. 3-b) from the moment of reaching the 820° temperature, and comes to an end in approximately 15

seconds (Fig. 3-c). Besides the merger of these three grains, the outer boundary of grain A at the same time moves to the left as indicated by arrows in Figure 3-a. Finally, one large grain formed from these three grains has as its boundaries the peripheral boundaries of the three initial grains, with the exception of the above mentioned segment of the grain A boundary. After heating at 820° for a period of 25 sec. the new grain boundaries remain practically the same as after the first 15 sec. of heating. Further heating (60 sec.) also failed to bring about any structural changes in this zone (Fig. 3-d).

Let us consider another example (see Fig. 1-a, -b, -c, -d). During the 5-sec. period of heating the group of grains (A, B, C, D, E) merge into one large grain. Within the same short period of time the growth of another large grain through boundary shifting sets in in some sectors. As a result of this, the contours of the new large grain after 5 seconds of heating coincide with the contours of the initial grains in some sectors (see the upper boundaries of grain A), but in other sectors the boundaries of the new grain pass across the body of the initial grains. For example, the boundaries of the fused A, B, C, D, E grains after 5-sec. heating have shifted to the right passing in the middle of grains F and G.

Further heating involves structural enlargement only as a result of boundary shifting (Fig. 1-c, -d). In this case, the boundary surface energy, evidently, begins to play an important role. Thus, the right-hand side boundary of grain A had a strongly developed surface at the initial state [a saddle and two ("promontories") protuberances marked by arrows in Fig. 1-b]. Heating at 820° for 5 sec. failed to change the boundary of grain A in this sector (Fig. 1-b), even though it has led to a merger of several grains with grain A. An additional holding for 10 seconds, however, caused a rapid shifting of the boundary in this sector as well (see Figs. 1-b and 1-c); in so doing, the boundary of the grain had straightened out and its length had been rapidly reduced. Characteristic thereat is the fact that in one sector (saddle) the boundary

of grain A has moved in the direction of grain H (indicated by arrow) while in the neighboring sector (the upper protuberance) the boundary of grain H has shifted in the direction of grain A. In other words, one and the same grain A has absorbed a portion of grain H in one sector, but in another adjacent sector it turned out to have been itself absorbed by the neighboring H grain. This is a typical case which may be very frequently observed.

In most cases, as in the one just reviewed, when the growth of grain occurs by way of boundary shifting, and is stimulated by a tendency to straighten the boundary and reduce its extent, this shift takes place in the direction of the center of the boundary curvature in the sector concerned. A similar character of boundary shifting in the course of collective recrystallization was previously determined for an alloy of tin with 1.5% antimony (7).

It should also be noted, that the growth of grains by way of boundary shifting is not a smooth, continuous process. It is characteristic for its intermittent and uneven nature with respect to time and direction (a peculiar type of anisotropy). The intermittent character of the grain boundary displacement may be seen from Figures 3-a, -b, -c, -d. The lower boundary of grain A has moved considerably during the first 5 seconds at 820° (see Fig. 3-a and 3-b). Thereafter, for the next 10 sec. at the same temperature the boundary remained in the same place (Fig. 3-c), but then during the following 10 seconds it rapidly moved again to come in contact with another large grain.

The non-uniformity of growth in different directions and its discontinuity with respect to time are illustrated also in Figure 4 (grain A). Heating for a period of 2 seconds at 820° did not change the contour of grain A. After additional heating at the same temperature for another 18 seconds, grain A still failed to change at the bottom and at the left-hand side, whereas at the top and to the right its boundaries showed a certain advance. After another 17-second heating cycle the left boundary remained in its original position, but the right boundary shifted further at a higher rate than during

Figure 4. Change in armco-iron structure in the process of holding at 820° after deformation to critical degree (8%). X 100.

a - structure before heating; b - structure after holding time of 2 sec.; c - 35 sec.

the preceding heating.

To gain a clearer picture of the peculiarities of recrystallization after deformation to critical degree, the progress of recrystallizations was also studied after deformation by 17%, i. e. for a degree of straining considerably higher than the critical.

In the case of transcritical deformation, in contrast to the critical point, not only the final recrystallized structure, but even the structure resulting after 5-minutes heating at 820°, is perfectly unlike the initial structure (Fig. 5). No connection between them can be established even after a most careful examination. This condition, apparently, may be ascribed only to

Figure 5. Variation of armco-iron structure in the process of holding at 820° after deformation to trans-critical degree (17%). X 100.

a - structure before heating; b - structure after holding time of 5 sec.; c - 60 sec.

the fact that at large-scale deformation recrystallization proceeds via nucleation, and the growth of the new grains occurs at the expense of the strained matrix.

The rate of nucleation and growth in this case is so high that the recrystallization of the deformed specimen terminates, in the main, in 5 to 10 seconds. Subsequent heating, particularly for periods in excess of 30 seconds, leads but to a minor change in structure caused by a slight boundary migration.

It is not excluded that after 17% deformation, along with nucleation, there occurs a direct collective recrystallization in some individual sectors. This is indicated by the highly consertal nature of the structure resulting

after deformation by 17% (Fig. 5-b) as compared with that following an 8% deformation. However, to substantiate this a special check to be carried out in the course of holding periods shorter than 5 seconds and, possibly, at temperatures below 820°, would be required.

The observations described above confirm the complex nature of the recrystallization process at critical strain and its dependence on a large number of varying factors, as to the nature of which only certain assumptions may be made at present.

It may be considered as firmly established that recrystallization in this case has a collective character and is not related to the formation of nuclei of new grains. The role of such nuclei is played by some of the initial grains.

However, as has been established, this collective recrystallization, may progress in two ways. The first possible mechanism consists in the union (coalescence) of the adjacent grains.

Ya. R. Rauzin and A. P. Zhelznyakova (5) feel that this is the only mechanism and tend to explain it by the special character of plastic deformation in the subcritical region. In their opinion no shearing within the grains occurs in this process. The grains turn with respect to each other as whole entities. This improves the contact between them, and their mutual position changes in the direction of equalized crystallographic orientations, which, in fact, facilitates the fusion of these grains. This theory, however, is not entirely valid, at least, not for iron. An X-ray study conducted by one of the authors of this paper revealed that even at the smallest deformations, considerably below critical, there occurs a shear within the individual grains, and the formation of slip bands is to be observed.

It is possible to assume that as a result of shearing strain accompanied by the formation of slip bands and their turn, the grain orientations undergo a certain change. Consequently, the probability that the adjacent grains and

their parts may acquire a close orientation, or may develop a twin relationship, increases, and the probability of their fusion accordingly augments. In this case, instead of boundary migration there occurs a reconstruction ("rectification") of the distorted atomic layers at the grain interface, i.e. a disappearance of the internal boundaries.

It is possible that a certain role in the process of grain coalescence is also played by the elastic stresses between the contiguous grains, and their elimination during heating.

The second mechanism is characterized by the absorption of some grains by the others via boundary migration. In this case, the absorbing grain may be some individual initial grain, or a group of them, previously fused together by means of the process referred to above. Characteristic is the fact that the "incubation" period of the process of grain growth through boundary shifts is greater than that in the process of grain coalescence. The merger, if it is possible, occurs, as a rule, before the beginning of noticeable boundary shifting.

The mechanism of structure coarsening due to boundary migration is subject to the general regularities of grain growth. The tendency to reduce the boundary surface energy appears to be the principal stimulus of this process. The existence of concave and convex boundary sections facilitates such migration to a considerable extent. Indeed, in this case the atoms located on the concave side will be surrounded by the atoms of their own crystal to a greater extent than the atoms on the convex side, and will, therefore, be in a more stable state. The migration of atoms from the convex to the concave side must, therefore, be accompanied by a decrease of energy in the surface layer and a rise in thermodynamic stability of the system. But, such shape of boundaries, alone, is evidently insufficient to produce this effect. The shifting of boundaries does not begin right away after a given temperature has been reached, but only after a certain period of incubation. Moreover, once started

the process does not develop continuously, its progress being intermittent. This constitutes a basis for the belief that, in addition to surface tension, the general energy state of the adjacent grains and of the boundary between them is likewise brought into play here. It may be assumed that in a number of cases the growing (absorbing) grain is the one which has experienced a lesser strain and the lattice of which is, therefore, less distorted. The process of relaxation proceeds with greater ease in such a grain during heating. Actually, the incubation period in this case must be associated with the relaxation process. Only after the relaxation will have developed with sufficient completeness, will the free energy of this grain reach a value considerably lower than that of the neighboring grain, and the process of its growth at the expense of the latter grain will become possible.

Another case is also possible, that is when the energy states of the adjacent grains differ little one from another, the distortions in them are minor, while the length of the boundary is considerable and its shape a pronounced convex-concave. Then, upon termination of relaxation and elimination of distortions in the crystal lattice, the surface energy differential becomes sufficient to stimulate the migration of atoms from the convex side of the boundary to the concave side, i.e. to cause the boundary to shift towards the center of the curvature.

REFERENCES

1. F. Göler u. G. Sachs, Zeitschrift für Physik, 1932, 77.
2. S. I. Gubkin, Teoriya obrabotki metallov davleniyem [Theory of Processing Metals by Pressure], Metallurgizdat, 1947.
3. D. M. Nakhimov, Metallovedeniye i termicheskaya obrabotka, Spravochnik [Metallography and Heat Treatment, Handbook], Metallurgizdat, 1956.
4. Ye. M. Savitsky, Aviapromyshlennost' [Aircraft Industry], 1940, No. 8.
5. Ya P. Rauzin and A. R. Zheleznyakova, Metallovedeniye i termicheskaya obrabotka, sb. statey VNITOMASH [Metallography and Heat Treatment, Symposium of Papers at the All-Union Scientific-Research Institute of Machine Building Technology], Mashgiz, 1955.

6. A. P. Gulyayev, Metallovedeniye [Metallography], Oborongiz, 1951.

7. H. Carpenter a. C. Elam. J. Inst. Met. 24, 1920, 83.

8. I. F. Burke a. D. Turnbull, Progress in Metall Physik 1952, No. 3.

9. M. G. Lozinsky, Trudy NTO ChM, [Transactions of the Scientific and Technical Department for Ferrous Metallurgy], vol. 3, Metallurgizdat, 1955.

Engineer V. E. KUCHNOV.
Department of Physics.

STRESS INVESTIGATION IN POLYCRYSTALS OF SILVER CHLORIDE BY THE POLARIZATION OPTICAL METHOD*)

Submitted by Professor B. N. Finkel'shteyn

METHODS OF STRESS STUDY

A. V. Stepanov (1) revealed the existence of a group of substances (silver and thallium halides, and various alloys based on them) which are distinguished by transparency and possess mechanical properties similar to those of metals. These substances were given the name of "transparent metals".

Of the "transparent metals" silver chloride is known best. Silver chloride is represented by ionic crystals with sodium-chloride structure, transparent, and optically isotropic. As shown by A. V. Stepanov (1), the extension curve of silver chloride is analogous to that of copper, but as if it were weakened 10 times. Silver chloride crystals are readily processed by pressing, rolling, forging, stamping, and heat treatment (2, 3, 4). The transparency of silver chloride and the appearance of birefringence, when stressed, make it possible to use the method of photoelasticity for research or the processes involved in plastic deformation. Previously this method was used only for investigation of stresses in isotropic amorphous bodies. The properties of amorphous materials, however, differ substantially from those of crystalline substances, including metals. In order to be able to simulate the processes of plastic treatment of metals and to investigate the stresses in them, it is important to have a material with properties similar to those

*) On the basis of the materials of a thesis presented for the award of the degree of Technical Sciences Associate. Scientific supervisors: Associate Professor M. P. Shaskol'skaya and Professor B. N. Finkel'shteyn.

of metal. Silver chloride meets all these requirements and is suitable for analog study of plastic deformation in metals. But one must first determine whether it is possible to utilize the photoelasticity method in a study of the strains and stresses arising in silver chloride, and to ascertain that the stress patterns obtained in silver chloride by this technique will correspond to the respective patterns in metals. The present work was devoted to the elucidation of these questions.

The following methods are being used in stress distribution studies: 1) optical analysis; 2) theoretical calculation of the stress trajectories; 3) study of Chernov-Lueders lines; 4) coordinate grid; 5) lacquer coatings; 6) tensometric method with utilization of varying types of tensometers; 7) comparison of the grain magnitude after crystallization; 8) hardness tests; 9) interferometric method. Some of these methods are used for direct study of stress distribution; in the main, however, research proceeds along the lines of studying strain propagation and distribution in the deformed area. The distribution of stresses is deduced on the basis of the strain distribution pattern since the stresses acting in the body element being studied must be related to the strains by a single-valued relationship.

POLARIZATION OPTICAL METHOD OF STRESS STUDY

The optical method of stress study in polarized light is based on the tendency of certain transparent optically isotropic materials to become optically anisotropic when acted upon by stresses. F. Neumann (5) has developed a theory of optical effects produced by internal stresses in amorphous bodies. The author made the following assumptions: optical anisotropy caused by internal stresses may be described by Fresnel's ellipsoid, and the elongations of the axes of this ellipsoid are proportional to the stresses. The validity of this assumption for amorphous materials has been experimentally confirmed.

The optical method of stress study in isotropic bodies is based on:

1) the law of direct proportionality of stress and strain values; 2) the tendency of certain transparent isotropic bodies (glass, celluloid, bakelite, special plastics, etc.) to acquire under stress a property of temporary birefringence, i.e. to become optically anisotropic, with the polarization planes in the material coinciding with the direction of the main stresses; 3) definition of the equilibrium equations for a two-dimensional stress condition as including neither the modulus of elasticity nor the Poisson ratio.

The latter condition is of substantial significance for the polarization optical method and for its possible application to the solution of practical problems.

The physical aspect of the phenomena, as well as the description of the method as such will not be dealt with here, since this information may be found in a number of monographs (6, and others).

We shall dwell only on certain problems which have an immediate bearing on this work.

Strains developing as a result of the main stresses produce an optical anisotropy in the material. Due to the strain differential in both main directions, a ray of light passing through the stressed transparent body will propagate in one main plane more rapidly than in the other. Each element of a stressed isotropic body behaves like a crystal with double refraction. The oscillations in a pencil (beam) of plane-polarized light, traversing a stressed plate, split up into two mutually perpendicular oscillating elements propagating through the body at different rates. This leads to a relative shift of the phases of both components, i. e. to optical difference of travel δ. The intensity of light passed through the analyzer is determined by formula

$$I = p^2 \sin 2\alpha \sin^2 \pi \frac{\delta}{\lambda}. \qquad (1)$$

where δ - optical difference of travel;

λ - length of light wave;

α - angle between the planes of polarization and one of the sample's polarization directions;

p - amplitude of oscillation in the beam which has passed through the analyzer (it is understood that the planes of polarization of the analyzer and the polarizer are at right angles).

When $\alpha = 0^\circ$ or 90°, total extinctions of the ray takes place. This case is of great interest for stress study, since it provides accurate data on the direction of the two main stresses σ and σ at any point of a sample in optically isotropic bodies.

If at a set arrangement of the planes of polarization of the polaroids the directions of the main normal stresses coincide with the directions of the planes of polarization, then a system of dark points or lines, called isoclinics, will appear in a corresponding spot on the screen. Synchronically rotating the polarizer and analyzer, we obtain the respective isoclinics for each angle of rotation.

The isoclinic line is a locus at the points of which the directions of both main normal stresses σ and σ are parallel to the planes of polarization of the polarizer and analyzer.

The isoclines, as such, do not determine the numerical value of the stresses and play but an auxiliary role in the construction of isostatic curves. The isostatics represent the trajectories of the main normal stresses, i. e. the curves, the tangentials to which coincide at each point with the direction of one of the main stresses σ or σ . The isostatics intersect the symmetry axes only at right angles, or run parallel to these axes. The maximum tangential stresses are directed at an angle of 45° to the main normal stresses.

PIEZO-OPTICAL PHENOMENA IN CRYSTALLINE BODIES

The optical phenomena which arise in transparent crystalline bodies, acted upon by internal stresses, are far more complex than the phenomena in isotropic bodies. The theory of these phenomena was formulated by the end of the last century by F. Pockels, who has elaborated Neumann's theory while proceeding from the following assumptions: 1) after the appearance of internal stresses in a crystal its optical anisotropy continues to be described by Fresnel's ellipsoid; 2) the variation of the ellipsoid equation coefficients is a homogeneous linear function of the stress. Like Neumann's theory, Pockel's theory is phenomenological. Its validity is confirmed by experiment. For the development of the optical method of stress study in polycrystals, a theoretical analysis of the elastic effects, arising in a polycrystalline body under the action of external forces, is required. A complete quantitative solution of this problem is very complicated. As to the qualitative determination of the stress distribution, it is possible to utilize the experimental data obtained by the method of photoelasticity and the symmetry of properties in crystalline bodies.

SYMMETRY OF PROPERTIES IN CRYSTALLINE BODIES

If the internal structure of a material possesses a symmetry of some kind, then symmetry will also be observed in its elastic properties. This symmetry is manifested in the body having symmetrical directions for which the elastic properties are identical (equivalent directions).

The relationship between the structural symmetry and the elastic symmetry in crystals is determined by the F. Pockels principle which may be formulated as follows: with respect to its physical properties (including the plastic properties) a material reveals a symmetry of the same type as that of its crystalline form (7). This principle may also be extended to the polycrystalline bodies which display anisotropy, i. e. to the textures.

If a body possesses a symmetry of physical properties, in particular of elastic properties, then the optical anisotropy, engendered by the action of forces applied to the body, will also reveal the same type of symmetry. The birefringence emerging in polycrystals and the optical patterns resulting therefrom will be related directly to the stresses produced by the load. According to F. Pockels' principle the symmetry of optical patterns must repeat the symmetry of the elastic properties of the material.

Thus, an approximated picture of the distribution of stresses may be obtained by utilizing only the optical patterns engendered by the load. V. M. Krasnov (8) worked on a solution for such a problem. He arrived at the conclusion that the directions of the optical ellipsoid axes, determined directly by experiment and defined by the isoclinic field, do not coincide with the directions of the main stresses. However, for purposes of qualitative analysis of stress distribution we may assume that in the case of a linear stress the isoclinic patterns, determining the optical ellipsoid, will also determine the ellipsoid of stresses in the first approximation. This assumption is valid only for qualitative analysis of the linear state of stress.

PLOTTING MAIN STRESS TRAJECTORIES

In plotting the trajectories of the main stresses the technique described in Frocht's paper (6) may be used. In dealing with the two-dimensional problem of the theory of elasticity by the optical method, the trajectories of the main stresses (isostatic curves) are constructed graphically on the basis of the isoclinic pattern obtained with the aid of a polariscope. The procedure of plotting trajectories of the main stresses, essentially constitutes a graphic solution of a differential equation on the basis of the experimentally determined values of the derivatives.

The method of "graphing" applied in this work is shown in Figure 1. A number of dashes sloping to the horizontal at an angle equal to the parameter

of the isoclinic are traced on each isoclinic line. Trajectory S_1' through point O_1 on isoclinic I_4 is traced approximately. This is a fairly rapid method yielding satisfactory results. Several more accurate, but more laborious, methods of graphing stress trajectories are known, on which we shall not dwell here.

The trajectories of the highest tangential stresses intersect the trajectories of the main stresses at a 45° angle and may also be constructed on the basis of the isoclinic field.

For the study of stresses by the optical method a projection-polarization unit was assembled in which polaroids were used.

Samples for investigation were prepared from bands of silver chloride, 3-mm thick, produced by pressing and subsequent recrystallization. Upon recrystallization the band was rolled to a 2-mm thickness and annealed for internal stress removal. The annealing temperature was $80\text{-}90^\circ$, the holding period 8-10 hours. Samples were cooled with thermostat for 6-8 hours. Sometimes

Figure 1. Trajectory curves for the main normal stresses.

the band was not subjected to recrystallization. After pressing, but not directly rolled into strip 2 mm thick; samples were cut out from the strip, and after proper surface treatment underwent recrystallization at $120\text{-}130^\circ$ for 4-6 hours.

Grinding and polishing of silver chloride in the annealed state is nearly infeasible due to the extreme softness and plasticity of the material. Deformation, computed by formula (2), may attain 99%.

$$\mu = \frac{\omega_1 - \omega_2}{\omega_1}, \qquad (2)$$

where μ - body deformation;

ω_1 and ω_2 - body cross-sections before and after deformation.

The high plasticity of silver chloride enabled a mirror-like smoothness to be imparted to the surface of the samples. The samples were etched in a hyposulphite or ammonia solution, washed and dried. Two organic glass plates were used in processing the samples. The glass plates were kept wrapped in paper, preserving them from damage; the wrapping was removed only immediately before the operation. The sample was placed between these plates and subjected to compression in a press.

A 3-4 t. pressure was sufficient for a 20 x 20 mm sample. After compression the specimen acquired a perfectly smooth mirrored surface, which remained unchanged after annealing and recrystallization. The microstructure of the samples was distinctly revealed by etching.

Silver chloride used for stress investigation in macro-volumes must have a fine grain measuring 0.01-0.03 mm. Only at such grain size, or smaller, it becomes possible to obtain distinct patterns of isoclinic and isochromatic lines for different methods of loading. At larger sizes of the grain the "pictures" turned out to be diffused revealing the granular structure of the material. For grain sizes of 0.1-0.3 mm no inhomogeneity was to be observed in polarized light (crossed Nicol prisms) in unloaded samples, but the granular structure was revealed as soon as the load was applied. The inhomogeneity of the stress condition was clearly visible in different grains.

EFFECT OF A SINGLE FORCE ACTING ON ANISOTROPIC POLYCRYSTALLINE PLATES

A sample of silver chloride, prepared as described above, was placed on

the reverser table of the loading press.

In studying the action of a single force on an anisotropic texturised plate it is assumed that at each point of a two-dimensionally stressed plate the main stress σ is directed along the radius traced from the point of application of the single force to the given point. Such character of the main stress direction was disclosed by S. G. Lekhnitskiy for the case of the single force acting on an infinite half-plane possessing elastic anisotropy of an arbitrary type (9).

Small size samples were used in our work. Measurements were taken, however, at points sufficiently far removed from the side and bottom edges of the sample. Consequently, the finiteness of the size, obviously, should not have affected substantially the state of stress in the zone where measurements were taken. The plastic deformation engendered at the point of the single force application, apparently, was hardly reflected in those sections where the stress was being determined.

EFFECT OF A SINGLE FORCE ACTING ON THE FACE PARALLEL TO THE DIRECTION OF ROLLING

A fine-grained band of silver chloride produced by pressing was annealed at 120° for a period of four hours. This is sufficient for total recrystallization. After recrystallization the band was rolled to a thickness of 3 to 2 mm. Samples were cut out from the rolled band, and their test faces were ground, whereupon the samples were subjected to low-temperature anneal at 80° for 25 hours. During this time all the residual stresses, resulting in the process of rolling, were totally eliminated, while no recrystallization could develop at this temperature. The grain turned out to be elongated in the direction of rolling.

A 20 x 40 mm, 2-mm thick, sample was cut for testing purposes. At such dimensions of the sample the character of the optical patterns was totally

Figure 2. Effect of a single force acting along the direction of rolling. The isoclinics are shown for every 15°. Passing polarized light. The polaroids are crossed.
a - 0°; b - 15°; c - 30°; d - 45°; e - 60°; f - 75°

unaffected by the lateral faces and an averaging of the optical properties through the thickness of the samples occurred. The annealed samples placed into the field of the polariscope showed no double refraction, which pointed to the absence of internal stresses.

Loading was effected by means of a wedge. At the beginning of the loading a brightening of the sample was to be observed in the zone of action of the internal stresses. The isochromatic lines were clearly discernible only near the place of load application. Figure 2 shows the isoclines for every 15° during the action of a point load of 800 g. Visible is the zone of residual stresses which occupies a very small area as compared to the field of the sample under load. A diagram of the complete isoclinic pattern is provided in Figure 3-a. On the basis of this pattern an attempt was made to construct a qualitative pattern of the trajectory of the main normal stresses, and of the tangential stresses, using the previously described graphing technique for an isotropic body (Fig. 3-b). Figure 3-c shows the trajectories of the tangential stresses. The isochromatic lines become discernible with

Figure 3. Effect of a single force acting along the direction of rolling:

a - the entire field of isoclinics; b - trajectories of the main normal stresses; c - trajectories of the maximum tangential stresses.

increasing load. The isoclinics remain as distinct as before. The character of variation of the optical patterns during rotation of the plane of polarization at 2400-g and 3000-g loads remains unchanged.

Just as in the case of an 800-g load, the character of variation of the parameters of optical isoclinics remains constant for loads of 2400 and 3000 g. Consequently, the trajectories of the main normal and tangential stresses will also have the forms similar to those registered for a load of 800 g.

The isoclinic parameters and the angle between the direction of the acting force and the optical isoclinic for several samples will be found in Table 1.

The parameters of the isoclinic lines obtained do not correspond to the parameters of the isoclinics resulting from the action of a single force upon an amorphous body (Fig. 3-a and Table 1). This shows that the distribution of stresses in an amorphous isotropic body is different than in a crystalline substance.

Table 1.

Variation of the Isoclinic Parameters During Rotation of the Planes of Polarization

Angle of rotation of the plane of polarization, degree	Angle between the direction of the acting force and the optical isoclinic line, degree						
	Sample No. 1 p = 800 g	Sample No. 1 p = 2400 g	Sample No. 4 p= 3000 g	Sample No 3. p = 2000 g	Sample No. 12 p = 1500 g	Sample No. 14 p = 1000 g	Mean Angle degree

Shown in Figure 4 are the isoclinics formed by forcing a wedge into a thin silver-chloride plate. The test procedure was as follows. A fine-grained silver-chloride plate was sandwiched between two thick glass plates to prevent it from transverse bending at the moment of load application. A wedge, the thickness of which was equal to that of the plate, was forced into the latter. No isochromatic lines are to be seen in view of the small thickness of the plate (0.5 mm).

Figure 4. Impression of a wedge into a flat sample of silver chorlide.

The isoclinics assume a rectilinear position in the elastic-plastic region and, as in the cast of thicker plates, they describe an optical ellipsoid.

The optical pattern cannot be observed in this case in the zone of plastic deformation (belt around the contour of the wedge visible on the photographs) owing to the distortion of the sample's surface. If the isoclinic lines be continued to the point of their intersection, it would be found that they issue from the point of application of the single load, as in the previously discussed cases. This experiment shows that outside of the zone of plastic deformation the character of the acting forces remains the same, as before the plastic flow sets in in part of the sample acted upon by the wedge.

EFFECT OF A SINGLE FORCE ACTING ON THE FACE PERPENDICULAR TO THE DIRECTION OF ROLLING

All samples were prepared from a single band. The dimensions of the test piece were 20 x 20 x 2 mm. No residual stresses were to be revealed by examination in polarized light. Loading of the sample was effected by means of a wedge. At the beginning of loading a brightening of the sample was to be observed in the zone of action of the internal stresses. Isochromatic lines become visible as loading increases. The isoclinics remain sharp, with the exception of the region around 0°, where the isoclinic does not represent a radial straight line but a sector encompassing the region of $25\text{-}35^{\circ}$, thereby suppressing all the isochromatic lines. Figure 5 shows photographs of the isoclinics taken after every 15° for a load of 1500 g. A complete diagram of the isoclinics and the trajectories of the main and tangential stresses is provided in Figure 6.

The parameters of the isoclinics and the angle between the direction of the acting force and the optical isoclinic line for the samples under consideration are to be found in Table 2.

Analysis of the optical patterns produced in this case reveals a still greater distinction from the behavior of an amorphous isotropic body. Owing to the presence of texture the distribution of stresses, and, therefore, also the optical patterns, have a peculiar character. From Figure 5 it may be seen

that the brightening of the samples, as compared with the preceding case, is far greater in the direction perpendicular to the acting force. This is strongly reflected in the curves of the normal stresses: there appears an ellipse elongated in the direction perpendicular to the acting single force. The shape of the curves of the maximum shearing stresses changes accordingly. It should be noted that when the plane of polarization is close to the axis

Table 2.

Variation of the Isoclinic Parameters During Rotation of the Plane of Polarization.

Angle of rotation of the plane of polarization, degree.	Angle between the direction of the acting force and the optical isoclinic line, degrees	
	Sample No. 18	Sample No. 19

Figure 5. Effect of an 800-g point load acting at right angles to the direction of rolling. The isoclines are shown for every 15°. Passing polarized light. The polaroids are crossed.

a - 0°; b - 15°; c - 30°; d - 45°; e - 60°; f - 75°.

Figure 6. Effect of a single force acting perpendicularly to the direction of rolling:
a - full field of isoclinic lines; b - trajectories of the main normal stresses; c - trajectories of the maximum tangential stresses.

of rolling, the optical isocline is very wide and does not appear as a ray, issuing from the point of the load application, but forms a sector subtending an angle of 20-35°. This makes it very difficult to graph the trajectories of stresses in such a zone, but it may be assumed that within the entire sector covered by the zero optical isocline the stresses are the same or differ little from one another, in direction. The stress curves were plotted with due allowance for this assumption.

EFFECT OF A SINGLE FORCE ACTING AT AN ANGLE OF 45° TO THE DIRECTION OF ROLLING

From a silver-chloride band, produced by pressing, a 28 x 28 x 3 mm sample was cut so that its lateral faces formed a 45° angle with the direction of the axis of rolling. The sample was processed in the same way as in the previous cases. The pattern of action of the single force is the same as in the preceding cases. Placed in the field of the polariscope the sample produced no double refraction. This indicated that there were no internal stresses.

Figure 7. Effect of a single force acting at an angle of 45° to the direction of rolling. The isoclines are given for every 15°. Passing polarized light. The polaroids are crossed. X 2.
a - 0°; b - 15°; c - 30°; d - 45°; e - 60°; f - 75°.

A brightening in the zone of stress action was to be observed upon application of the load. Photographs of the sample under 3000-g load are reproduced in Figure 7. The optical patterns formed in this case differ strongly from those reviewed earlier. For the zero position there are three isoclines instead of one. No such phenomenon may be observed in optical isotropic material. The appearance of such a pattern in the pressed band may be explained only by the presence of a texture and the resulting anisotropy in the distribution of stresses within the tested sample. The isoclinic field was plotted in the diagram on the basis of the data contained in the photograph, and also by sketching during direct projection of the optical patterns on the screen. In graphing the trajectories of the main and maximum tangential stresses use was made of the technique applied in the study of optical isotropic amorphous bodies. The resulting distribution curves of the main and maximum tangential streeses are recorded in Figure 8.

COMPARISON OF THE TRAJECTORIES OF MAXIMUM SHEARING WITH THE SLIP LINES

The trajectories of the maximum tangential stresses obtained by optical

method for the action of a single force on the silver-chloride plates are shown in Figures 3-c, 6-c, and 8-c. The distribution of the maximum tangential stresses in metals may be appraised by the slip lines. Figure 9 shows the slip lines revealed by etching of the polished surface of steel after deformation. Comparing the pattern of the slip lines in metals with the trajectories of tangential stresses in silver chloride (Fig. 9), one finds a considerable resemblance between them. This resemblance is manifested with particular distinctness in the case of the forces acting at an angle of 45°.

Thus the utilization of silver chloride makes it possible to simulate the processes of plastic deformation of metal in the first approximation, and to determine the distribution of stresses in them.

INVESTIGATION OF THE PROCESS OF CUTTING OF SILVER-CHLORIDE PLATE SAMPLES

In the case of the action of a single force on silver chloride a correspondence with the action of a single force on real metals was observed as shown above. It may, therefore, be assumed that a similar correspondence of the acting forces will take place in more complicated cases as well. The cutting of silver-chloride plate samples is discussed below and a comparison made with the cutting of steel plate specimens.

The deformation mechanism and the physical phenomena involved in the process of metal cutting were discussed in study (10). A complex deformation process develops during cutting, including crumpling, setting, punching, bending, extension, and contraction. The change of shape during cutting occurs as a result of plastic, elastic, and breaking strains. The mechanism of deformation involved in cutting was studied by the authors on samples of carbon steel with varying contents of carbon. In order to plot the stress-strain curves for different zones of the samples the authors (10) studied the cutting of plate samples in a die, permitting observation. In view of the complexity of the phenomena to be studied various research methods were used. In addition

Figure 8. Action of a single force at an angle of 45° to the direction of rolling.

a - the entire isoclinic field; b - trajectories of the main mormal stresses; c - trajectories of the maximum tangential stresses.

Figure 9. Chernov-Lueders lines in steel (Nadai)

to direct measurement of the thickness of samples at different stages of cutting, studies were made of the cracking of lacquer coatings, the method of coordinate grid was applied, and the slip lines on the blue-finished and polished surfaces of samples were investigated. A considerable unevenness of the plastic flow was revealed. In the region bounded by one pair of cutting edges six zones with different strain conditions were observed.

Discussed below is the cutting of plate samples of silver chloride without

Figure 10. Diagram of plate sample cutting.

clamping. The stress and plastic deformation were studied in polarized light.

Samples measuring 5 x 40 x 2 mm were cut from a rolled band of fine-grained silver chloride. The faces were ground, and the samples were then annealed at 80° in the course of 8-10 hours. As a result of such anneal the residual stresses in the silver-chloride samples were completely removed. Later on the samples were subjected to cutting with the punch of the polarization unit. In addition to these samples, specimens measuring 2 x 20 x 0.5 mm were also prepared. These were cut from a rolled silver-chloride band and then subjected to recrystallization at 120° for a period of 6-7 hours. A fine-grained structure was thereby obtained. This series of samples were subsequently cut in a special unit. A polarization microscope was used to examine the character of stress distribution.

The samples prepared for cutting were placed between two thick glass plates. The thickness of the punch and the die were equal to the thickness of the sample.

The width of the punch used for cutting the plate samples of the first series amounted to 9 mm, and 6 mm - for the second series. Observations in polarized light showed identical optical patterns.

A diagram of plate-sample cutting is shown in Figure 10.

When pressure is applied to the punch, the sample begins by bending under

the punch and partially beyond its limits. The bending of the sample occurs as a result of the force exerted by the punch, and the die reaction forces which produce a torque. At the very beginning of force application the stresses are revealed only at the rim of the punch and the cutting edges of the die.

Figure 11 shows the part of the sample under the punch. Clearly visible is the variation of the isoclines during rotation of the plane of polarization. The isocline rotates about the center of that part of the sample which is exposed to the action of the punch. In this case, the pattern resembles that of pure bending. On further loading the isocline in the middle of the sample remains all the time in its place. This incicates that the stress in the central part remains unchanged, and delineates the boundary between the zones of extension and contraction.

For the given case the total isoclinic field was plotted and on the basis of these lines the isostatic field was obtained (see Figure 14, the left-hand side of the diagram).

Let us now consider that part of the sample which is directly contiguous to the cutting edges.

The action of the punch initially entails an elastic deformation of the sample, which on observation in polarized light appears as a brightening of the region adjacent to the cutting edges. On rotation of the plane of polarization the isocline smoothly moves along the sample (see Fig. 11). With the removal of the load the sample as observed in polarized light, becomes completely dark. This indicates the presence of elastic strain only.

When the load applied to the punch is increased, the picture gradually begins to change. The isocline changes only in a rigidly restricted region, which attains a certain limit and then remains unchanged (Fig. 12). Before the beginning of permanent plastic deformation and the cut proper, in the part of the sample which is under the punch and immediately adjacent to the cutting edges, a "triangle of deformation" (see Figs. 12-14) becomes visible. It is

so called because it may be observed even after the sample has been cut. In this case the shape of the isoclinic lines is still smooth, without bends.

Upon further increase of load the isoclinics observed in polarized light become sinuous. This probably signifies the beginning of shearing processes in the individual sections of the material located in the zone of action of the cutting edges. At the same time a crumpling of the sample occurs near the cutting edges (see Fig. 12 -2,-3). The crumpling of the sample surfaces which abut on the cutting edges, and the bending of the sample, increase continuously up to the moment of the beginning of the cut. At the start of the "crumpling" a plastic deformation referred to here as "contraction" takes place (see Figures 12-15.)

Figure 11. Initial stage of cutting of a plate sample (part of the sample located under the punch). Variation of the parameter of the isoclinic lines on rotation of the plane of polarization. Passing polarized light. The Nicol prisms are crossed. X 4.
a - 0°; b - 5°; c - 15°; d - 45°; e - 75°; f - 85°.

With further increase of the load the punching of the material begins. The fibers of the material begin to warp and there occurs a kind of shearing

Figure 12. Process of cutting of a plate sample (observed in polarized light). The Nicol prisms are crossed. Isoclinic lines 45°. x 4.

1 - beginning of loading; 2, 3 - crumpling sets in at the cutting edges; the zone of crumpling is indicated by an arrow; 4 - enlargement of the crumpling zone, the triangular zone of deformation is visible; 5 - beginning of shearing and punching; 6, 7 - punching and cut.

process in them. The microstructural changes involved therein will be discussed later on. As soon as the shearing process attains the stage of full development the severable part of the sample begins to separate from the ends. The fracture proceeds without any increase of load (see Fig. 16), but at the same time a marked contraction is to be observed, particularly, at the ends.

CUTTING OF PLATE-SAMPLE AT A LARGE CLEARANCE BETWEEN THE PUNCH AND THE DIE

At first the sample bends under the action of the punch. As observed in polarized light initially there appears a brightening around the cutting

edges. It then spreads over the entire area located under the punch extending partially to the free ends of the sample. The isocline in this case has the form of a straight line passing through the center of the sample. The changes occur in the same manner as shown in Figure 11. As the load increases the punch begins to exert greater pressure upon the sample and causes it to bend still more. As compared with the sample cut at a small clearance between the punch and the die, the variation of an identical isocline is to be observed at considerably higher loads. The first twisting of the isocline occurs approximately at loads 1.25 times higher than in the preceding case. The so-called "triangle of deformation" appears also much later and at higher stresses. As compared with the previous case, the triangle is more elongated (approximately by a factor of 1.5) in the direction of the center of the portion to be cut out.

The zone of crumpling is almost 1.5 times smaller for this type of cutting than in the preceding case, but indrawing (contraction) is considerably higher. The breaking strain appears after significant indrawing. All these distinctions from the preceding case may be attributed only to the fact that a greater effect results from the action of a couple owing to the greater gap between the punch and the die. The arm of couple in this case is greater than in the one previously examined. As a result of this, a greater flexure is produced and the indrawing is considerably larger. A diminution of the crumpling zone is due to greater bending of the sample. The breaking strain arises at a higher load. The indrawing is considerably larger than in the preceding case. This was also revealed in steel specimens in work (10). In studying the width of a contact (slip) ring the authors came to the conclusion that some grades of steel and aluminum display a tendency towards a reduction of the contact ring's width when the gap between the punch and the die is larger. The width of the contact surface, both in the case of metal and silver-chloride cutting is, in the first place, determined by the bending of the sample and then by its

crumpling near the cutting edges. In the given case it may be clearly seen that with an increase in the clearance the bending of the sample increases, the zone of crumpling diminishes, and as a result the width of the contact surface decreases.

On observing the cutting of samples in passing non-polarized light, the zones of crumpling and the varying flexure of the sample may be seen (Fig. 13).

Figure 13. Cutting of a plate sample of silver chloride (passing, non-polarized light). X 2.
a - small clearance; b - large clearance.

On the basis of optical patterns, as observed during the cutting of plate samples, the trajectories of the normal and the maximum tangential stresses may be plotted provided the conclusions relative to the case of single force action are taken into account, and certain assumptions, made pertaining to the process of cutting. The isoclinic lines were traced directly according to the optical pattern projected on the screen or were photographed. The isoclinic field obtained in the polariscope varies with changing punch loads.

At the beginning of deformation at low loads the isoclinics appear as straight lines which traverse the sample center, and their field covers a large area. As the load grows, however, the isoclinic field shrinks and the lines commence to bend. They become even more warped on further growth of the load, and after the first macroshears they begin to vary differently in the severing parts of the sample. The trajectories of the main and the maximum tangential stresses are plotted on the basis of the isoclinic fields (Fig. 14).

Figure 14. Trajectories of the main normal stresses (σ_1 on the right) and the field of isoclinics (the left part of diagram) for two loads.

In analyzing the trajectories of the normal stresses three different zones may be observed: 1) the zone of compression stresses; 2) the zone of tensile stresses, and 3) the zone of complex stresses in which an increase of load causes the sample to fail. On the basis of a comparison of the optical patterns of the trajectories of normal and tangential stresses and the variation of the geometrical form of the sample certain conclusions on the cutting process may be drawn.

Initially the punch produces an elastic compression of the silver chloride sample. In this case no change in the sample's shape can as yet be observed, but the optical patterns in polarized light already disclose the presence of elastic bending. A local plastic deformation occurs near the cutting edges after a further increase of the load. In the severable part of the sample, it becomes possible to observe in polarized light the "triangle of the complex state of stress", the base of which abuts on the cutting edges, while its summit lies on the neutral line between the extension and compression zones. The smaller the gap between the punch and the die, the smaller the "triangle of the complex state of stress". In passing light and at the surface of the sample no changes are visible. Observation of the microstructure in reflected light also reveals no changes. It is at this moment that permanent deformation (bend) sets in, and the contraction of the material begins around the cutting edges.

Figure 15. Trajectories of the maximum tangential stresses (at the right) for two loads.

With further loading "crumpling" sets in under the cutting edges, and

the character of the optical patterns observable in passing polarized light exhibits a sharp change. If up to this moment the isoclinics in the samples had the aspect of straight lines, now they begin to bend, this condition taking place only in the zone of the "triangle of the complex state of stress". No changes are visible in observations made in non-polarized light. After a certain increase of the load the character of the isoclinic lines manifests a still more drastic change. A sharp bend appears in the 45° isocline, and the latter, following a certain curve, connects the points in the sample located around the cutting edges. At a further increase in load shear sets in, and the optical pattern in polarized light changes again. The beginning of shear, as observed in polarized light, is shown in Figure 12,-5; for passing non-polarized light and a small clearance between the punch and the die - in Figure 13-a; and in case of a large gap - in Figure 13-b. In this condition a bending of the material's fibers occurs, as well as a glide of bands in individual grains (Fig. 16). At this moment the maximum shearing stresses attain a peak along some line which connects the areas of the sample near the cutting edges. On further action of the punch the portion of the sample to be cut out is squeezed out to be, finally, followed by the splitting of the sample into parts.

Figure 16. Microstructure of the sample at the initial moment of shearing. In polarized light this structure reveals patterns similar to those shown in Figure 13. Reflected light. X 500.

For purposes of comparison of the cutting processes in silver chloride and

in steel, the different stages of cutting are shown in Figure 17. The character of the separation of samples into parts is identical in the cutting of metal and silver chloride. This points to the similarity of the processes developing in the cutting of metals and silver chloride. After the sample has been cut, residual stresses may be observed both in the severed section and in the waste ends. The cut out part manifests a highly inhomogeneous state of stress, particularly, at the place of cutting. The flexure imparted at the beginning of the punch action still remains, as indicated by the neutral line in the middle of the sample. In the area near the cut the "triangle of the complex state of stress" is still visible.

CONCLUSIONS

1. In deformation fine-grained silver choloride behaves as a quasi-isotropic body. The grain size exerts a major effect on the sharpness of the optical patterns visible in polarized light. Coarse grain fails to produce a clear picture. A redistribution of stresses from grain to grain is to be observed in such samples.

2. Anisotropy of the elastic and piezo-optical properties is to be observed in rolled polycrystalline plates of silver chloride acted upon by a single force. For the three cases reviewed (single force is perpendicular, parallel, and slanted at a 45° angle to the direction of rolling or the axis of compression), the action of the forces and the stress patterns are different and differ strongly from the stress arising under single force action in isotropic bodies. For a single force acting at an angle of 45° to the axis of compression or rolling elastic and piezo-optical anisotropy is most strongly manifested. The isoclinic distribution patterns have a peculiar aspect distinct from the isoclinic lines emerging under the action of a single force in isotropic plates. The main stresses show their highest values not in the direction of the acting force but at a certain angle approaching 45°.

Figure 17. The different stages of cutting of unclamped plate samples:
a - silver chloride; b - steel sample (according to V. V. Gubarev).

3. Plotting of curves of the main normal and the maximum tangential stresses is possible for elastic and elastic-plastic deformation. After the plastic deformation has been completed, the surface of the sample at the place of load action suffers a distortion and the observation of optical patterns becomes impossible. In the regions of minor plastic deformation the optical pictures remain preserved and may be readily photographed or sketched.

4. The trajectories of the maximum shearing stresses in silver chloride coincide with the Chernov-Lueders lines which appear at the surface of the deformed metal. In metals they may be revealed by etching of ground samples cut from the deformed body.

5. The polarization optical method enables studies to be made of the stresses and of the process of deformation in cutting plate samples. The optical patterns obtained thereat indicate the qualitative distribution of stresses and reveal the different stressed areas.

6. Combining of the optical method with metallographic techniques enables certain conclusions to be drawn as to the mechanism of plastic deformation in the process of cutting. The zone of the principal plastic deformation is determined by the "triangle of complex stress condition", the base of which lies between the cutting edges and the summit - at the end of the line which .

separates the zone of compression from that of extension. Cutting is accompanied by the bending of fibers in the area delineated by the triangle and by the splitting of the grain (initially in individual grains and then over the entire volume) into slip bands resulting from the shearing action of the punch and die edges.

7. The behavior of silver chloride in the process of cutting is similar to that of metal. The picture obtained in work (10) for the cutting of sheet metal is to be observed also in the case of silver chloride. Thus wider possibilities for the study of stresses with the use of polarized light, are created.

REFERENCES

1. A. W. Stepanow, Sow. Phys., 1934, 6, 312, 1935, 8, 25.
2. A. V. Stepanov, ZhTF [Journal of Technical Physics], 1949, 19, 205.
3. R. D. Moeller, Trans. Amer. Soc. for Metals, 1951, 43, 39.
4. R. A. Zhitnikov & A. V. Stepanov, ZhTF, 1956, 26, 772, 779, 786.
5. F. Neumann, Vorlesungen über die Theorie der Elastizität Leipzig, 1885.
6. M. Rrocht, Fotourpugost' [Photoelasticity], v. 1 & 2, GIZ, 1948.
7. F. Pockels, Annalen der Physik, 1889, 37, 144, 269, 372, 1890, 39, 440.
8. V. M. Krasnov & A. V. Stepanov, ZhETF [Journal of Experimental and Theoretical Physics], 1953, 25, 98.
9. S. G. Leknitskiy, Teoriya uprugosti anizotropnovo tela [The Theory of Elasticity of Anisotropic Bodies], 1950.
10. V. I. Zalesskiy & V. V. Gubarev, Sb. XXXIII Moskovskovo instituta stali [Symposium of the Moscow Steel Institute], Metallurgizdat, 1955.

Prof. Dr. of Chemical Sciences N. D. TOMASHOV,
Assistant M. A. VEDENEYEVA, Engineer K. N. GEDGOVD
Department of Metal Corrosion.

EFFECT OF TENSILE STATIC AND ALTERNATING STRESSES ON THE CORROSION OF 1Kh18N9 STEEL

A number of studies (1-8) has been devoted to the investigation of corrosion in stressed austenitic steels of the 1Kh18N9 type. Studied in these works was the effect of the internal stresses, resulting from various heat treatments of steel, and of the externally applied static tensile stresses upon the tendency of steels to cracking.

It was established that a boiling $MgCl_2$ solution, a saturated aqueous solution of H_2S, a saturated solution of Hg_2Cl_2, the $FeCl_3$ solution, chlorobenzene in the presence of H_2O and a number of other media may cause the cracking of steels in the presence of tensile stresses. Fissures may occur between the crystals or run through them depending on the state of metal, the aggressiveness of the medium, and the stresses. For an accelerated determination of the susceptibility of steels to cracking it is recommended to use boiling $MgCl_2$ solution (3) and aqueous solution of H_2S (7) under conditions of static tensile stresses being applied.

The purpose of this work was to investigate the influence of the state of steel 1Kh18N9 on its resistance in a solution promoting intercrystalline corrosion, under conditions of simultaneous application of static tensile and alternating stresses.

The effects of the static tensile stresses were studied with the aid of a device designed by the Moscow Institute of Steel (9). The wire sample to be tested was placed in a glass test tube, the lower opening of which was sealed by a rubber stopper, and fixed to the hooks of the frame and the lever. The required stress was produced by moving a corresponding load along the lever arm. The corrosive solution was poured into the test tube. Corrosion

fatigue was investigated in an apparatus designed by the Moscow Institute of Steel (10). The wire sample was placed in a vessel made of organic glass which was filled with the aggressive solution. The sample was stressed by bending and simultaneous rotation about its longitudinal axis. Various stresses were produced by imparting corresponding radii of curvature to the sample in the process of bending.

The stress tests were carried out on wire samples 1 mm in diameter. In addition to this, corrosion tests were conducted with flat samples without application of stresses. The chemical composition of the steel is given in Table 1.

Prior to the tests the wire was cleaned by No. 280 emery cloth and washed in alcohol.

Table 1.

Chemical Composition of the Investigated Grade 1Kh189 Steel

Type of Sample	Compositon, %							
	C	Mn	Si	Cr	Ni	S	P	Ti
1 - mm diameter wire 0.4-mm thick band								

In carrying out the tests in the equipment referred to above, it was found expedient to use as corrosion media the solutions ordinarily employed to investigate the tendency of steel 1Kh18N9 to intercrystalline corrosion, since most of these solutions are used at elevated temperature as, for example, sulfur-copper solution (11, 12) nitric acid (12), etc. Solutions of fluorides in nitric acid which promote intercrystalline corrosion not only on heating (12, 13), but also at room temperature (14), are also unsuitable in this work owing to their high aggressiveness and their tendency to attack the glass parts of the apparatus for tensile tests.

On the basis of special research a solution, containing 0.8 g-equiv./

/liter of nitric acid (5%)and 0.1 g-equiv./liter of ferric chloride, was adopted as the aggressive medium.

The effect of the contents of varying amounts of $FeCl_3$ in nitric acid on the corrosion of 1Kh18N9 steel was investigated on 70 x 5 x 0.4 mm plate samples. After heat-treating the samples were etched in a 4% solution of HNO_3 containing 1% HCl. The specimens were weighed before and after testing and their electric resistance was measured by means of an MD-6 bridge. All tests were run at a temperature of 19-20°.

The degree of intercrystalline corrosion was determined by the change in resistivity of the sample as a result of corrosion, and quantitatively expressed by ratio $\frac{\Delta\rho}{\rho}$, where $\Delta\rho = \rho - \rho_1$ - resistivity variation:

ρ_1 - resistivity of the metal prior to corrosion test;

ρ - resistivity of the sample after the test.

Total corrosion was determined by weight losses of the sample. It should be noted that intensive intercrystalline corrosion may entail a possible crumbling of the grains which may cause appreciable losses in weight.

For purposes of comparison of intercrystalline corrosion with uniform corrosion, the latter was also expressed quantitatively by ratio $\frac{\Delta\rho_s}{\rho}$, where $\Delta\rho_s$ is the change in resistivity as a result of general corrosion calculated on the basis of weight losses. By a simple calculation it may be shown (6), that

$$m = \frac{S_2}{S} \approx \frac{\Delta\rho}{\rho}, \qquad (1)$$

where m - degree of attack of the sample cross-section by intercrystalline corrosion;

S - total cross-sectional area of the sample;

S_2 - cross-sectional area of the sample attacked by intercrystalline corrosion;

ρ - resistivity of metal after corrosion;

$\Delta\rho$ - resistivity change resulting from corrosion.

From equation (1) it follows that ratio $\frac{\Delta\rho}{\rho}$ shows what part of the specimen's section is attacked by corrosion.

In addition tc resistivity variation, determinations of the change in tensile strength resulting from corrosion were made in the course of the study of static tensile stresses. Tensile strength was calculated from formula:

$$K_{\sigma} = \frac{\Delta\sigma_B}{\sigma_B} \cdot 100, \qquad (2)$$

where

$$\Delta\sigma_B = \sigma_B - \sigma'_B;$$

σ_B - tensile strength before corrosion;

σ'_B - tensile strength after corrosion.

In corrosion fatigue tests the resistance of the metal was evaluated on the basis of the number of cycles before the breakdown of the sample.

EFFECT OF FERRIC CHLORIDE CONTENTS IN 5% NITRIC ACID ON THE CORROSION OF STEEL.

The results of tests of 1Kh18N9 steel samples measuring 70 x 5 x 0.4 mm, hardened from 1080-1100° and held at 650° for three hours in 0.8 N. HNO_3 with varying $FeCl_3$ contents, are given in Table 2 and in Figures 1 and 2.

Figure 1. Effect of the $FeCl_3$ contents in 0.8 N. solution of HNO_3 on intercrystalline and uniform corrosion of 1Kh18N9 steel: 1 - intercrystalline and uniform corrosion; 2 - uniform corrosion. a) $FeCl_3$ content, g-eq/lit.

The severity of the attack by intercrystalline corrosion suffered by the metal increased as the proportion of $FeCl_3$ in the investigated solutions was augmented to 0.3 g-eq/lit. (Fig. 1, curve 1). Uniform corrosion (Fig. 1,

Figure 2. Photomicrograph of 1Kh18N9 steel after a three-hour exposure of the polished cross-section of the sample in a solution containing 0.8 g-eq/lit HNO_3 + 0.3 g-eq/lit $FeCl_3$. X 358.

Table 2.

Effect of $FeCl_3$ Contents in 0.8 N. HNO_3 on Intercrystalline and Uniform Corrosion of 1Kh18N9 Steel*) (Duration of Test 3 Hours).

$FeCl_3$ contents in 0.8 N. HNO_3 g-eq/lit.	Variation of the sample's resistivity as a result of corrosion, ΔR, ohm.	Intercrystalline and uniform corrosion, $\frac{\Delta \rho}{\rho}$	Proportion of uniform corrosion $\frac{\Delta \rho}{\rho}$	Losses in weight g/m^2

*) Average values for 2-3 samples.

curve 2) also showed a growth, but its value was minor. The proportion of uniform corrosion in comparison with intercrystalline corrosion is small, and it varies negligibly with increasing concentration of $FeCl_3$.

On further increase of the $FeCl_3$ concentration up to 0.5 g-eq/lit intercrystalline corrosion manifests a slight decrease, but uniform corrosion increases appreciably. This may be explained by the rising proportion of the depassivating chlorine ion in the solution.

On the basis of the obtained data, the solution containing 0.8 g-eq/lit

HNO_3 and 0.3 g-eq/lit $FeCl_3$ may be considered as the more effective for determination of the tendency to intercrystalline corrosion. Comparative corrosion tests carried out in sulfur-copper solution showed that the rate of intercrystalline corrosion in the solution containing 0.3 g-eq/lit $FeCl_3$ and 0.8 g-eq/lit HNO_3 at room temperature is 3-4 times lower than in a boiling sulfuric acid solution $CuSO_4$.

EFFECT OF STATIC TENSILE STRESSES

The influence of tensile stresses ranging from 0.77 to 51.3 kg/mm^2 on corrosion was studied. The wire samples were subjected to the following two types of heat treatment before testing: 1) hardening from 1050-110° (water quench); 2) hardening with subsequent tempering at 650° for 2 hours. The solution containing 0.8 g-eq/lit HNO_3 and 0.3 g-eq/lit $FeCl_3$ turned out to be too aggressive to be used in tests with simultaneous application of stresses. The samples failed too rapidly. Consequently, a solution containing 0.1 g-eq/lit $FeCl_3$ and 0.8 g-eq/lit HNO_3 was used for these tests. The samples were tested in the course of three hours. The degree of corrosion was determined by resistivity variation measured before and after the test over a 70-mm long section and by variation of tensile strength. In addition, a metallographic investigation was carried out. The results of the tests will be found in Table 3 and Figures 3 and 4.

From Table 3 and Figure 3 it may be seen that the corrosion of steel increases with increased application of load. Comparison of the values of corrosion index $\frac{\Delta\rho}{\rho}$ (Table 2 and 3) leads to the conclusion that 1Kh18N9 steel becomes subject to intercrystalline corrosion after tempering, and to uniform corrosion - after hardening.

The tensile strength of 1Kh18N9 steel samples decreases after tempering as a result of corrosion. The losses in strength increase in proportion to the growing load. Tensile strength shows practically no changes during

Figure 3. Effect of tensile stresses on the corrosion of steel 1Kh18N9 in a solution containing 0.8 g-eq/lit HNO_3 and 0.1 g-eq/lit $FeCl_3$:
1 - steel hardening from 1080°-1100°;
2 - steel after temper hardening at 650° for 2 hours.
a) Stress, kg/mm^2

corrosion of hardened steel (Table 3). This is confirmed by the uniform character of hardened steel corrosion and by the local character of tempered steel corrosion. A high loss in strength (22%) of one sample of hardened steel at 51.3 kg/mm^2 stress (Table 3) indicates the possible appearance of individual cracks in the defective spots of the sample at high stresses. The formation of such a fissure is not typical, since otherwise there would be several such cracks, and in the presence of a number of fissures the resistivity of the sample should have manifested a noticeable change. In our tests,

Figure 4. Photomicrograph of 1Kh18N9 steel sample (temper hardened at 650°) after a three-hour exposure in a solution containing 0.8 g-eq/lit HNO_3 and 0.1 g-eq/lit $FeCl_3$ with simultaneous application of tensile stresses (25.7 kg/mm^2). Longitudinal section of sample. Etched in HCl and $CuSO_4$. X 600.

however, the $\frac{\Delta \rho}{\rho}$ ratio of the sample, which was found to have lost 22% in tensile strength, and of the sample with unchanged strength, shows close by approaching values (0.054 and 0.057) resulting from uniform corrosion. Metallographic analysis also confirms the development of intercrystalline corrosion of the steel after tempering (See Fig. 4). No cracks were revealed by metallographic examination on hardened samples, even on the one which was

Table 3.

Effect of Tensile Stresses on the Corrison of 1Kh18N9 Steel in a Solution Containing 0.1 g-eq/lit $FeCl_3$ and 0.8 g-eq/lit HNO_3 (duration of test - 3 hours) *)

Heat Treatment	Hardening from 1080-1100°		Hardening from 1080-1100° with subsequent temper at 650° (2 hours)	
Stress, kg, mm/2	Restivity variation $\frac{\Delta \rho}{\rho}$	Tensile strength variation $\frac{\Delta \sigma_B}{\sigma_B} \cdot 100$	Resistivity variation $\frac{\Delta \rho}{\rho}$	Tensile strength variation $\frac{\Delta \sigma_B}{\sigma_B} \cdot 100$
	Sample No. 1 Sample No. 2			

*) Average values for 2-3 samples

**) Tensile strength of the samples after the test exceeded the tensile strength of the samples before the test (within the limits of the method's error).

found to have lost 22.6% of its strength.

EFFECT OF ALTERNATING STRESSES

A study was made of the effect of alternating stresses, ranging from 20 to 45 kg/mm^2, upon the corrosion of 1Kh18N9 steel in a solution containing 0.8 g-eq/lit HNO_3 and 0.1 g-eq/lit $FeCl_3$. The steel was tested in two states: after hardening from 1080-1100° and after temper hardening at 650° for two hours. In addition, a Weler curve - mechanical fatigue versus magnitude of stress on testing in oil - was obtained for the steel after tempering. The cycle frequency was 4200 r.p.m. The test results are recorded in Table 4 and Figures 5-8.

Table 4.

Mechanical and Corrosion Fatigue of 1Kh18N9 Steel

Stress kg/mm^2	Number of cycles before breakdown of the samples.*)		
	Hardening from 1080-1100° (0.8 g-eq/lit HNO_3 + 0.1 g-eq/lit $FeCl_3$)	Hardening from 1080-1100° + tempering at 650° (2 hours)	
		0.8 g-eq/lit HNO_3 + 0.1 g-eq/lit $FeCl_3$	Oil
			(no failure)

*) Average values for 2-3 samples

Figure 5. Fatigue curve for 1Kh18N9 steel (hardening from 1080-1100° in oil, tempering at 650°, 2 hours)
a) Stress, kg/mm^2;
b) Number of cycles before breakdown, N·10^{-6}

Figure 6. Corrosion fatigue curves for 1Kh18N9 steel in a solution containing 0.8 g-eq/lit HNO_3 and 0.1 g-eq/lit $FeCl_3$:
1 - steel after hardening from 1080-1100° and tempering at 650° for 2 hours; 2 - steel after hardening from 1080-1100°.
a) Stress, kg/mm^2; b) Number of cycles before breakdown, N·10^{-5}.

The tensile strength of 1Kh18N9 steel after tempering approaches 30 kg/mm^2. For tests conducted in HNO_3 + $FeCl_3$ solution the number of cycles preceding breakdown of samples diminishes sharply. Corrosion-fatigue resistance of hardened steel is higher than its resistance after tempering. At 20 kg/mm^2 stress the resistance of the samples differs by more than a factor of 2. This difference diminishes as the stress increases. For a 45 kg/mm^2

Figure 7. Photomicrograph of 1Kh18N9 steel sample (after 650° temper for 2 hours) after corrosion-fatigue test in a solution containing 0.8 g-eq/lit HNO_3 + 0.1 g-eq/lit $FeCl_3$ under a stress equal to 35 kg/mm^2. Longitudinal section of sample. Etched in HCl and $CuSO_4$. X 600.

Figure 8. Photomicrograph of 1Kh18N9 steel sample (hardening from 1080-1100°) after corrosion-fatigue test in a solution containing 0.8 g-eq/lit HNO_3 and 0.1 g-eq/lit $FeCl_3$, under stress of 35 kg/mm^2. Longitudinal section of sample. Etched in HCl and $CuSO_4$. X 600.

stress the number of cycles before failure of differently heat-treated samples is the same.

The declining effect of heat treatment upon the resistance of steel under conditions of rising stress is attributable to the fact that with increased stresses the role of the mechanical factor in the corrosion-fatigue breakdown of steel grows and it assumes a prevalent significance when the loads are high.

The photomicrographs of samples with differing heat-treatment show that the corrosion-fatigue cracks in the samples pass across the crystals after hardening, and between the grains of the metal - after tempering.

It should be noted that the single cracks in hardened samples begin between the crystals and then turn into transcrystalline fissures. In tempered samples minor single cracks were found to be passing through the metal grain.

CONCLUSIONS

1. The application of tensile static or alternating stresses greatly accelerates the intercrystalline corrosion of stainless 1Kh18N9-type steel treated by solutions which promote intergranular breakdown.

2. The method of revealing the tendency of steel to intercrystalline corrosion may be made more sensitive through application of tensile stresses during tests of steel in a corrosive solution.

3. The use of a solution containing 0.8 g-eq/lit HNO_3 (5%) and 0.1 g-eq/lit $FeCl_3$ is recommended for intercrystalline corrosion tests with simultaneous application of tensile stresses.

4. A solution containing 0.8 g-eq/lit HNO_3 and 0.3 g-eq/lit $FeCl_3$ may be successfully used for intercrystalline corrosion tests not involving the application of tensile stresses. The rate of intercrystalline corrosion in this solution is 2-3 times lower than in the standard liquor. Yet this solution has a number of advantages: it is simple in preparation, safe, and the tests for intercrystalline corrosion in it may be carried out at room temperature.

5. After hardening, 1Kh18N9 steel shows no tendency to crack formation under the action of static tensile stresses up to 51.3 kg/mm^2 in a solution containing 0.8 g-eq/lit HNO_3 and 0.1 g-eq/lit $FeCl_3$.

6. The corrosion-fatigue cracks in samples of 1Kh18N9 steel have a predominantly transcrystalline character after hardening from 1080-1100°.

7. In samples of 1Kh18N9 steel tempered at 650° for a period of 2 hours the corrosion-fatigue cracks, and those forming as a result of corrosion with application of static tensile stresses, show a predominantly intercrystalline character.

REFERENCES

1. S. L. Hoyt, M. A. Scheil, Transactions of the American Society for Metals, 1939, 27, 191-226.

2. J. C. Holge, J. L. Miller, Transactions of the American Society for Metals, 1940, 28, No. 1, 25-62.

3. M. A. Scheil, Symposium of Stress-Corrosion Cracking, 1945, 395-410.

4. O. B. Ellis, Symposium of Stress-Corrosion Cracking, 1945, 421-424.

5. R. Franks, W. O. Binder, C. M. Brown, Symposium of Stress-Corrosion Cracking, 1945, 411-420.

6. F. K. Bloom, Corrosion, 1955, No. 8, 351-361.

7. V. M. Nikiforova, A. V. Ryabchenkov, N. A. Reshetkina, Vliyaniye korroziynykh sred na prochnost' stali, TsNIITMASh [Effect of Corrosive Media on the Strength of Steel, Central Scientific-Research Institute of Heavy Machinery], 1955, vol. 77.

8. V. M. Nikiforova, N. A. Reshetkina, Ibid, 79-102.

9. N. D. Tomashov, V. A. Titov, Zavodskaya laboratoriya [Plant Laboratory] 1949, No. 1.

10. N. D. Tomashov, V. A. Titov, Zavodskaya laboratoriya, 1951, No. 7.

11. GOST (State Standard) 6032-51, Metody ispytaniya na mezhkristallitnuyu korroziyu [Methods of Intercrystalline Corrosion Testing].

12. H. W. Gillet, Symposium on Evaluation Tests for Stainless Steels, 1950, 41-55.

13. B. I. Medovar, N. A. Langer, Avtogennaya svarka [Gas Welding], 1951, No. 5.

14. V. Sh. Shekhtman, M. A. Vedeneyeva, N. P. Zhuk, ZhFKh - Zhurnal Fizicheskoy khimiyi [Journal of Physical Chemistry], 1954, 28, vol. 12, 2199-2209.